Isern, A.R., Anselmetti, F.S., Blum, P., et al., 2002
*Proceedings of the Ocean Drilling Program, Initial Reports* Volume 194

# 1. Leg 194 Summary[1]

Shipboard Scientific Party[2]

## ABSTRACT

Estimating the amplitude and timing of past eustatic sea level changes is essential both for the establishment of an accurate Phanerozoic sea level curve and for the interpretation of sediment sequences on continental margins. The magnitude and timing of sea level changes can be estimated in tectonically stable environments by correlating seismic data with lithologic facies, biofacies (for paleowater depths), and chronostratigraphy.

During Leg 194, a series of eight sites was drilled through Oligocene–Holocene mixed carbonate and siliciclastic sediments that record the depositional history and past sea level variations on the Marion Plateau, northeast Australia. Seismic sequence stratigraphy provided the geometric framework to locate the drill sites on two carbonate platforms, their slopes, and the plateau for optimal sampling of highstand and lowstand sequences with geometries that enable quantification of Miocene relative sea level variations. At each site, ~500–700 m of sediment was drilled, and five sites penetrated into acoustic basement. During this leg, ~2 km of sediment was recovered from a total cored interval of 5 km. Water depths of the drill sites ranged from 304 to 419 m.

In addition to determining sea level magnitudes, Leg 194 drilling also addressed the following scientific themes:

1. The development of carbonate platforms in a current-dominated environment,
2. The development of subtropical carbonate platforms,
3. Facies changes and the development of sequence stratigraphic units controlled by sea level changes in a mixed carbonate and siliciclastic sediment system,
4. The record of Oligocene–Pliocene third-order sea level fluctuations,

[1]Examples of how to reference the whole or part of this volume.
[2]Shipboard Scientific Party addresses.

Ms 194IR-101

5. The mechanisms and causes of fluid flow within pure carbonate and mixed siliciclastic/carbonate depositional environments, and
6. The role of climatic and paleoceanographic change in the subtropical South Pacific and its influence on carbonate platform development.

The original hypothesis for Leg 194 drilling postulated that the magnitude of the late middle Miocene (calcareous nannofossil Zones N12–N14; 12.5–11.4 Ma) sea level fall could be estimated from seismic sequences and facies relationships between the top of the Northern Marion Platform (NMP), which was deposited during the sea level highstand, and the base of the Southern Marion Platform (SMP) initiated during the lowstand. Drilling results showed, however, that the southern platform is not solely composed of late Miocene age sediments as previously thought. Instead, ~120–160 m of upper Miocene carbonates overlie a thick middle to lower Miocene platform similar in age to portions of the northern platform. The magnitude of the middle Miocene sea level fall, therefore, was estimated by reconstructing the paleobathymetry of the northern platform top with respect to an upper middle Miocene lowstand ramp immediately adjacent to the platform margin. Physical properties information was used to remove the compaction effects imparted by the overlying sediments at both sites. The base of the lowstand unit after decompaction lies 96 m below the top of the NMP. Paleowater depths estimates are 10–50 m for the platform surface at Site 1193 and 30–50 m for the lowstand unit at Site 1194. Combining the decompaction with the paleowater depth estimates, a late middle Miocene sea level drop between 56 and 116 m is required to produce today's sediment geometries at Sites 1193 and 1194. These values assume infinite crustal strength between the sites. If zero flexural strength is assumed for the crust, the local isostatic compensation would reduce the required magnitude of the sea level drop to 12–53 m. The undisturbed and consistently dipping sediments, as well as the horizontal basement geometry between the two sites, however, show no signs of differential subsidence, and favor the infinite flexural strength model over local isostacy.

Lithologic and biostratigraphic data obtained from the Neogene carbonate platforms of the Marion Plateau during Leg 194 reveal that platform architecture was controlled by a series of complexly related factors including sea level change, bottom-current action, and the nature of biological assemblages. Two platform to slope transects were drilled across the Miocene carbonate platforms of the Marion Plateau. An important finding is that the oldest platform phase of the southern carbonate platform developed in a topographic depression as opposed to the more common condition of nucleation on a topographic high. Furthermore, the steep-sided geometry of both Marion Plateau carbonate platforms is typical of tropical to subtropical carbonate platforms. Despite this, cores retrieved during Leg 194 document a cool subtropical faunal assemblage consisting primarily of red algae, bryozoans, and larger foraminifers. These calcite-dominated biogenic sediments have a lower diagenetic potential than their aragonite-dominated counterparts in the tropical realm. Therefore, they can be reworked more easily as they undergo less cementation. In addition, the fragmentation of these sediments leads to the formation of silt- to fine sand–sized particles rather than carbonate mud. Another important finding of Leg 194 is that unlike other carbonate systems, the morphologies of which are predominantly controlled by wind direction, the carbonate platform architecture observed on the

Marion Plateau was strongly influenced by high-energy currents near the seafloor, similar to those that exist on the modern Marion Plateau. These currents inhibit sedimentation in the upcurrent position and form wide low-angle clinoforms in the downcurrent position, resulting in an asymmetric platform shape.

Pore waters from Leg 194 sediments provide clear evidence that seawater is circulating through the sediments proximal to the carbonate platforms on the Marion Plateau. The dolomitization found in both platforms is itself indirect evidence for past fluid circulation, as dolomite formation on a large scale requires fluid exchange to deliver magnesium to the precursor calcium carbonate sediments. Although sampling of pore waters from within the SMP was not possible because of low recovery, samples taken from the adjacent periplatform sites are characterized by seawater values for most elements. These samples provide evidence that seawater is circulating through these sediments even though they are overlain by ~200 m of hemipelagic deposits. Evidence also indicates that seawater is circulating through the NMP.

Acoustic basement was penetrated at five sites during Leg 194, and the basement rocks that were collected differ greatly from those drilled on the Queensland Plateau. Rather than metasedimentary rocks, highly altered volcanic flows and volcaniclastics were recovered. The lack of deformation in hand samples and thin sections suggests that these volcanics may have formed during the Late Cretaceous–Paleocene rifting along northeastern Australia from the Papuan Plateau in the north and the Lord Howe Rise in the south. High-quality paleomagnetic data collected from these basement volcanics, when compared with the Australian apparent polar wander path, may provide age estimates for both the emplacement of the basalts and the timing of their low-temperature alteration.

## INTRODUCTION

Carbonate platforms and their slopes are sensitive indicators of sea level variations, as they predominantly record growth during sea level highstands and shut down during sea level lowstands. Sampling these platforms records sea level change in a "dipstick" fashion. On the other hand, sediments on platform margins and slopes record sea level variations as alternations of shallowing and deepening sequences. Leg 194 drill sites on the Marion Plateau, northeast Australia (Figs. F1, F2), were positioned to establish the magnitude of the late middle Miocene (calcareous nannofossil Zones N12–N14; 12.5–11.4 Ma) sea level fall using both of these depositional systems. This information will provide an independent calibration of a significant part of the global sea level curve. An important characteristic of the stratigraphic relationships investigated during Leg 194 is that the drill sites are located in an area without major basement structuring. Thus, subsidence of the platform is likely to have affected all sites equally, enabling the true amplitude of the sea level fall to be determined.

High-resolution seismic data collected during the Leg 194 site survey provides quasi-three-dimensional geometry of Oligocene to Pliocene depositional sequences on the Marion Plateau. The correlation of these seismic images with drill core and logging data provides a synoptic view of depositional processes in a mixed carbonate-siliciclastic carbonate platform setting. The seismic sequence geometry shows that the depositional systems of the Marion Plateau are predominantly controlled by

F1. Map showing DSDP Site 209 and ODP Legs 133 and 194 sites, p. 61.

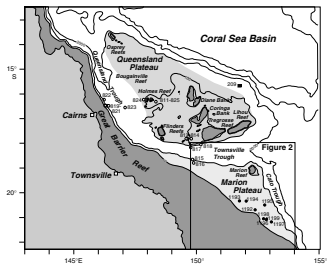


F2. Map showing ODP Legs 133 and 194 sites with multichannel seismic lines, p. 62.

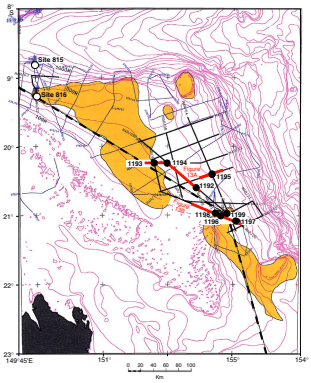

current flow and provide insight into the genesis of a current-dominated platform system. In addition, the carbonate platforms and slopes drilled during Leg 194 preserve a record of third-order sea level variations within a mixed carbonate-siliciclastic depositional environment. Pore water geochemical records from slope sites and platform sites will provide insight into possible fluid flow processes and diagenesis. Finally, the composition and age of basement will yield crucial information on the tectonic history of this passive margin.

# BACKGROUND

## Geologic Setting of the Marion Plateau

The Marion Plateau and its carbonate platforms, located between 18°S and 23°S, seaward of the south-central Great Barrier Reef on the northeastern Australian continental margin (Fig. F1), provide an ideal case study to address the causes, magnitudes, and effects of sea level change on continental margin sediments. This plateau is the most southerly of the northeast Australian marginal plateaus, forming a deeper extension of the Queensland continental shelf, and is bounded by the Townsville Trough along its northern margin, the Cato Trough along its eastern margin, and the south-central Great Barrier Reef to the west (Fig. F1). The Marion Plateau is part of a slowly subsiding margin. It is thought that the gently northeastward-dipping plateau top remained exposed throughout much of the Paleogene, forming a relatively smooth plateau surface (Pigram et al., 1992).

### Tectonics of the Marion Plateau

The western Coral Sea has been affected by two distinct tectonic events. The earlier event, Late Jurassic–Early Cretaceous in age, was responsible for the formation of the Queensland and Townsville Basins that underlie the present-day bathymetric features of the Queensland and Townsville Troughs (Fig. F1). These basins formed as a result of oblique extension along preexisting Paleozoic structural trends (Struckmeyer and Symonds, 1997). The Queensland and Townsville Basins do not appear to have been affected by the later tectonism responsible for seafloor spreading in the Tasman and Coral Sea Basins (Struckmeyer and Symonds, 1997). In the Late Cretaceous to early Paleocene, rifting in the Coral Sea Basin created numerous continental fragments that are now capped by carbonate platforms such as on the Marion Plateau (Figs. F1, F2). This rifting in the Coral Sea was an extension of Late Cretaceous (80 Ma) seafloor spreading in the Tasman Basin, which extended to the north to form the Cato Trough and the Coral Sea Basin by 64 Ma (Weissel and Hayes, 1977; Hayes and Ringis, 1973; Shaw, 1978). Spreading is thought to have ceased along the length of this system by the earliest Eocene (52 Ma) (Gaina et al., 1999). Thus, the main physical elements of the western Coral Sea were in place by the early Tertiary (Davies et al., 1989). Although the exact structural style and development history of the rift system are still not completely understood, it is clear that the Late Jurassic–Early Cretaceous rifting event controlled the gross architecture of the margin and the shape and distribution of the high-standing structural elements on which the carbonate platforms are located. The Marion Plateau is an internally largely undeformed basement block with structural elements existing only on its margins

(Fig. F3). Basement along the northern margin of the plateau consists of gently dipping ramps that gradually deepen toward the Townsville Trough until a fault is encountered. Normal extensional faults along this northern margin are restricted to the edge of the plateau (Symonds et al., 1988). The eastern margin of the plateau is free of major structural offsets (Mutter and Karner, 1980), and the slope is apparently simple and continuous. Faults along this margin are steeply dipping to vertical from the margin of the plateau into the Cato Trough. A southeasterly plunging, gently arched basement high forms the southern part of the plateau. The top of the arch is unstructured, and faults are confined to the flanks of the arch (Pigram, 1993).

## Subsidence History of the Marion Plateau

The tectonic histories of the Marion and Queensland Plateaus are well constrained by Ocean Drilling Program (ODP) Leg 133 drill holes and extensive multichannel seismic data. Subsidence curves for these plateaus have been produced using both benthic foraminifers (Katz and Miller, 1993) and geohistory modeling (Fig. F4) (Müller et al., 2000). Geohistory models were produced using integrated geophysical logs, biostratigraphic and lithologic information, and seismic reflection data (Müller et al., 2000). These models predict post-9-Ma subsidence of 1300 ± 200 m in the Queensland Trough and 650 ± 200 m on the western margin of the Queensland Plateau, and post-5-Ma subsidence of 500 ± 30 m on the southern margin of the Queensland Plateau and 660 ± 50 m on the northern margin of the Marion Plateau (Fig. F4) (Müller et al., 2000). Although the Marion and Queensland Plateaus are located on a passive margin, ~1000 km south of the Pacific/Australian plate boundary, geohistory models record a greater amount of post-9-Ma subsidence than simple elastic models can predict. This subsidence occurred in pulses between 9 and 5 Ma on both plateaus. It is difficult to account for this observed subsidence either by means of thrust loading in Papua New Guinea or by a combination of the latter and in-plane stresses originating from collision along the Pacific/Australian plate boundary (Müller et al., 2000). Despite the occurrence of post-9-Ma subsidence events on the Marion Plateau, the observed rates of tectonic subsidence are much slower than those of third-order sea level changes and thus can be differentiated from glacial eustasy. In addition, because of the methodology proposed here to investigate sea level change, any unaccounted subsidence should be similar for all sites. Although we will attempt to quantify in detail the additional water depth added to all sites as a result of tectonic subsidence, this increase is likely to be <10 m between Zones N12 and N14 and thus will not greatly affect our attempts to quantify sea level variations.

## Stratigraphy of the Marion Plateau: Evidence from Prior Drilling

Stratigraphies for the Marion Plateau were obtained during Leg 133 (Figs. F1, F5) (Davies, McKenzie, Palmer-Julson, et al., 1991), and these data supplement extensive seismic surveys over the plateau. Initiation of shallow marine carbonate sedimentation on the Marion Plateau began during the latest Paleogene, as the sea transgressed across basement (Megasequence A) (Pigram, 1993). These first sediments over basement are thought to be primarily siliciclastic, with temperate-water carbonates occurring in the eastern part of the sequence.

**F3.** Topography of acoustic basement, p. 63.

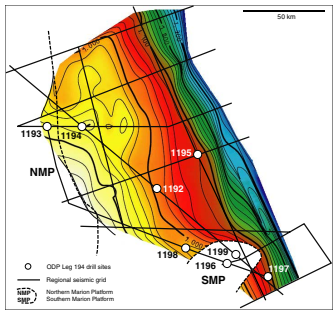


**F4.** Water-loaded tectonic subsidence, p. 64.

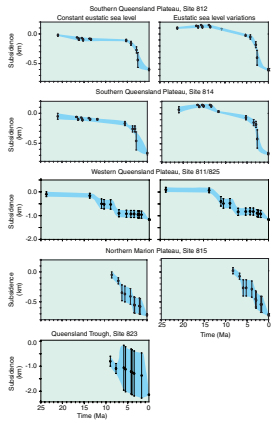


**F5.** Stratigraphic summary of previously cored sites near Leg 194 sites, p. 65.

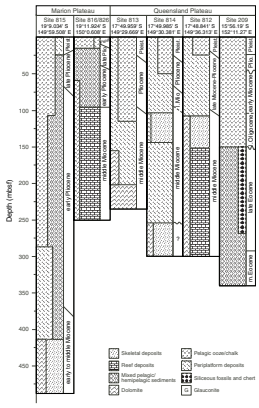

Sedimentary facies recovered during Leg 133 and correlation to seismic profiles indicate that tropical–subtropical reef development was initiated on the Marion Plateau in the early Miocene, and by the middle Miocene, there was extensive reef growth on the plateau surface. These reefal sediments are part of seismic Megasequence B. In the late middle Miocene, carbonate bank productivity rapidly diminished on the Marion Plateau, as shown by a reduced fine-grained, bank-derived component in slope sediments. This decline was primarily the result of subaerial exposure resulting from a sea level regression, which caused the demise of the NMP. During the late Miocene, the SMP continued to grow, whereas carbonate production on the northern platform did not reinitiate even after being reflooded during subsequent sea level increases. During continued growth of the southern platform, the western two-thirds of the Marion Plateau was exposed, forming a broad, low-relief karstic surface. At the end of the Miocene, the southern platform underwent partial drowning that may have resulted from sea level variations in conjunction with reduced sea-surface temperatures (SSTs) (Isern et al., 1996) and greatly increased platform subsidence rates (Müller et al., 2000). Carbonate production from the Pliocene to Holocene never again achieved the areal extent of the Neogene. Instead, hemipelagic drift sediments have since dominated sedimentation on the Marion Plateau.

## Determining the Magnitude of Eustatic Sea Level Variations

Measuring the amplitude and timing of eustatic sea level fluctuations is essential both for the establishment of an accurate eustatic sea level curve for the Phanerozoic and for the accurate interpretation of sediment sequences on continental margins. Defining the amplitude of the eustatic sea level curve remains one of the major challenges in sea level research (COSOD II, 1987; Sahagian and Watts, 1991; JOIDES Planning Committee, 1996). Several attempts have been made to determine the amplitude of glacioeustatic fluctuations, including passive-margin sequence stratigraphy (Vail et al., 1977; Vail and Hardenbol, 1979; Haq et al., 1987), modeling of sedimentary depositional regimes (Watts and Thorne, 1984), calibration of the oxygen-isotope curve (Major and Matthews, 1983; Miller et al., 1987; Williams, 1988), and analysis of the depositional history of carbonate sediments on atolls (Schlanger and Premoli Silva, 1986; Halley and Ludwig, 1987; Moore et al., 1987; Lincoln and Schlanger, 1987, 1991). These analyses yield a wide range of results that are often in agreement with regard to the timing of sea level events. However, there are significant differences between the different independent data sets in regard to estimates of the magnitude of sea level fluctuations.

### Influence of Subsidence on Sea Level Magnitudes

The inability to extract tectonic subsidence effects from relative sea level signatures has hindered the quantification of eustatic sea level variations in many areas. However, a sea level shift that occurs between two sites of equal tectonic subsidence will provide an accurate record of the magnitude of eustatic change. For estimating sea level between sites on the Marion Plateau, it is necessary to demonstrate that there is no differential subsidence along the drilling transect. Two lines of evidence support this assertion. First, the Marion Plateau is not structurally com-

partmentalized and, therefore, behaves as a single structural entity (Symonds et al., 1988). Seismic lines between Leg 194 sites show that no structural elements such as faults are present that could cause these sites to have differential relative subsidence. Second, because the Marion Plateau basement surface is planated with minimal dip to the northeast, depths to basement surface contours can be considered isosubsidence lines (Fig. F3). The eight sites drilled are all near the 1-s basement contour. Thus, there is minimal basement gradient between sites and negligible differential subsidence.

Calibration of eustatic sea level variations can only be estimated realistically on slowly subsiding, structurally well-understood margins, where an accurate tectonic subsidence history can be established, and where sites of equal tectonic subsidence that have both the highstand and the lowstand history preserved, can be located. For the predicted middle Miocene Marion Plateau subsidence rates, the increase in water depth added to both sites as a result of tectonic subsidence is an order of magnitude less than that resulting from eustatic sea level change over the same interval. This additional depth is <10 m over the 1-m.y. interval of middle Miocene eustatic sea level fall, which is smaller than the error of paleowater depth estimates in these sediments.

## SCIENTIFIC OBJECTIVES

The scientific themes of Leg 194 include the following:

1. Magnitude of the second-order eustatic sea level fall during calcareous nannofossil Zones N12–N14: The Marion Plateau provides ideal targets to address the magnitudes and effects of sea level change on continental margin sediments. Although one of the fundamental controls on the nature and geometry of continental margin deposition is sea level change, much of the information on the relationship between sea level and depositional facies is qualitative. Leg 194 drilling will determine the magnitude of the Zone N12–N14 sea level fall to help calibrate the Phanerozoic sea level curve.
2. Development of carbonate platforms in a current-dominated environment: Slope sedimentation adjacent to most carbonate platforms is controlled by the prevailing wind direction with the windward side of the platform being relatively sediment starved and the leeward side having higher depositional rates. On the other hand, carbonate platforms and slope sediments of the Marion Plateau are controlled by strong seafloor currents. These currents determine the morphology and growth potential of the platforms as well as the location and amount of sediment transported from the platform top. The results of Leg 194 drilling, along with available seismic data, will enable the characterization of these current dominated carbonate platform systems.
3. Development of subtropical carbonate platforms: The carbonate platforms of the Marion Plateau are dominated by subtropical and cool subtropical carbonates. The results of Leg 194 coring will bridge the gap between the cool-water carbonates sampled during Leg 182 (Great Australian Bight: Cenozoic cool-water carbonates) and the tropical to subtropical carbonates recovered during Legs 133 (Northeast Australian Margin) and 166 (Bahamas Transect). Stable isotopic data from Leg 133, Site 811, on the

more northerly Queensland Plateau, showed that during the late Miocene, regional SSTs were cool (~20°–22°C), as were global SSTs (Isern et al., 1996). Given the more southerly location of the SMP with respect to Site 811 (Queensland Plateau), temperatures were probably similar to, if not cooler than, those over the Queensland Plateau. SSTs at or below 20°C would not prevent tropical coral growth but would make it more likely that the platforms were constructed of a "cooler," more subtropical bioassemblage. Documenting the transition of cooler water biota into warmer water forms will be an important outcome of Leg 194.

4. Facies change and development of sequence stratigraphic units controlled by sea level changes in a mixed carbonate and siliciclastic sediment system: Leg 194 coring recovered a detailed record of carbonate and siliciclastic sediment facies variations resulting from the mixing of sediment from carbonate banks on the Marion Plateau and the continental margin of Australia. In general, carbonate sediment export increases during sea level highstands as carbonate banks have additional accommodation space for increased growth of carbonate-producing organisms. On the other hand, terrigenous sedimentation generally decreases during highstands because of the elevated erosional base level. Detailed analysis of the cumulative result of these different sedimentological responses to sea level forcing will be an important result of Leg 194 drilling.
5. Oligocene–Pliocene third-order sea level fluctuations: The Oligocene–Pliocene sea level record preserved in the carbonate platform growth phases of the Marion Plateau includes a third-order event stratigraphy within the second-order sea level falls that dominate the sequence stratigraphic framework. Analyses of these variations, and the higher order fluctuations that are contained within them, provide information on the timing and influence of sea level on the carbonate growth phases and sedimentation of the Marion Plateau.
6. Mechanisms and causes of fluid flow within pure carbonate and mixed siliciclastic/carbonate depositional environments: Determining the mechanism and rate of fluid transport through carbonate platforms and reef structures is critical to understanding diagenetic processes (Buddemeier and Oberdorfer, 1986) and the geochemical cycling of many elements. Fluid movement has the ability to chemically alter the mineralogic composition of the sediment by hastening the conversion of metastable minerals such as high-Mg calcite and aragonite to more stable calcite and dolomite (Mullins et al., 1984; Simms, 1984). Alteration of carbonate sediments to dolomite has been significant in both the Bahamas (Varenkamp, 1991) and the carbonate platforms of northeast Australia (McKenzie et al., 1993; Davies, McKenzie, Palmer-Julson, et al., 1991). Studies using $^{87}Sr/^{86}Sr$ isotopic ratios have shown that carbonate sediments off northeast Australia were dolomitized by multigenerational fluids flowing through the platforms (McKenzie et al., 1993). Fluid flow can also alter sedimentary structure, permeability, and porosity of a carbonate deposit, thus having important effects on flow pathways and reservoir potential. The existence of fluid flow has been described in tropical carbonate platforms such as the Great Bahama Bank and the Queensland Plateau (Eberli, Swart, Malone, et al., 1997;

Elderfield et al., 1993) and also in temperate-water carbonates (Feary, Hine, Malone, et al., 2000). However, the mechanisms causing this flow are neither well documented nor understood.

7. Role of climatic and paleoceanographic change in the subtropical South Pacific and its influence on carbonate platform development: In addition to sea level fluctuations, paleoceanographic variations in the western Coral Sea have significantly affected the development of carbonate platforms and reefs off northeast Australia. Paleocirculation has been modified both by the movement of continental fragments resulting from local rifting events and by the northward movement of the Indo-Australian plate. Northward movement of the Indo-Australian plate also resulted in significant variations in climate caused by movement across climatic boundaries. These changes, in addition to global climatic variations, influenced the depositional environments in the Coral Sea, which today are dominated by tropical carbonates.

## SITE SURVEY OVERVIEW

Previous investigations of the seismic stratigraphic architecture of the Marion Plateau have produced a model for the evolution of the carbonate platforms on this plateau (Davies et al., 1989; Davies, McKenzie, Palmer-Julson, et al., 1991; Pigram et al., 1992). These studies proposed that the geometric relationship between the Miocene carbonate platforms and their slopes can be used to estimate the magnitude of Miocene sea level changes (Pigram et al., 1992). In order to image these geometric relationships in more detail and to provide additional site survey information for potential ODP drill holes, a 1-month site survey cruise in April 1999 was funded by the Australian Geological Survey Organisation (AGSO). A high-resolution multichannel seismic grid consisting of 1700 km of seismic lines, gravity cores, dredges, and bottom photographs was acquired from the *Franklin* (FR 03/99; AGSO 209), operated by the Commonwealth Scientific and Industrial Research Organisation (CSIRO) data (Isern and Anselmetti, unpubl.; Heck et al., 1999). Acquisition and processing parameters for the seismic site survey data are summarized in Table **T1.**

**T1.** Acquisition and processing parameters for seismic site survey data, p. 86.

### Bottom Samples and Photographs

Seafloor sediment samples were collected using pipe dredges, chain dredges, a Van-Veen grab, and a 1-T gravity corer with 10-cm-diameter barrels. Seafloor photographs were taken using a Benthos deep-sea camera and flash mounted on the standard *Franklin* conductivity/temperature/depth recorder frame. Sediment samples and seafloor photographs showing prominent current ripples (Fig. **F6A, F6D**) document the strong influence of currents in the modern environment at the Leg 194 sites on this open plateau (Heck et al., 1999). The study area is characterized by subtle bathymetric changes as drift sedimentation in the Pliocene–Pleistocene infilled much of the preexisting relief. Strong seafloor currents also favor early submarine diagenesis as shown by the cemented worm tubes that were dredged at the location of Site 1194 and seen on the seafloor photographs (Fig. **F6A**). Sediments on the plateau surface consist of wackestone to packstone containing abundant planktonic foraminifers. Minor skeletal grains include bryozoans, scapho-

**F6.** Seafloor photographs, p. 66.

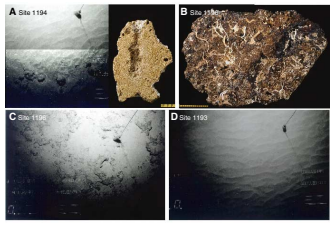

pods, solitary corals, sponge spicules, and pteropods. The top of the southern platform edifice is coated with a red-stained submarine hardground surface that is encrusted with serpulids and bryozoans with patches of soft sediment that partly overlie this crust (Fig. F6B, F6C).

## Seismic Stratigraphy

Seismic data collected during the site survey cruise provided excellent images of late Oligocene–Holocene sedimentation on the Marion Plateau. Following the nomenclature of Pigram (1993), four unconformity-bounded megasequences (A–D) are identified overlying the continental basement (Figs. F7, F8). These five seismic units can be mapped through most of the survey area. The following section describes the seismic facies, geometry, and the general seismic stratigraphic architecture of these megasequences. Seismic sequence boundaries separating megasequences are labeled in uppercase letters that represent the name of the two bounding megasequences (A/B, B/C, etc.). Because of the nature of the carbonate platform sediments drilled during Leg 194, in this volume we do not follow the nomenclature of Pigram (1993) when referring to the platform phases. Instead, the NMP is discussed as the northern platform and the SMP as the southern platform. All major seismic stratigraphic elements can be recognized in Figures F7 and F8, which show two transects along which all Leg 194 sites are positioned. Figures F9A and F9B show lithologic columns, chronostratigraphic frameworks, and petrophysical signatures for the same two transects.

### Seismic Megasequence D (Latest Miocene–Holocene)

Megasequence D has variable thickness and is composed of latest Miocene to Holocene hemipelagic sediments. Megasequence D sediments were deposited under the influence of strong currents in thick sediment drifts characterized by numerous downlap surfaces defining individual drift packages (Fig. F7). The thickness of Megasequence D is controlled largely by the preexisting relief existing at the end of the late Miocene, as strong currents moved the sediments over the plateau and filled existing topographic depressions. Sediment sequence geometry indicates a predominant progradation of drift units, and thus a current direction, from north to south.

### Seismic Megasequence C (Late Miocene)

In the southern portion of the study area, Megasequence C contains the seismically opaque SMP edifice. Originally, this platform was thought to be purely of late Miocene age, and thus would have been initiated on distal sediments of NMP during the middle to late Miocene sea level lowstand (Pigram et al., 1992). Sites 1196 and 1199 were drilled into this platform to test this hypothesis (Fig. F8).

Scattering of the seismic signal from the well-indurated SMP top makes it difficult to determine the geometry and architecture within this platform. On the seismic data, the southeast margin of the platform displays a completely different geometry from the northwest margin. The northwestern margin is composed of a nondepositional escarpment separating deeper-water Megasequence C from platform equivalents. Megasequence C thickens toward the platform, providing evidence for the accumulation of platform-derived carbonates in a talus at the base of the escarpment. Site 1198 was located to recover these sediments. In

F7. Seismic overview of characteristics of seismic megasequences, northern transect, p. 67.

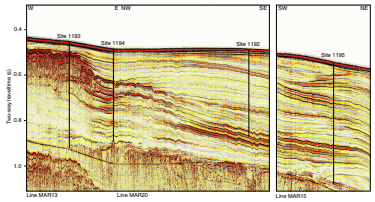


F8. Seismic overview of characteristics of seismic megasequences, southern transect, p. 68

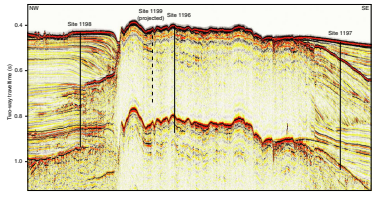


F9. Stratigraphic correlation summary, p. 69.

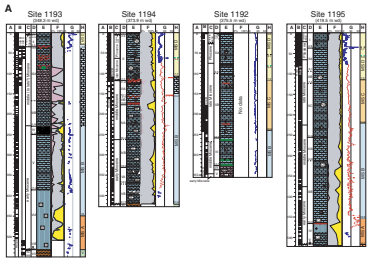

contrast, the southeastern margin (Site 1197) shows a thick prograding package consisting partly of Megasequence C sediments similar to those penetrated at Site 1198. At this site, the top of Megasequence C can be traced into the platform. Previous work indicates that the SMP was likely to have drowned near the end of the late Miocene, possibly in the earliest Pliocene (Pigram, 1993).

The deeper-water facies of Megasequence C, as drilled at Sites 1192 and 1195, is restricted toward the west by the topographic high of the northern platform margin on which Megasequence C downlaps and wedges out. Toward the east, Megasequence C thickens toward the plateau edge (Fig. F7).

### Seismic Megasequence B (Early Miocene–Middle Miocene)

Seismic Megasequence B is generally thicker toward the west, thinning eastward and southward. In the western part of the study area, Megasequence B is dominated by the early middle Miocene NMP. The upper portion of this sequence is characterized by a generally transparent to chaotic seismic section with hummocky reflections, representing a vertically aggrading carbonate platform (Fig. F7). Below these chaotic reflections, a sequence of moderately continuous reflections dipping to the east indicates an eastward prograding slope system over which the NMP initiated. Reflections at the top of Megasequence B can be traced from the platform top, to the margin, and into the deeper water sequences. Close to the northern platform margin, the uppermost portion of Megasequence B is characterized by a near horizontal high-amplitude reflection pattern that can be interpreted as a downstepped carbonate platform during a phase of lower sea level. Further out on the plateau, Megasequence B is composed of a thick package of gently eastward-dipping reflections.

### Seismic Megasequence A (Paleogene?–Early Miocene)

Megasequence A, the oldest depositional megasequence over basement, is generally limited to the eastern part of the plateau, over which there is only limited seismic coverage. This thin sequence is characterized by highly continuous reflections prograding westward over basement. Because Megasequence A overlies and infills basement irregularities, it is variable in thickness.

### Acoustic Basement

Acoustic basement is characterized by a high-amplitude reflection at the interface with overlying sediments and numerous diffractions caused by the irregular bedrock surface. In some places, distinct morphologic structures, such as narrow highs and depressions, can be recognized clearly even on unmigrated seismic profiles. In general, the basement surface occurs at a similar two-way traveltime with a slight northeastward dip toward the edge of the plateau, where it is downfaulted to the Cato Trough (Fig. F7).

## SITE SUMMARIES

Site locations, water and drilling depths, core recovery, etc., are listed in Table T2. For stratigraphic and lithologic summaries of all sites, see

T2. Summary of operations, p. 87.

Figures F9A and F9B. Seismic lines and stratigraphic summaries are also presented in Figure F10.

F10. Partial seismic sections for sites and stratigraphic correlation summary, Leg 194, p. 72.

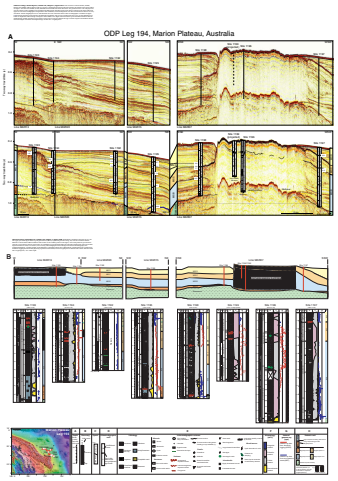


## Site 1192

The main objective at Site 1192 (proposed Site CS-13A) was to perform a feasibility test of the Hydrate Autoclave Coring Equipment (HYACE), including the pressure core sampling tool (H-PCS) developed at the Technische Universität Berlin and the vibracore sampling tool (HF-VS) developed by Fugro Geotechnical Engineering. In July 2000, the HYACE team was awarded 72 hr of testing time at the beginning of Leg 194. The HYACE developer did not specify a particular test site, so ODP selected proposed Site CS-13A, a contingency site of the Leg 194 scientific program. The scientific objectives at this contingency site were to investigate the slope sediments ~40 km east of the paleomargin of the early middle Miocene NMP carbonate platform margin. In particular, Site 1192 was drilled to provide information on the facies and age range of seismic Megasequences B through D, which together form the carbonate platform to slope architecture of the Marion Plateau from early Miocene time to today. Specifically, the aim of drilling at this site was to recover the marginal slope sediments shed from the NMP, the lithologic signature of basinward unconformities adjacent to the NMP, and the age of the erosional top of NMP by dating the correlative seismic horizon, and to calibrate regional seismic sequence stratigraphy.

### Operations

Leg 194 began at 2200 hr on 3 January 2001, ~2 days earlier than scheduled. The ship departed Townsville at 0700 hr on 8 January, 3 days ahead of schedule, and operations at Site 1192 began at 1720 hr on 9 January. During the initial fit test of the HYACE tools in the bottomhole assembly (BHA), it was discovered that the outside diameter of the top 1 m of the H-PCS tool was several thousandths of an inch too large to pass through the latch sleeve of the ODP advanced piston corer/extended core barrel (APC/XCB) BHA. Therefore, the latch sleeve was left out of the BHA in the hope that pump pressure would generate enough resistance to offset the rotation and torque caused by rotation of the small bit.

Hole 1192A was cored continuously with the APC to refusal at a depth of 241.5 meters below seafloor (mbsf). Twenty-five APC cores were retrieved with 101.7% average recovery. The HF-VS was deployed three times, at 28.5–29.5, 86.5–87.5, and 192.0–193.0 mbsf. The corer recovered 0.19, 0.91, and 0.77 m of sediment, respectively. The shear pin parted in the first and second run, but not in the third run. The hammer could not be activated in the first run, presumably because the formation was too soft. The hammer did operate in the subsequent runs for several seconds. The flapper only closed in the second run, and a sample chamber pressure of 609 psi (close to estimated in situ pressure) was maintained. The flapper did not close in runs one and three, presumably because of difficulties with the polyvinyl chloride liners.

The H-PCS was run two times in Hole 1192A, from 231.0 to 232.0 mbsf and from 241.5 to 242.5 mbsf. This tool is designed to operate in more indurated sediment than the HF-VS tool. The positive displacement motor was not activated in either run, and the end of stroke was not indicated. After the instrument was recovered, the inner barrel was still retracted in the autoclave and the flapper valve was not properly

seated. It is possible that the lack of a latch sleeve in the BHA allowed the upper part of the tool to rotate instead of the lower section. Prior to the second deployment, the tool was marked with paint on the upper and lower sections in order to ascertain if slippage occurred and if the tool was seated. After deployment, the marking was reviewed. Abrasions of the paint suggested that the upper section had rotated and that the bottom section had not seated properly. It was decided to recover the drill string and add the latch sleeve. The rig mechanic machined the top 1 m of the tool to the same diameter as the tool body.

Hole 1192B was spudded at 1145 hr on 11 January. Following a single mudline core that established the seafloor depth at 387.1 m, the hole was drilled ahead to 179.9 mbsf. Five more APC cores were retrieved with 43.6 m recovery (87.3%), followed by 13 XCB cores with 60.43 m recovery (48.3%), to a total depth of 355.5 mbsf. Total recovery in Hole 1192B, including test cores, was 105.1 m, representing 59.1% of the cored interval.

The HF-VS tool was deployed once more from 179.9 to 180.9 mbsf. The results of this test were similar to the last test in Hole 1192A. The shear pin did not part, hammering was detected for a few seconds, and when the tool was recovered, it showed that the latching pawls were jammed, which prevented full retraction of the liner into the inner barrel. The flapper was not closed. The corer recovered 0.84 m of sediment.

Immediately following this last HF-VS deployment, the H-PCS tool was run for the third time from 180.9 to 181.9 mbsf. This time, the inner barrel did stroke out and rotate, but no sediment sample was obtained.

During the fourth and final run of the H-PCS (335.2 to 336.2 mbsf), the inner barrel stroked out, rotated, and recovered ~0.27 m of sediment. The formation was too soft for the type of core catcher employed (the only type available), and it was thought that some sediment was lost in the recovery process. The retraction mechanism was not released, so the core was not under pressure.

The allocated testing time expired, and operations at Site 1192 ended at 1440 hr on 12 January.

## Principal Scientific Results

The sediments recovered at Site 1192 provide a record of the middle to late Miocene evolution of distal carbonate platform sediments on the Marion Plateau. The recovered upper Miocene to Pleistocene hemipelagic carbonates document the interfingering of subtropical neritic carbonates with pelagic carbonates and terrigenous siliciclastics. These constituents were deposited in extensive sediment drifts on the Marion Plateau. Breaks in the production of shallow-water carbonates, caused by exposure and/or drowning, coincide with the sudden appearance of glauconite-rich and phosphate-rich lithologies. A significant increase in the terrigenous fraction of the sediment beginning 4 m.y. ago, together with drift geometries as seen on the seismic data, indicate increased current activity or increased continental erosion and sediment transport.

Site 1192 penetrated seismic Megasequences D and C and part of Megasequence A/B. The site is located midway between the NMP and SMP (Figs. **F1, F2**). The biostratigraphic results and zonal assignments of Holes 1192A and 1192B indicate a Pleistocene to upper Miocene succession that was subdivided into five main lithologic units according to texture, color, and the presence or absence of quartz, glauconite, and phosphate grains. The entire sequence is generally heavily bioturbated

and in many places reveals distinctive ichnofossils. Color variations are generally subtle, and most of the succession is light to dark green-gray or olive green in color.

Unit I (0–2.4 mbsf) includes the modern seafloor, a current-swept hardground with various stages of lithification as indicated by intraclasts with brown iron oxide–stained sediment. Carbonate content is more than 90 wt%.

Unit II (2.4–258.1 mbsf) is an upper Miocene to Pleistocene heavily bioturbated, planktonic foraminifer mudstone to packstone with clay. Sediments of Subunit IIA (2.4–103.1) show highly variable grain density and magnetic susceptibility (MS), indicating a high and variable amount of terrigenous grains. An increase in bulk density at 85 mbsf may correlate with an impedance contrast imaged as a high-amplitude reflection on the seismic data. In Subunit IIB (103.1–258.1), sediment physical properties are nearly constant, reflecting an overall more homogeneous sedimentary composition. Carbonate concentrations vary between 73 and 82 wt% in Subunit IIA and between 80 and 92 wt% in Subunit IIB, reflecting the increased siliciclastic content in Subunit IIA.

Sediments in Units III–V (258.1–355.5 mbsf; middle Miocene) record the distal influence of a platform (periplatform/hemipelagic) and the adjacent continent. Unit III (258.1–325.6 mbsf) contains abundant quartz, glauconite, and phosphate grains within a foraminifer packstone with clay that contains more shallow-water benthic foraminifers than the units above. Unit IV (325.6–336.2 mbsf) consists of alternating intervals of planktonic foraminifer mudstone and packstone with clay. Quartz and glauconite grains as well as dolomite rhombs are present. Unit V (336.2–355.5 mbsf) is a silt-sized dolomitic grainstone with clay that coarsens toward the bottom of the hole. Unlike Subunit IIB, Units III through V are characterized by more variable grain density and MS, indicating changing concentrations of siliciclastic sediment components. This variability is supported by a large range of carbonate concentrations (66–94 wt%). For the entire site, bulk density, porosity, *P*-wave velocity, and thermal conductivity data show consistent downhole trends.

Nannofossil datums provided modest biostratigraphic resolution for the Pleistocene through middle early Miocene. Holes 1192A and 1192B in general reveal good to moderate planktonic foraminifer preservation from the Pleistocene to upper Miocene. Preservation is poor at the base of the hemipelagic sequence, which affects age assignments in the middle to lower Miocene samples from Hole 1192B. The average sedimentation rate of the entire sequence at Site 1192 is ~20 m/m.y.

The presence of small, flat specimens of the larger benthic foraminifers, *Amphistegina* and *Operculina,* of which modern equivalents host algal endosymbionts, along with several porcellaneous taxa at the top of Hole 1192B, indicate a deep euphotic (~50–120 m) habitat (middle to outer neritic), suggesting reworking and lateral transport within Unit I. Further downcore, benthic foraminifers are relatively rare in all samples examined from Hole 1192A, although the relatively diverse assemblages of rotaliid, buliminid, nodosarid, and agglutinated taxa are characteristic of upper bathyal habitats.

Magnetostratigraphic interpretation of the uppermost 150 m of Site 1192 resulted in an average sedimentation rate of 20 m/m.y. However, the age model derived from the paleomagnetic data is offset from the biostratigraphic age model. The data are compromised by unremoved, possibly high-coercivity magnetic overprint. In addition, potential hiatuses may prevent an accurate interpretation of observed polarity inter-

vals. Below 150 mbsf magnetostratigraphic interpretation is not possible as a result of incomplete core recovery, low intensities, and magnetic overprint.

The sediment and pore water chemistry of Site 1192 is fairly typical of hemipelagic to pelagic, carbonate-rich sediments with low sedimentation rates. Sedimentary organic carbon content is low (0.1–0.3 wt%) and is predominantly of marine origin. As a result of the low organic carbon content, carbon reoxidation rates are also low. The primary products of diagenesis are iron sulfides, celestite, and dolomite, all of which appear as accessory minerals in the sediments. The low gas content at Site 1192 is a function of low organic matter contents that prevent complete sulfate reduction and immature organic matter that does not provide a thermogenic gas fraction.

A seismic traveltime to depth conversion was achieved using shipboard velocity data measured with the *P*-wave sensor tool. Seismic Megasequence D incorporates lithologic Unit I and part of Unit II, ranging in age from late Miocene to Pleistocene. The absence of Holocene sediments at this site confirms the assumption that modern sedimentation is strongly reduced or absent and the seafloor represents an unconformity, which is also supported by relatively low porosity in the uppermost sediments. The time-depth correlation places the Megasequence C/D boundary at 120 mbsf, which results in an age of ~7.2 Ma. In the area of Site 1192, this sequence boundary is conformable, and no large stratigraphic hiatus was observed in the drill cores across this boundary. The sediments of the underlying Megasequence C consist mostly of the late Miocene age lower part of lithologic Unit II, which is characterized by a rather uniform lithology, resulting in a seismic facies mostly characterized by low-amplitude reflections. The Megasequence B/C boundary at 240 mbsf correlates approximately with the boundary between lithologic Units II and III (259 mbsf). The sedimentological and geochemical signatures of lithologic Unit III point toward a relative increase of noncarbonate sediments (quartz, glauconite, and phosphate) into the depositional system during a period that can be seismically correlated with the exposure of the NMP. Using the compiled age model, an age of ~11.9 Ma can be assigned to seismic Megasequence B/C boundary.

## Site 1193

Site 1193 (proposed Site CS-01A) is located on the Marion Plateau, ~80 km east of the south-central Great Barrier Reef, in 348 m of water (Figs. **F1, F2**).

The main objective at this site was to recover the sedimentary rocks of the NMP carbonate platform. The platform is an important element for the reconstruction of Miocene sea level, because its top marks the last platform growth phase before the late middle Miocene sea level fall. Regional seismic line MAR13, along which Site 1193 is located, indicates that an irregular, karstic platform top is buried under a relatively thin cover of hemipelagic drift deposits. Further, seismic geometry suggests that the NMP was established on gently dipping slope deposits, as indicated by inclined reflections underneath the platform.

The northern edge of the NMP was drilled during ODP Leg 133 (Davies, McKenzie, Palmer-Julson, et al., 1991). Sites 816 and 826 showed that the top of NMP at these locations consists of a tropical reefal assemblage deposited in water depths <20 m. This depth defines the approximate point from which sea level began to fall at approxi-

mately the middle/late Miocene boundary. Results from Leg 133 also indicated that the top of NMP had been subjected to subaerial exposure.

Site 1193 provides a record of the total thickness of NMP near the platform edge, the history of its growth phases and episodes of exposure, and by investigating the hemipelagic sediments overlying NMP, the timing of its burial. Biostratigraphic data from Site 1193 also provide crucial information for dating the regional seismic sequence boundaries necessary to calibrate the established sequence stratigraphic framework for the region. In addition, Site 1193 sediments will yield a record of fluid flow and diagenetic processes in this carbonate platform, parts of which are extensively dolomitized. The age and nature of the underlying deeper water sediments, together with the facies of the basal sediments directly overlying basement, document the timing of and processes linked to the initial basement transgression. Finally, Site 1193 provides a lithologic record of the age and nature of acoustic basement.

The total sediment thickness at Site 1193 is 531 m. Holes 1193A through 1193C penetrated to total depths of 515, 138, and 548.5 mbsf, respectively. Acoustic basement was encountered in Hole 1193C. Site 1193 was the first ODP site at which the advanced diamond core barrel (ADCB) was used to drill a sedimentary section. Recovery with the ADCB in the platform carbonates was significantly better than XCB recovery over a comparable interval until the ADCB bit was damaged.

## Operations

Operations began at 2200 hr on 12 January 2001. Hole 1193A was APC cored to 37.1 mbsf (101% recovery) (Table T2), where the carbonate platform was encountered. XCB coring continued to 450.4 mbsf with an average recovery of 28%. The pipe had to be pulled as a result of the "bent pipe event," and coring resumed 8 hr later. From 450 to 515 mbsf, average recovery was 17%. At 515 mbsf, the pipe became stuck and was freed after 5 hr of working the hole; however, the BHA had to be retrieved soon after because of a stuck barrel caused by a broken latch.

On 13 January, the rendezvous boat from Mackay arrived with three scientists and two ODP technicians who had remained on shore so that the HYACE engineers could be accommodated during the first 3 days. In addition to the HYACE team, the personnel leaving the *JOIDES Resolution* included Lamont-Doherty Earth Observatory (LDEO) and ODP representatives and an ODP technician. On 17 January, a helicopter from Mackay landed on the vessel and removed a roughneck who was diagnosed with probable kidney stones.

The vessel was offset 20 m, and Hole 1193B was spudded at 1730 hr on 17 January with the rotary core barrel (RCB). After the hole was washed ahead to 35.0 mbsf, rotary coring penetrated the hard cover of the carbonate platform and advanced 53.8 mbsf with 19% recovery. A free-fall funnel (FFF) was deployed and the pipe was tripped to make up the ADCB system with a 7.25-in polycrystalline diamond compact (PDC) drill bit. The developmental ADCB was deployed in anticipation of improved recovery of reefal limestone. The ADCB reentered Hole 1193B, and coring started at 53.8 mbsf. After Core 194-1193B-4Z was cut, the pipe had to be pulled to retrieve a stuck barrel and it was found that the inner tube had collapsed. Hole 1193B was reentered with the ADCB on 19 January, and coring resumed at 63.2 mbsf. Total recovery over the interval from 53.8 to 91 mbsf was 16% compared to 2.6% for the XCB over a similar interval. Below that interval, bit problems, per-

haps associated with a clayey formation, reduced recovery dramatically. After cutting Core 194-1193B-11Z, an improvised bit deplugger was run in an attempt to clear the core blockage. Several blows of the wireline jars succeeded in landing the barrel, but subsequent cores had dismal recovery. The drill string was pulled, and it was found that ~50% of the cast matrix pilot portion of the bit that trims the core had been broken off by the earlier jarring with the bit deplugger. Hole 1193B was thus terminated.

On 20 January, a second medical evacuation by helicopter was required for a scientist diagnosed with a fractured femur. The diagnosis was confirmed on shore, and the patient underwent surgery in a local hospital. The roughneck evacuated earlier returned to work on the same helicopter.

The vessel was offset 20 m, and Hole 1193C was spudded with the RCB at 1800 hr on 20 January with the primary objective of providing a dedicated logging hole. After drilling through the overlying hemipelagic section, the top of the carbonate platform was cored for a third time, from 35 to 70.1 mbsf, with an average recovery of 16.2%. A center bit was deployed and continuous drilling advanced to 510 mbsf. Four additional cores were taken from 510 to 548.5 mbsf (39.9% recovery), where acoustic basement was penetrated. The hole was then displaced with 172 barrels of sepiolite mud, and the drill string was pulled in preparation for logging. The pipe got stuck at ~297 mbsf, and circulation or rotation could not be established despite a 3-hr attempt. The pipe was therefore severed with explosives at 434 m drill string length (75 mbsf). The fragmented end of pipe was on deck by 2100 hr, ending operations at Site 1193. Logging plans had to be abandoned. As the drill string was being recovered, several attempts to retrieve the beacon failed.

## Principal Scientific Results

Drilling of Site 1193 penetrated to a depth of 548.5 mbsf, and at the base of the hole we recovered an immature fine marine sandstone consisting of volcanic detritus mixed with carbonate skeletal fragments. This acoustic basement is overlain by a 531-m-thick sedimentary succession ranging in age from early Miocene to late Pleistocene. The lowest part of the sedimentary sequence is a basal transgressive succession that deepens upward as indicated by early Miocene age upper-slope sediments. The 302-m-thick transgressive and slope sequence is overlain by a 194-m-thick, middle Miocene carbonate platform (NMP). This interval represents one of the major Miocene platform growth phases on the Marion Plateau. The platform rocks consist mostly of a bryozoan and larger foraminifer assemblage that is almost barren of corals. This assemblage is indicative of a cool subtropical depositional environment at paleowater depths within the euphotic zone (i.e., <100 m). In some intervals the rocks are heavily dolomitized. In the upper part of the platform, a series of exposure surfaces is observed. In addition, a couple of submarine hardground formations occur close to its top. Cessation of carbonate production on the NMP platform could have occurred as early as the early middle Miocene. Unconsolidated uppermost Miocene through upper Pleistocene hemipelagic carbonates cover the platform, indicating that platform growth was not reestablished at Site 1193.

The lithology of Site 1193 is divided into seven principal units. Unit I consists of a 4-m-thick skeletal grainstone, composed mostly of planktonic foraminifers, that reflects the modern current-swept conditions at

the seafloor. Unit II (4–35 mbsf) is an unconsolidated Pleistocene to uppermost Miocene hemipelagic foraminiferal packstone. The heavily bioturbated sediment consists mostly of very fine sand-sized planktonic foraminifers in a clay-rich carbonate matrix. Carbonate content ranges between 70 and 90 wt%. These first two units are equivalent to seismic Megasequence D.

The boundary between lithologic Units II and III marks the top of the 194-m-thick NMP. This boundary is characterized by a major hiatus that, according to nannofossil and planktonic foraminifer datums, spans most of the late Miocene and possibly of the middle Miocene. If the broad age constraint imposed by the benthic foraminifer assemblage (12–24 Ma) is included, the hiatus spans from 5.6 to at least 12 Ma, and possibly to ~15 Ma. The hiatus at 35 mbsf corresponds seismically to the top of Megasequence B and is marked by distinct changes in all shipboard data sets. The platform rocks consist of coarse skeletal grainstone to rudstone and subordinate dolostone. In general, the sediments of lithologic Unit III have a diverse biotic assemblage of bryozoans and larger benthic foraminifers, with subordinate mollusks and coralline algae but rare coral. This assemblage indicates cool subtropical environmental conditions. The platform sequence is divided into two subunits based on a 10-m-thick clay-rich mudstone to floatstone interval rich in larger benthic foraminifers. This interval was deposited in a more protected, possibly lagoonal environment. Several irregular and reddish colored horizons occur within the uppermost part of Unit III and likely represent exposure horizons. The shallowest of these has a thin veneer, probably phosphatic coating, that indicates submarine hardground formation during a depositional hiatus. Analyses of benthic foraminiferal abundance and morphology verify that the paleowater depth was always within the euphotic zone (i.e., <100 m and more likely <60 m), with some intervals that were deposited in <10 m of water. Dolomite content is variable and generally higher in the upper part of the platform. Some intervals of the platform rocks are completely dolomitized and display an intense orange to red color. Physical properties of the platform rocks show large scatter. For example, bulk density varies from 1.95 to 2.65 g/cm$^3$, porosity from 10% to 45%, and *P*-wave velocity from 2700 to 5200 m/s.

Immediately below these high-energy, relatively shallow water sediments is a 20-m-thick interval of mudstone with up to 50% clay (Unit IV). This unit passes downcore into 136 m of fine-grained bioturbated skeletal packstone (Unit V), representing the progradational platform slope. The slope sediments can be correlated to seismically imaged clinoforms underlying the hard platform cap. Carbonate content in Units IV and V average ~60 and ~80 wt%, respectively. Dolomite content in Unit V is relatively constant, averaging ~10%. The paleowater depth indicated by the benthic foraminiferal assemblages of Units IV and V sediments is consistently deeper than 100 m. The sediments below the NMP can be recognized by a consistent and nearly linear downhole trend in bulk density, grain density, porosity, *P*-wave velocity, and thermal conductivity.

The lowest part of the drilled sedimentary section consists of 146 m of interbedded grainstone and subordinate quartzose sandstones (Unit VI). The siliciclastic content of the sediment varies widely as a result of the presence of the sandstone beds. The depositional setting was probably inner to middle neritic, as indicated by abundant larger benthic foraminifers.

The deepest core from Site 1194 (540–549 mbsf) recovered what was possibly the top of acoustic basement (Unit VII), consisting of a marine sandstone with occasional organic-rich layers and quartz grains showing undulose extinction. These quartz grains likely originate from deformed terrains on the continental margin.

At Site 1193, well-preserved calcareous nannofossils and planktonic foraminifers provided 15 latest Miocene to Pleistocene age-depth control points in the top 35 m of the cored section and six early Miocene control points below 230 mbsf. The two biostratigraphic data sets agree well within these intervals, which broadly constrain the age of growth and times of nondeposition and flooding of the NMP (35–229 mbsf) to ~5.6–~16 Ma. No age diagnostic assemblages were found within the platform sequence. Larger benthic foraminiferal assemblages were observed throughout the platform interval (35–229 mbsf) and further constrain the time of platform buildup to 12–24 Ma. However, the 12-Ma time constraint does not necessarily exclude younger platform growth that could have been eroded.

Preliminary interpretation of the sequence of observed polarity reversals above the platform (lithologic Units I and II; 0–35 mbsf) provides ages offset by up to 0.5 m.y. from the depth-equivalent biostratigraphic ages. Within the platform sequence (35–220 mbsf), recovery was insufficient to allow development of a reliable magnetostratigraphic record. Below the platform (225–375 mbsf), discontinuous polarity sequences were identified, but their interpretation is not reliable without further investigation. Preliminary rock magnetic studies suggested that magnetic remanence may be carried by magnetite, hematite, goethite, and pyrrhotite.

Because of the difficulties with the magnetostratigraphy, biostratigraphic control points were used to construct the shipboard age model for Site 1193. Average sedimentation rates are 10 m/m.y. for the middle early Miocene, 100–150 m/m.y. for the late early Miocene and 0–25 m/m.y. for the Pliocene–Pleistocene. The significant late early Miocene increase (one order of magnitude) in sedimentation rate can be interpreted as the onset of shedding from the carbonate platform, augmented by clay from the continent and modified by current activity. This high rate of sedimentation evolves directly into carbonate platform growth at Site 1193 near the early/middle Miocene boundary. The period of platform growth, erosion, and nondeposition probably contains several depositional hiatuses. The Pliocene–Pleistocene sequence shows one distinct hiatus at 3.3–6.3 mbsf, which is constrained by nannofossil datums to at least 2.8–1.7 Ma. This hiatus correlates with peaks in the natural gamma radiation (NGR) and MS to 5.7 mbsf, coinciding with a change in sediment texture from packstone to wackestone, an iron-stained interval, and a seismic sequence boundary within Megasequence D.

Poor core recovery in the cemented shallow-water carbonate intervals at Site 1193 limited pore water sampling to finer-grained, more clastic rich sediments above, below, or within the platform carbonates. Overall, however, obtaining a general picture of the pore water chemistry was still possible. The interstitial water chemistry suggests that the fluids within sedimentary Units I–III, extending to the base of the carbonate platform facies, have probably not evolved from seawater. Even the strontium concentration, which might be expected to increase as a result of ongoing carbonate recrystallization, shows no increase until below the platform facies. The best explanation for the lack of change in fluid chemistry is that the platform sediments were completely al-

tered to stable carbonate mineralogies, dolomite, and low-magnesium calcite before the platform was reflooded.

In the platform and underlying sediments, horizons defined by decreased $CaCO_3$ content, increased total organic carbon (TOC) weight percent values, low hydrogen index (HI) values, and relatively elevated total S concentrations correlate with intervals containing increased clay content and transported and transport-abraded benthic and planktonic foraminifers.

The low gas content at Site 1193, as at Site 1192, is likely a function of appreciable pore water $SO_4^{2-}$ concentrations limiting methanogenesis to the deepest strata cored at the site. Also, the organic matter that does exist is immature relative to petroleum generation, so no thermogenic component to the gas fraction is expected.

## Site 1194

Site 1194 (proposed Site CS-02A) lies on regional seismic line MAR13 (shotpoint 3951) and at the crossing of lines MAR24 (shotpoint 355) and MAR27 (shotpoint 1123). This site is located ~20 km east of Site 1193 (Figs. F1, F2). Drilling at Site 1194 provided information on the age and facies of Megasequences A, B, and D. The purpose of this site was to investigate the growth history of the NMP as recorded in the adjacent marginal slope sediments. A prominent seismic horizon overlying these slope sediments can be traced to the surface unconformity on the NMP platform. Thus, this horizon and the underlying section provide information concerning the causes for the demise of the NMP. This site also provided information on the age and duration of unconformities within the prograding, proximal slope sediments of NMP that are part of Megasequence B, the age of Megasequence A that represents the initial marine transgression over the Marion Plateau basement, and the nature of this basement.

### Operations

Hole 1194A was APC cored to refusal at 117.4 mbsf, with an average recovery of 104.1% (Table T2). APC temperature measurements were obtained at four depths. The hole was deepened with the XCB system to 169.9 mbsf, with an average recovery of 7.6%. Hole 1194A was abandoned at that depth because of poor recovery. At 145.3 mbsf, the drill string became temporarily stuck and circulation was lost. The drill string was freed after it was worked for 30 min. Inspection of the bit at the end of operations in this hole revealed that all four bit nozzles were plugged with sediment.

The vessel was moved 20 m east of Hole 1194A, and Hole 1194B was drilled ahead with the RCB to near the bottom of Hole 1194A. RCB coring advanced without incidents to the target depth at 427.1 mbsf, with an average recovery of 28.1%. Afterward, the hole was flushed with a sepiolite sweep, the bit was released on bottom, the hole was displaced with sepiolite mud, and the drill pipe was pulled up to logging depth.

With the LDEO temperature tool at the bottom and the LDEO gamma ray tool (MGT) at the top, the triple combination (triple combo) tool (natural gamma ray, density, porosity, and resistivity) was the first wireline logging run in Hole 1194B. Hole conditions were good and the tools reached the base of the hole at 423 mbsf. The Formation MicroScanner (FMS) and dipole sonic imager (DSI) were deployed for the second logging run. Electronic problems precluded the collection of

DSI sonic data. One successful pass was completed with the FMS before the DSI was replaced with the Long-Spaced Sonic tool for a second logging run. The second pass detected a narrow spot in the hole at ~230 mbsf, which was passed after several attempts.

The last run was the check-shot survey with the well seismic tool (WST). The air gun developed a leak, so only the water gun was used. Downhole measurements were complicated by a strong current, which generated considerable drill string noise due to vibration. The end of the drill pipe was placed at 78.2 mbsf, and the deepest station was at 156.2 mbsf. However, the unclear source signature of the water gun resulted in an arrival waveform that could not be picked accurately by the software.

## Principal Scientific Results

The lowest portion of the sedimentary succession at Site 1194 is characterized by an early Miocene age shallow-water transgressive deposit (Unit V) overlying a basement high (Unit VI). This interval was followed by an early to early middle Miocene high sea level episode characterized by abraded carbonate particles indicative of transport (Unit IV and Subunit VA). A late middle Miocene sea level fall led to the formation of shallow water facies (Subunit III) followed by ~4 m.y. of sediment starvation. The late Miocene sea level rise led to deposition of hemipelagic sediments (Unit II) that are capped by highly winnowed Pleistocene deposits (Unit I) indicating strong bottom currents.

The sediments at Site 1194 are divided into six lithologic units. Unit I (0–3.8 mbsf; late Pleistocene in age) consists of a foraminiferal packstone without mud that reflects current-influenced deposition on the seafloor.

Lithologic Unit II (3.8–117.4 mbsf) is composed of late Miocene to Pliocene age hemipelagic mudstone/wackestone. Potential hiatuses and intermittently high sedimentation rates inferred from the shipboard biostratigraphy suggest that these sediments were deposited by small-scale gravity flows. Carbonate content in this unit varies from 60 to 90 wt% with an increasing trend downcore. The sediments in lithologic Units I and II have similar physical properties with slightly increasing bulk density (averaging ~1.75 g/cm$^3$) and velocity (averaging ~1600 m/s) and decreasing porosity (~70%–50%) downcore. MS and NGR show cyclic variations within these two units. Lithologic Units I and II correspond with the seismically defined Megasequence D.

The boundary between lithologic Units II and III (equivalent to seismic boundary B/D) consists of a sharp contact between poorly lithified wackestones and underlying lightly cemented neritic-rich grainstones. This surface is coated with a reddish brown crust of laminated phosphate interpreted as a hardground. Micropaleontological data suggest that this surface may represent a hiatus from 11.8 to 7.7 Ma. A second strong reflection below seismic boundary B/D correlates with a wireline signature similar to the hardground above, but this layer apparently was not recovered.

Lithologic Unit III (117.4–177 mbsf), deposited in the middle Miocene, was divided into two subunits. Subunit IIIA (117.4–158 mbsf) consists of bryozoan-dominated packstones and floatstones in the upper part and by small benthic foraminifers in the lower part. This subunit was likely to have been deposited on a middle neritic ramp in 30–50 m of water during the late middle Miocene (~13 to ~11 Ma) lowstand. Carbonate content in Unit III varies between 68 and 98 wt%.

Here, dolomite content is as high as 40 wt% but decreases toward the base of the unit. The near absence of bryozoans and the predominance of benthic foraminifers differentiate Subunit IIIB from Subunit IIIA.

The top of the early middle Miocene to early Miocene Unit IV consists of a 1-cm-thick layer of grainstone with a sharp contact to Unit III. This horizon is interpreted to be a firmground and is recorded as a prominent reflection in Megasequence B, a peak in physical properties data sets and low calcium carbonate values (~46 wt%). The lower to middle Miocene sediments of Unit IV (177–331.1 mbsf) are characterized by silt-sized packstones with physically abraded, unidentifiable skeletal components indicating high-energy long-distance transport. The likely source for these skeletal components was the NMP. Paleoenvironmental information and seismic sequence geometry indicate that lithologic Unit IV was deposited at outer neritic depths and displays an overall shallowing-upward trend. Carbonate content in Unit IV is variable (62–97 wt%). Unit IV was subdivided into two subunits. Subunit IVA has higher dolomite content (up to 20 wt%) and generally contains more clay. The common occurrence of angular quartz sand and the absence of clay differentiates Subunit IVB. Physical properties data from this interval show overall normal compaction trends with increasing bulk density and velocity and decreasing porosity.

The lower Miocene lithologic Unit V (331.1–421.1 mbsf) is characterized by partially burrowed dark layers. No clay was observed in this unit. Lithologic Unit V is interpreted as a shallow marine transgressive deposit over a topographic high on the Marion Plateau basement. Within lithologic Unit V calcium carbonate content varies between 76 and 99 wt% and generally increases downhole. Subunit VA is dominated by packstones with unidentifiable silt-sized skeletal components. The distinguishing characteristic of Subunit VB is that the skeletal components are coarse, sand sized, and dominated by planktonic foraminifers. Near the base of the unit, the larger benthic foraminifer *Lepidocyclina* is abundant, and glauconite infillings indicate reworking. Dolomite concentrations within lithologic Subunit V are ~10 wt% near the top and decrease to zero near the base. Porosity values show greater variability than in the overlying units superimposed onto the general decreasing trend resulting from compaction. Velocity and bulk density increase downhole within Unit V. MS and NGR show evidence of cyclicity. Unit V unconformably overlies the reddish brown olivine basaltic basement of Unit VI (421.1–421.7 mbsf).

Benthic foraminiferal assemblages suggest that water depths at Site 1194 increased from <100 m near the bottom of Subunit VB to >200 m near the base of Subunit IVA (264.5 mbsf). Above this interval, water depths progressively decreased to 30–50 m at the base of Subunit IIIA and increased to >200 m for the top 117.4 m of the section at Site 1194.

Well- to moderately preserved nannofossils and planktonic foraminifers are generally abundant above 117.3 mbsf at Site 1194 and are rare to few and poorly preserved below this depth. Correspondingly, biostratigraphic resolution is relatively good above 117.3 mbsf and poor below. A hiatus of ~4 m.y. duration occurs at the upper Miocene hardground at 117.3 mbsf. Average sedimentation rates for Site 1194 are estimated to be 30 m/m.y. for the early to middle Miocene and 25 m/m.y. for the late Miocene to Pliocene.

Paleomagnetic measurements on long cores over the upper 100 mbsf were pervasively corrupted by core-top magnetic anomalies. Susceptibility peaks, indicating that new magnetic material had been introduced at the top of cores and then magnetized in the direction of the

downhole overprint often accompanied these anomalies in magnetization intensity. To correct for these difficulties, the data were filtered, high intensities were removed, and the z-component was used in an attempt to obtain a magnetostratigraphy. Ultimately this effort provided only limited agreement with late Miocene biostratigraphic data. Apart from the hardgrounds, where there was evidence for hematite, the predominant magnetic material was magnetite.

The pore water chemistry of Site 1194 suggests two different chemical regimes divided by the contact between lithologic Units II and III. In the hemipelagic sediments of Units I and II, a strong correlation of downhole decreasing magnesium and sulfate concentrations indicates the formation of authigenic dolomite. The reoxidation of organic matter via sulfate reduction supplies carbonate ions for dolomitization, with the required calcium and remaining carbonate supplied from biogenic calcite. Pore water profiles in lithologic Unit III and below show little or no change for most constituents. Continued decreases in magnesium and increases in calcium concentrations in this interval are considered to be driven by reactions occurring in the mafic basement coupled with diffusional exchange with the sediment pore fluids. Taken as a whole, lithologic Units III–V do not appear to be undergoing further low-temperature diagenesis, but are acting as a passive aquifer.

TOC content at Site 1194 is <0.5 wt%. Hydrogen index values at Site 1194 range from 29 to 300 mg HC/g TOC, although the low TOC values in some intervals limit the reliability of the HI values. S content in Site 1194 sediments ranges from 0 to ~0.67 wt%; the sulfur profile is similar to that of TOC. Sediments from ~118 to 300 mbsf at Site 1194 can be organized into three geochemically defined units, which consist of a conspicuous horizon of increased TOC weight percent values, low HI values, and relatively elevated weight percent total S content, overlying a broader interval of relatively high $CaCO_3$, low TOC, and higher HI values. The horizons appear to coincide with hardgrounds and firmgrounds. The low gas content at this site is likely a function of appreciable pore water $SO_4^{2-}$ concentrations to total depth limiting methanogenesis. The immaturity of the organic matter meant that there was no thermogenic component to the gas fraction.

Downhole logging measurements from Hole 1194B produced a continuous geophysical record extending from basement (425 mbsf) to sediments at 84 mbsf. The measurements can be grouped into three logging facies (logging Units 1–3) that correlate well with seismic facies of the drift, slope, and shelf packages. Logging Unit 1 (84–114.5 mbsf), with generally low values of density, resistivity, and natural gamma ray, correlates to the onlapping sediments of Megasequence D. Logging Unit 2 (114.5–260 mbsf) is characterized by increased variability and distinct peaks in all logging data sets and roughly coincides with the high-amplitude inclined slope reflections of the NMP slope. Lithologically, neritic outer-ramp and upper-slope deposits above shallowing-upward deeper slope deposits characterize this interval. Thus, the variability and especially the peaks in the logs are most likely the combined result of variations in sedimentation rates, clastic content, and cementation, as might be expected in proximal slope sediments. For example, peaks of uranium and velocity appear to correlate with hardground surfaces. Logging Unit 3 (260–425 mbsf) contains low values in all logs but has regular variability, suggestive of distal cyclic shelf sedimentation. Changes in log signatures in Hole 1194B correlate well with lithologic unit boundaries, indicating that facies changes across unit boundaries produce distinct petrophysical signals.

## Site 1195

Site 1195 (proposed Site CS-10A) is located on the Marion Plateau, ~60 km northeast of the south-central Great Barrier Reef margin, at a water depth of 420 m (Figs. F1, F2). The main objective at this site was to recover a lower Miocene to Holocene sedimentary section that would provide a complete chronostratigraphy of the Neogene Marion Plateau depositional succession. Site 1195 is located at the intersection of regional seismic lines MAR15 (shotpoint 3505) and MAR04 (shotpoint 3928), 70 km east of the early middle Miocene NMP and 60 km north of the Miocene SMP platform. The sediments at Site 1195 record a distal shelf facies with the combined effects of changes in platform shedding, detrital input, and pelagic sedimentation, all of which can be linked to sea level and paleoceanographic changes.

A successfully drilled complete deepwater section, such as that which was recovered at Site 1195, provides an ideal sedimentary archive with which to accurately date seismic reflectors and seismic sequence boundaries. The ages for these horizons can be correlated with the other sites in the seismic grid to refine the age constraints in environments with lower age resolution.

In addition to calibrating the chronostratigraphy of the regional seismic sequences, Site 1195 will provide information on paleoceanographic changes recorded by variations in sedimentologic composition, physical properties, geochemistry, and stable isotope signatures. Results from Site 1195 will also provide insight into the age and sedimentologic response of the postrift drowning of the Marion Plateau.

### Operations

Operations at Site 1195, located 40 nmi south-southeast of Site 1194, began at 0700 hr on 26 January 2001. Hole 1195A was cored with the APC to 80.7 mbsf, where the wireline parted and the drill string had to be recovered. Average recovery was 98.2% (Table T2). The APC temperature tool was deployed at 33.2 and 71.2 mbsf. Cores were oriented starting with 194-1195A-4H (23.7 mbsf).

The vessel was offset 20 m east of Hole 1195A, and Hole 1195B was cored with the APC to refusal depth at 207.9 mbsf, with an average recovery of 101.1%. XCB coring deepened the hole to a total depth of 521.2 mbsf, with an average recovery of 60.4%. The recovery for the entire hole was 399.5 m (76.7%).

To evaluate the magnetic overprint imparted by the drill bit, a Russian-made 9.875-in APC/XCB PDC bit was used in Hole 1195B, instead of the standard 11.4375-in APC/XCB bit used in Hole 1195A. The Davis-Villinger Temperature Probe (DVTP) was deployed at 112.9 mbsf (following Core 194-1195B-12H) and 150.9 mbsf (following Core 16H). Cores were oriented starting with Core 194-1195B-3H.

Wireline logging operations were shortened because of deteriorating hole conditions. The triple combo tool string had to be pumped out of the pipe but subsequently descended to within 2 m of the bottom of the hole (~600 mbsf) without problems. For the second run, a successful check-shot survey with the WST was the highest priority. The WST also had to be pumped out of the pipe, but it failed to descend into the hole. In a few instances, the drill pipe became stuck and the WST had to be recovered. After the pipe was freed, the WST was run back in the hole but could not be lowered below 121 mbsf. Three levels were shot at 118, 95, and 86 mbsf using the air gun. No further logging was attempted.

## Principal Scientific Results

Drilling at Site 1195 recovered a 517-m-thick sedimentary succession ranging in age from the early Miocene to Pleistocene and showing little change in average sedimentation rate. In the lowest part of the sedimentary section (517.5–517.7 mbsf), 20 cm of well-indurated grainstone with nummulitids of possible Eocene age were recovered. The lithostratigraphy of Site 1195 comprises five main units that are defined by texture, color, biotic associations, and the presence or absence of glauconite, quartz, and pyrite. Induration increases from unlithified at the top to strongly lithified at the base of the succession. With the exception of Units I and V, which are mainly pale yellow and light yellowish brown, most of the succession displays subtle color variations from light to dark greenish gray or olive gray. A complete and well-established biostratigraphy provides an accurate framework to date this succession and to calibrate the entire sequence stratigraphy of the Neogene Marion Plateau. The basal sediments record a transgression with lithoclast-bearing sandstone and grainstone, containing abundant quartz and glauconite (~500–517.5 mbsf; lithologic Unit IV). Unit IV was deposited in a proximal periplatform setting in <100 m of water. The overlying 467 m of sediment (lithologic Units III–I) were deposited in upper bathyal depths (>200 m). This deeper-water section records changes in carbonate platform growth, detrital input, and current dynamics by changes in texture, neritic constituents, clay content and, glauconite content. The end of the NMP (lithologic Unit II/III boundary), and the associated sea level drop near the middle to late Miocene boundary are recognized at Site 1195 as an upcore decrease in neritic components and the occurrence of a major glauconite-rich unit that coincides with the seismic Megasequence B/C boundary (~11 Ma).

Lithologic Unit I (0–36.9 mbsf) is composed of skeletal grainstone with planktonic foraminifers and subordinate mollusks. Deposition was strongly current controlled. The base of Unit I consists of a 20-cm-thick rudstone with phosphatized lithoclasts, which is visible in the seismic sections as an unconformity within seismic Megasequence D. Unit II (36.9–255.9 mbsf) consists of bioturbated skeletal packstone with clay and minor wackestone, and grainstone intervals are present. The top 15 m of this unit is glauconite rich. Compared to Unit I, Unit II is darker and has greater biotic diversity. In the upper 200 m of Site 1195, rare to common larger benthic foraminifers indicate deposition in upper bathyal water depths. The relative proportion of coarser and finer planktonic foraminiferal fractions varies among samples, possibly indicating winnowing variations in a current-influenced environment. To a depth of 95 mbsf, sediments of Units I and II, are characterized by high-frequency variability in NGR and MS, which contrasts sharply with the underlying intervals to 220 mbsf, where values approach zero. The high NGR and MS amplitudes above 95 mbsf are likely caused by increased terrigenous clay deposition, an observation supported by carbonate measurements of 80–90 wt% with clay dominating the noncarbonate fraction. Between 220 mbsf and the base of lithologic Unit II, NGR and MS values are reduced and more consistent than in the uppermost section.

Three subunits separated by prominent glauconite-rich horizons can be distinguished within lithologic Unit II. Subunit IIA (36.9–93.9 mbsf) is a fine-grained, poorly bioturbated packstone and grainstone with clay defined by the absence of pyrite and textural recurrent variations. Subunit IIB (93.9–123.9 mbsf) is composed of silt-sized skeletal packstone

with common burrows. Subunit IIC (123.9–255.9 mbsf) is characterized by a series of 2-m-thick fining-upward intervals, which display color changes presumably related to variations in clay content. Some of these intervals have a scoured base and display a gradual change into the overlying coarser interval. Subunit IIC coincides with seismic Megasequence C and thus is coeval with growth of the SMP to the south of Site 1195. The base of Unit II is glauconite rich. Based on both foraminiferal assemblages and the presence of fine sand-sized fragments of neritic origin, the lower part of Unit II (below 200 mbsf) and all of lithologic Unit III (255.9–467.3 mbsf) were deposited in a distal periplatform environment at outer neritic to upper bathyal water depths. The Unit III to II boundary corresponds to the top of Megasequence B and thus marks the time at which the NMP to the east ceased carbonate production. In addition to the increase in neritic components, Unit III sediments contain more organic matter and, especially in the lower part, more clay and quartz. The base of Unit III is glauconite rich.

Unit IV (467.3–517.5 mbsf) consists of grainstone to sandstone with quartz, rounded glauconite, carbonate lithoclasts, nannofossils, and rare broken foraminifers. The biotic assemblage and coarse fraction, mixed with neritic and pelagic components, indicate a proximal periplatform depositional environment in outer neritic water depths. This unit was deposited during flooding and initial transgression over acoustic basement. Similar to Unit I, Unit IV NGR and MS values display high amplitude variability.

At the base of Site 1195, 20 cm (Unit V; 517.5–517.7 mbsf) of a well-cemented skeletal grainstone with coralline algae, larger benthic foraminifers, and mollusks was recovered. This light yellowish brown limestone contains abundant nummulitids that may be late Eocene in age. These rocks/sediments are overlain by or possibly are encased in sediment containing benthic foraminifers and nannofossils that indicate early Miocene deposition.

Overall, bulk density shows a decreasing downhole trend to 60 mbsf (1.68 to 1.45 g/cm$^3$) followed by a slow but consistent increase to 380 mbsf (1.45 to 2.08 g/cm$^3$). Below this, density is approximately constant to the bottom of the hole. Porosity and thermal conductivity reflect these bulk density trends; porosity ranges between 30% and 80%, whereas thermal conductivity ranges from 0.8 to 1.4 W/(m·K). In contrast, *P*-wave velocity increases from 1541 to 2241 m/s at 370 mbsf. Below this depth, the mean velocity remains constant to the bottom of the hole.

Calcareous nannofossils and planktonic foraminifers ranging from late Pleistocene to late Miocene age are generally well preserved, whereas early to middle Miocene microfossils vary from poorly to well preserved. Calcareous nannofossils are abundant for most of the sequence recovered at Site 1195. Unlike other sites, the sequence cored at Site 1195 is virtually complete, with no apparent hiatuses. Interval (0.5–4 m.y.) sedimentation rates range from 20 to 65 m/m.y.

Magnetostratigraphy obtained at this site is in agreement with the biostratigraphic datums for the middle Miocene and early late Miocene intervals. However, the late Miocene to Pleistocene magnetostratigraphy suggests ages ~0.6–0.8 m.y. younger than the biostratigraphy suggests. Nevertheless, the interpreted magnetostratigraphy between Chrons C1n and C2An provides the best record of all Leg 194 holes. A comparison between APC cores taken with the reduced magnetic PDC drill bit in the BHA with those taken with the standard bit reveals that the core top intensity anomalies in the vertical component are much reduced

with the non-magnetic bit. At this site, glauconite layers coincide with intervals of high magnetic intensity, suggesting the presence of magnetite. Magnetic intensity peaks could be correlated between Hole 1195A and 1195B, indicating a depth offset of ~6 m between the holes.

The low gas content at Site 1195 is likely a function of appreciable pore water $SO_4^{2-}$ concentrations limiting methanogenesis and the lack of mature organic matter that could provide a thermogenic component to the gas fraction. The pore water chemistry at Site 1195 can be subdivided into two zones. In the upper ~80 mbsf, the chemistry is similar to seawater and appears to be the result of pore fluid exchange between the sediments and overlying waters. Strong oceanographic currents in the area might play a role in driving fluid exchange. Between 80 mbsf and basement, pore water chemistry varies little with depth and shows evidence for authigenic dolomite formation and organic matter remineralization during sulfate reduction.

Wireline logging in Hole 1195B provided a continuous geophysical record from 80 to 517 mbsf. Five logging units were distinguished. Logging Unit 1 (80–240 mbsf) has low gamma ray, bulk density, and resistivity values and displays little variability, which is consistent with the homogeneous lithology of lithologic Unit II. The boundary with logging Unit 2 at 240 mbsf coincides with the seismic sequence B/C boundary. This boundary is marked by an increase in bulk density, resistivity, and natural gamma ray values. The onset of cyclic alternations of light gray and greenish gray sediment correspond to a cyclic appearance in all logging data within logging Unit 2 (240–418 mbsf). At the top of logging Unit 3 (418–451 mbsf), bulk density and resistivity values increase slightly and neutron porosity and NGR decrease. Toward the bottom of this unit, higher amplitudes in gamma ray and resistivity logs were observed. This pattern of higher variability in the lower part and less variability in the upper part of the unit is similar to logging Unit 2, perhaps indicating a repetition of the sedimentation pattern, although with a reduced thickness. At the top of logging Unit 4 (451–468.5 mbsf), the various logs become relatively constant and values decrease slightly. The base of this unit, however, includes a dramatic gamma ray peak that correlates with a glauconite-rich layer. The last significant change in log character was detected at 468.5 mbsf with a significant drop in the resistivity and an increase of gamma ray values, dominated by an increase in uranium from 3 to 6 ppm. The lithologies corresponding to logging Unit 5 (468.5 mbsf to the bottom of the logged section) consist of glauconitic sand and packstone.

## Sites 1196 and 1199

Sites 1196 and 1199 were both drilled into the top of the SMP. Site 1196 (proposed Site CS-06A) was drilled in 304 m of water, 20 km east of the Great Barrier Reef margin (Figs. **F1, F2**). The site is positioned at the intersection of regional seismic line MAR07 (SP 2808) and local grid line MAR70 (SP 178). Two holes were drilled (Hole 1196A: 0–672.2 mbsf; Hole 1196B: 0–265.3 mbsf) through a 663-m sequence of carbonate platform sediments overlying a phosphate-rich substrate. One hole was drilled at Site 1199 (proposed Site CS-16A; 0–419.5 mbsf). This site is located in 316 m of water ~5 km northeast of Site 1196 and is positioned on regional seismic line MAR20 (SP 2690).

Sites 1196 and 1199 were drilled to provide information on the initiation and facies development of the SMP carbonate platform, the nature of unconformities separating each platform phase, and the age and

nature of the section equivalent to the NMP drilled at Site 1193. Post-cruise analysis on recovered samples will enable the study of fluid flow processes within the carbonate platform as interpreted from the pore waters from adjacent slope sites (1197 and 1198).

Scattering of seismic energy within the well-indurated SMP makes it difficult to determine the stratigraphy and nature of sediment deposition underneath the platform cap. Despite this, analysis of regional seismic data suggested that Sites 1196 and 1199 should penetrate a thick sequence of upper Miocene–Pliocene carbonate platform sediments representing the deposition of the SMP. The base of this sequence was predicted to overlie basinal sediments shed from the NMP drilled at Site 1193. Drilling at Sites 1196 and 1199 only partially confirmed this interpretation. Although not conclusive, evidence from these sites suggest that only the upper 130 to 150 m of the platform facies could have been accreted during the late Miocene, overturning the working hypothesis that this platform was completely of late Miocene to early Pliocene age. This discovery also necessitates a lower-amplitude sea level change for this time interval than was originally predicted.

## Operations

### *Site 1196*

Site 1196 is located within the Great Barrier Reef Marine Park. All operations adhered to the guidelines established by the Great Barrier Reef Marine Park Authority. Hole 1196A was spudded with the RCB into the hard carbonate cap of the SMP and advanced to 85.8 mbsf. Coring was interrupted for 10 hr because the drill string became stuck and had to be freed. To reduce the risk of the pipe becoming stuck, the hole was flushed with mud sweeps following the retrieval of each core and additional wiper trips were made at 285 and 429 mbsf. The pipe was stuck and freed again after a connection was made with the bit at 499 mbsf. Coring was terminated at 672.2 mbsf, well below the original target depth of 570 mbsf. Acoustic basement was not penetrated. A total of 86.34 m of core was recovered (12.9% average recovery) (Table T2).

The wireline triple combo was run with the MGT on the top and the LDEO temperature tool on the bottom for the first logging run in Hole 1196A. The MGT experienced electrical problems when it was lowered in the pipe and was subsequently removed. The shortened string was deployed but could not pass a tight spot at ~520 mbsf, and the hole was logged up from that depth. The tool string was recovered with loosened connections and without the brass bottom nosepiece (~4 in long) of the LDEO temperature tool, most likely a result of current-induced vibration of the drill pipe. For the second wireline run, the FMS-sonic combination was deployed, but an obstacle was encountered in the pipe—possibly the missing piece of the temperature tool—that had to be pushed out by a core barrel. The FMS-sonic tool combination was subsequently run starting from a tight spot at 524 mbsf. The third run was a check-shot survey with the WST with 13 stations successfully shot between 94.4 and 523.5 mbsf.

Hole 1196B was spudded with the RCB to prepare a pilot hole for ADCB coring. Following the recovery of Core 194-1196B-6R, the vessel was forced to wait on weather for 11 hr as the heave was routinely exceeding the shallow-water guideline threshold of 2 m. Coring then resumed and advanced to the target depth of 110 mbsf. Average recovery for that interval was 10%.

Once the bit was on deck, the weather remained unfavorable for shallow water operations and the seas were deemed too rough for ADCB coring. In response, drilling operations were moved to Site 1197, with a planned return to Site 1196 when the environmental conditions might provide better success for ADCB reentry and coring. The vessel departed Site 1196 at 0415 hr on 6 February, with the beacon left on the seafloor. After initial operations at Site 1197 and completion of Site 1198, the weather abated, and ADCB coring in Hole 1196B appeared feasible. Reoccupation of Hole 1196B began at 0545 hr on 11 February.

Hole 1196B was reentered with the RCB, without the use of an FFF, and washed ahead to 110 mbsf to ensure a clean and stable hole for the ADCB reentry. The drill string was recovered, and the ADCB drilling assembly was reentered. ADCB coring advanced from 110 to 265.3 mbsf (Cores 194-1196B-13Z through 51Z). Coring was terminated before reaching the target depth of 360 mbsf because of diminishing core recovery and to conserve time for an additional site. Total recovery from the 155.3-m interval cored was 17.92 m, or an average of 11.5%. The RCB recovery for a comparable interval (17 cores from 105.0 to 268.4 mbsf) from Hole 1196A was 10.4%. The heave rarely exceeded 1 m during coring operations in Hole 1196B. Although still in the development stage, the ADCB system operated continuously for 35 hr without hardware problems, broken parts, improper seating of the core barrel, or downtime of any kind.

### *Site 1199*

After a revisit of nearby Site 1197 (13–17 February 2001), the vessel proceeded to Site 1199 (proposed Site CS-16A) in dynamic positioning mode. After waiting on weather for 3.5 hr, Hole 1199A was spudded with the RCB at 1235 hr on 18 February. Rotary coring advanced to a final depth of 419.5 mbsf (Table T2). The recovery from the top 159.8 m of the hole was 83.6 m (52.3%). The average penetration rate (ROP) (4.7 m/hr) was slow until the hole deepened and the increased bit weight gradually helped to increase the ROP. Below 159.8 mbsf, the recovery dropped off dramatically and the ROP increased substantially. The average recovery from 159.8 to 419.5 mbsf was 3.3%. The total recovery for the hole was 92.16 m, or 22.0%.

Because of time constraints, after completion of coring the hole and drill string were prepared for logging and the triple combo tool string was lowered to a depth of 418 mbsf, ~2 m above total depth of the hole. A successful logging run was completed. The FMS-sonic velocity tool suite was subsequently lowered in the hole but would not move past an obstruction at 129.2 mbsf, presumably because of a karst cave. The logging tool indicated a hole inclination of up to 7°. After countless attempts to pass the tight spot, which included lowering the pipe and adding sections to the tool string, logging was initiated above this horizon, and good data was obtained over the short interval. Logging operations were terminated at 1000 hr on 19 February. The drill string was recovered and the beacon retrieved for the last time during Leg 194. The BHA was disassembled and the vessel was secured for the extended sea voyage to Guam, leaving the site at 1415 hr on 22 February.

## Principal Scientific Results

### *Site 1196*

The SMP drilled at Site 1196 was established on an upper Oligocene (to early Miocene?) siliciclastic, phosphate-rich substrate. Above this

substrate, an ~660-m-thick edifice of shallow-water carbonates was established from the early (to late?) Miocene that underwent several phases of growth, exposure, and dolomitization. The oldest platform, undated but probably mostly early Miocene in age, is ~300 m thick and is pervasively dolomitized, nearly obliterating the initial depositional facies. This dolomitized platform is the foundation for a growth phase that spans the middle Miocene and may have begun in the late early Miocene and continued into the late Miocene. Within these two packages, platform development starts with a reefal unit, which is overlain by a sequence of shallow-water sediments with highly variable facies, ranging from high-energy grainstone to seagrass roots and blades and larger benthic foraminiferal assemblages. The lack of mud in the 200-m-thick middle Miocene succession suggests a high-energy environment of deposition throughout the sequence. This platform is capped by a 25-m-thick dolomitic interval. Overlying this dolomitic interval is a nondolomitized reef with evidence of exposure on its surface. The youngest phase of platform growth is represented by 125.5 m of dolomitic floatstone/mudstone.

Five lithologic units were defined at Site 1196 (here, depth references are only given for Hole 1196A). Sediments recovered in lithologic Unit I (0.0–182.2 mbsf; middle to late? Miocene to Pliocene? in age) were deposited in inner to middle neritic water depths. This unit was subdivided based on biotic assemblages. Subunits IA, IB, and ID are mostly dolomitic, whereas Subunit IC is predominantly composed of calcite. Subunit IA (0.0 to 117.2 mbsf) consists of dolomitic floatstone/rudstone characterized by the occurrence of centimeter-sized rhodoliths in a moderately sorted sandy matrix containing larger benthic foraminifers, coralline algae, mollusks, and rare bryozoan fragments. Both intergranular and moldic porosity occurs, and some pores are filled by a complex succession of cements and internal sediments. Lithologic Subunit IB (117.2 to 125.9 mbsf) is ~8 m thick and consists of a well-lithified dolomitic skeletal floatstone with a recrystallized grainstone matrix. The coarse (>2 mm) fraction is >30% of the rock volume and includes elongated fragments of branching coralline algae and centimeter-sized mollusk shells. Numerous molds of flat, larger benthic foraminifers also are present. The base of this subunit corresponds to a peak in NGR in both core and downhole logging records. Lithologic Subunit IC (125.9 to 162.8 mbsf) is composed of skeletal rudstone, floatstone, and boundstone rich in centimeter-sized hermatypic coral debris, mollusk shell fragments, and rhodoliths. Coralline algal and bryozoan clasts, broken echinoid spines, and larger benthic foraminifers occur also in the finer-grained matrix. Both intergranular and moldic porosity is frequent throughout this predominantly calcitic interval. Lithologic Subunit ID (162.8–182.2) is mostly a dolomitic floatstone with a grainstone matrix. The main constituents include elongated fragments of branching coralline algae, small (<1 cm) rhodoliths, mollusk shells, rare bryozoan detritus, and molds of larger benthic foraminifers. Overall sorting is poor; however, distinct laminae are present in some intervals.

The top of lithologic Unit II (182.2 to 345.8 mbsf; middle Miocene in age) is composed of floatstone/rudstone containing abundant molds of branching coral and rare fragments of branching coralline algae. This lithology corresponds to peaks in resistivity and velocity in the downhole logging data. Unit II can be divided into two subunits, both of which were deposited in shallow water (<10 m). Lithologic Subunit IIA (182.2 to 335.9 mbsf) consists of well-lithified, poorly sorted skeletal floatstone with a silt-sized grainstone matrix and common moldic po-

rosity. The predominant constituents include porcellaneous small (miliolids) and larger benthic foraminifers, and centimeter-sized mollusk shells. Coral, bryozoans, and rare *Halimeda* debris also occur. Thread-like, dark patches up to 1 cm long are interpreted as preserved seagrass roots. The lower part of Subunit IIA contains thin horizons with brown micrite mottles. This interval also contains exceptionally high values of NGR, shallow and deep resistivity, and sonic velocity in the downhole logging data. Lithologic Subunit IIB (335.9–345.8 mbsf) is characterized by a thin unit of well-lithified, poorly sorted skeletal rudstone/boundstone. The coarse (>1 cm) fraction includes colonial hermatypic corals, red algae, and mollusk fragments in a micritic matrix. *Lithophaga* borings are common, as is moldic porosity. The boundary with underlying Unit III is marked by a change from pure calcite to a mixed calcite and dolomite mineralogy.

Lithologic Unit III (345.8 to 617.1 mbsf, early [to middle?] Miocene in age) consists of coarsely crystalline dolostone lacking primary textures. This unit is divided into four subunits on the basis of color, presence or absence of molds, and identification of primary rock components. Lithologic Subunit IIIA (345.8 to 355.3 mbsf) consists of a mottled, recrystallized dolomitic rudstone with a grainstone matrix. Ghosts of rhodoliths, branching and massive corals, and dissolved mollusk fragments were also identified. The majority of the sediments within this subunit were deposited in water depths <30 m. Lithologic Subunit IIIB (412.7 to 470.4 mbsf) contains a brilliant white sucrosic dolostone with rare relicts of centimeter-sized rhodoliths and branching coralline algae and millimeter-sized lenticular molds of larger benthic foraminifers. The recovered portion of this subunit is visually homogenous. Downhole logging data, however, shows several peaks in sonic velocity suggesting a more heterogeneous composition in the unrecovered horizons. The lower boundary of Subunit IIIB corresponds to a reddish interval at 470.4 mbsf.

Lithologic Subunit IIIC (470.4 to 537.7 mbsf) is a mottled, recrystallized, dense dolostone. Ghosts of rhodoliths, mollusk shells, and coralline algal fragments are visible. Intercrystalline, shelter, moldic, and possibly, fenestral porosity were observed. The lower portion of Subunit IIIC contains several millimeter- to centimeter-thick, dense, brown or red layers interpreted to be exposure surfaces. Lithologic Subunit IIID (537.7 to 617.1 mbsf) is a well-lithified dolostone, with larger benthic foraminifers. Other constituents include rhodoliths, coralline algae, and mollusk fragments. Most original texture has been lost.

Lithologic Unit IV (617.1 to 662.6 mbsf; early Miocene in age) includes various dolostone facies that occur in meter-thick sequences separated by iron-stained zones interpreted to be exposure surfaces. The lower limit of this unit occurs at 653 mbsf. The deepest core at Site 1196 contains lithologic Unit V, which consists of a dark, phosphate-rich sandstone and claystone representing the Oligocene substrate of the carbonate platform.

Nearly all core catcher samples from this site contained lithified platform facies and thus were not processed for nannofossil or planktonic foraminifers once a number of samples were shown to be barren. One thin section from a few centimeters below the seafloor contained age-diagnostic planktonic foraminifers that provided a maximum age of 3.2 Ma. Few planktonic and no outer neritic/upper bathyal foraminifers were recovered within the platform sediments. Calcareous nannofossils found within lithologic Subunit IIA provide an age range of 13.6 to 18.2 Ma. This age was further constrained between 183 and 327 mbsf by the

occurrence of the benthic foraminifer *Flosculinella botangensis,* with an age range of 13.3 to 15.2 Ma. Nannofossils were also found in the last core directly below the carbonate-platform sequence, providing an age of 24.2 to 24.6 Ma.

Benthic foraminifers characteristic of subtropical carbonate-platform environments at inner to middle neritic depths (<100 m) are abundant throughout most of Site 1196. Within the platform sequence, several shallowing and deepening sequences occur, although highly dolomitized intervals and poor core recovery seriously limited resolution, particularly below 335 mbsf. The interval from 183 to 336 mbsf indicates a shallow (<10 m) depositional setting, probably on a seagrass-dominated open platform. A complex interval from 117 to 183 mbsf includes exposure surfaces that bracket a skeletal boundstone interpreted to be a reefal facies. The upper 117 m of Site 1196 are open platform sediments deposited at middle neritic depths, shallowing to inner neritic depths with possible carbonate beach sands just below the hiatus surface at the top of the platform. The discovery of the larger benthic foraminifer *Lepidocyclina* in limestone at the top of the SMP appears to support recent evidence that this genus survived into the late Miocene in the western Pacific. Most interpretations from northern Australia concluded that the youngest unreworked occurrence of this genus was in the late middle Miocene.

At Site 1196, bulk density ranges between 1.9 and 2.75 g/cm$^3$ and generally increases downhole. Bulk density shows a high degree of scatter throughout the drilled interval and no apparent relation exists between density variations and lithologic units. Grain-density values average 2.80 g/cm$^3$ and range between 2.55 and 2.95 g/cm$^3$. The downhole trend correlates well with dolomite abundance. Porosity mirrors bulk density and decreases with depth (51% to 2%). The highest porosity values are found in dolomite-rich intervals due to the abundant intercrystalline porosity. *P*-wave velocity varies between 2300 and 6600 m/s. Anisotropy of *P*-wave velocity ranges from –9% to 14%. Most of the anisotropy values (71%) have a positive sign, meaning that the velocity in the z-direction is lower than average velocity in the x- and y-directions. MS ranges from –8 to 5 $\times$ 10$^{-6}$ SI. A diamagnetic interval from 20 to 105 mbsf correlates with Subunit IA. NGR ranges from 0 to 65 counts per second (cps). Maximum NGR values follow trends observed in the downhole logs.

Based on conventional downhole logging data and FMS images, four logging units can be distinguished. Each of these units can be interpreted as a platform growth phase, where logging Unit 1 (76–128 mbsf) appears to correlate with the late Miocene SMP, logging Unit 2 (128–163 mbsf) is a reef growth phase of undetermined age, and logging Units 3 and 4 (163–524 mbsf) are middle and possibly early Miocene platform phases. Within the logging units, subunits are recognized that may be related to facies changes during the progressive development of these platforms.

Results from sporadic paleomagnetic measurements indicate that the sediments are relatively weakly magnetized with average intensities of 10$^{-4}$ A/m increasing downcore. Magnetostratigraphic interpretation of the sedimentary section was not possible because of poor recovery. Rock magnetic analyses performed throughout the recovered section to 600 mbsf indicate that magnetite is the predominant mineral phase recording magnetization. Below 600 mbsf, however, both magnetite and hematite are present. The varying role of the magnetite and hematite in

magnetization and in associated color changes may provide a record of oxidizing fluid migration in the lower portion of this platform.

Carbonate ($CaCO_3$) content at Site 1196 ranges from ~0.5 wt% in the siliciclastic interval at the bottom of the hole to 100 wt% in the carbonate-dominant intervals. TOC content is close to zero except from ~180 to 260 mbsf and from ~250 mbsf to the bottom of the section, where values of 0.3 and >0.8 wt%, respectively, were measured. The upper organic carbon-containing interval corresponds to samples containing seagrass, whereas in the lower interval, HI values and C/N ratios are indicative of terrigenous organic matter inputs. These relative TOC enrichments coincide with decreased carbonate contents, particularly in the lower horizon. Sulfur content in Site 1196 sediments ranges from 0.0 to ~5.38 wt%, and its distribution is similar to that of TOC. No volatile gases were detected at Site 1196. The dolomitized and highly indurated lithologies, as well as the low core recovery, prevented pore water sampling at this site.

### *Site 1199*

The geologic setting and lithologic units recovered at Site 1199 were similar to those at 1196, although the thicknesses of the units are different in some intervals. The 419.5-m-thick stratigraphic succession retrieved from Site 1199 consists of diverse carbonate facies, reflecting variations of accommodation space during the middle, and probably late, Miocene. This succession was subdivided into three major units on the basis of carbonate mineralogy and nature of constituent particles. Unit I (0.0–159.8 mbsf; middle–late Miocene in age) was divided into four subunits. Subunit IA (0.0–106.6 mbsf) is a rhodolith-bearing, dolomitic floatstone deposited in a neritic, open-platform environment at water depths estimated between 30 and 80 m. Varying hydrodynamic energy during the deposition of this subunit, possibly due to storm action, is recorded by the presence of distinctive facies and crude coarse-tail grading in some intervals. Dense pink-colored zones in this subunit correspond either to exposure horizons or, more likely, to submarine hardgrounds.

Subunit IB (106.6–114.1 mbsf) consists of well-lithified, dolomitized skeletal floatstone with a recrystallized grainstone matrix rich in coralline algae fragments. These sediments were deposited in an open-platform setting, possibly at slightly deeper water depths than the overlying and underlying subunits.

Subunit IC (114.1–121.9 mbsf) is characterized by rudstone/boundstone textures with centimeter-sized hermatypic coral debris, branching coralline algae fragments, and larger benthic foraminifers representative of shallow reefal facies. Unlike the corresponding interval at Site 1196, this subunit is pervasively dolomitized. These sediments overlie, and are overlain, by reddish crusts interpreted as exposure surfaces. Widespread vuggy porosity and reddish silt in large vugs support this interpretation. Downhole logging data, as well as these diagenetic features, suggest that Subunit IC has been pervasively karstified. Subunit IC corresponds to low NGR, density, and resistivity values in both the core and downhole physical properties data.

Subunit ID (121.9–159.8 mbsf) was deposited in a low-energy open-platform setting. Sediments are composed of dolomitic floatstone with a grainstone matrix with elongated fragments of branching coralline algae, small (<1 cm) rhodoliths, mollusk shells, rare bryozoan detritus, larger benthic foraminifers (as molds), and rare coral debris.

Lithologic Unit II (159.8–410.0 mbsf; early? to middle Miocene in age) is divided into two subunits. Hardground horizons observed at the top of Unit II at Site 1196, were not seen at Site 1199. This suggests that the uppermost part of the sequence was not recovered or was of a different composition because of lateral facies variability. Lithologic Subunit IIA (159.8–285.0 mbsf) consists of a well-lithified, slightly dolomitized skeletal floatstone with a silt-sized grainstone matrix rich in porcellaneous benthic foraminifers (alveolinids), mollusk shells, and rare coral fragments. This subunit corresponds to an interval of relatively high NGR values in the downhole logs. Lithologic Subunit IIA was most likely deposited in an inner platform setting at very shallow (<30 m) water depths, although in contrast to its lateral equivalent position at Site 1196, no evidence of seagrass roots or blades was found.

Lithologic Subunit IIB (285.0–410.0 mbsf) is characterized by a highly porous, friable limestone comprised of two facies that form meter-scale alternations. The first facies consists of well-sorted, skeletal grainstones with leached grains. The second facies is slightly darker and includes centimeter-sized rhodoliths. The sediments of Subunit IIB were deposited in shallow water depths (<60 m).

The core catcher of the last core recovered at Site 1199 contains 10 cm of sucrosic dolostone similar to that found at the same depth in Hole 1196A. Because of the similarity with rocks at Site 1196, this interval has been classified as lithologic Unit III (410.0–419.5 mbsf; early to middle? Miocene in age), although it is possible that it represents a dolomitized interval in lithologic Subunit IIB.

No age constraints were obtained from nannofossils or planktonic foraminifers. Benthic foraminifers characteristic of shallow-water carbonate platform environments are abundant throughout most of the sequence recovered at Site 1199. The larger benthic foraminifer assemblages indicate a Miocene age throughout, and distinctive benthic foraminifers in several samples from 170.3 to 265.9 mbsf indicate an age of 13.3–15.2 Ma.

Paleowater depths during deposition of the platform were consistently within the euphotic zone (0–150 m), as indicated by the dominance of red algae and larger benthic foraminifers. Shapes and sizes of the larger benthic foraminifers in lithologic Unit I indicate depths consistently <100 m and probably much shallower near the top of the platform. Miliolid foraminifers are abundant throughout lithologic Subunit IIA, whereas the larger porcellaneous taxa (alveolinids and soritids) were only observed occasionally. Paleowater depths are conservatively interpreted as <30 m throughout lithologic Subunit IIA. They were likely much shallower, including exposure surfaces and eolian episodes. Lithologic Subunit IIB is dominated by larger foraminifer-rich grainstone and floatstone with varying proportions of red algae. The abundance, robustness, and sorting of *Lepidocyclina* indicate paleowater depths of <60 m and possibly shallower. At Site 1199, bulk density ranges between 1.4 and 2.7 g/cm$^3$ showing high scatter throughout the entire interval with no apparent relation between density and the lithologic units. Grain density averages 2.79 g/cm$^3$ and is nearly constant throughout the drilled interval. Porosity values range from 3% to 48% with values at ~30% at the top of the hole, decreasing to 3% at 90–110 mbsf and increasing to 20% at 170 mbsf. Below 170 mbsf, porosity values are scattered between 14% and 48%. Velocity mirrors the porosity profile and varies between 3000 and 5500 m/s with values at ~4000 m/s at the top of the hole, increasing to 5500 m/s between 100 and 110 mbsf and decreasing to 3950 m/s at 170 mbsf. MS ranges from –2 to 20

$\times 10^{-6}$ SI with little variability except for a spike to $22 \times 10^{-6}$ SI at 141 mbsf. NGR values increase between 0 and 40 mbsf (~10 to ~24 cps) and between 40 and 114 mbsf (~10 to ~83 cps). A peak in NGR is visible at 170 mbsf.

The average sediment magnetization at Site 1199 is $10^{-3.5}$ A/m ranging between $10^{-4.5}$ to $10^{-2.5}$ A/m. An intensity increase of two orders of magnitude occurs at ~103 mbsf at the Subunit IA/IB boundary. The predominant magnetic mineral carrying remanence is magnetite.

Downhole logging data from Hole 1199A provide important information on the lithology and architecture of the SMP, especially in the lower part of the site, where core recovery was low. Two karst holes are inferred from the logs, each ~10 m thick, at 118–129.2 and 155–162 mbsf, respectively. The logs show significant differences between this site and Site 1196. However, as with Site 1196, the logging data can again be subdivided into four logging units related to the growth stages of the SMP.

## Site 1197

Site 1197 (proposed Site CS-08A) is located on the southern Marion Plateau, 40 km east of the Great Barrier Reef margin and ~5 km southeast of the downcurrent, windward slope of the SMP (Figs. **F1, F2**) The site is located on regional multichannel seismic lines MAR07 (shotpoint 3721), MAR65 (shotpoint 645), and MAR66 (shotpoint 907) in 348 m of water. The main purpose of this site was to retrieve a proximal platform margin record of the SMP sedimentation; to document and date platform growth, shedding, and subsequent current reworking; to study the fluid flow within the platform and adjacent slope sequences; and to determine the age and nature of acoustic basement.

### Operations

Operations at Site 1197 began at 0711 hr on 6 February 2001 (Table **T2**). Hole 1197A was spudded with the APC. Piston coring advanced to 54.6 mbsf, where a hardground was struck. The average recovery for this interval was 101.6%. Coring continued with the XCB to 203.8 m, where operations were terminated because of very low recovery (0.48% average recovery). Eleven of the 16 XCB cores had zero recovery. An inspection failed to identify any mechanical reason for the lack of recovery, so operations at Site 1197 were terminated with the option to return at a later time. Before the vessel departed for Site 1198, it remained in standby mode on location to wait for the third helicopter arrival of Leg 194 to evacuate an injured ODP technician.

After completion of Site 1198 and a return to Site 1196, Site 1197 was reoccupied to drill the hole to basement. The second operation at Site 1197 began at 1900 hr on 13 February. Hole 1197B was spudded with the RCB, drilled to 50 mbsf, and cored to a total depth of 674.9 mbsf. Erratic torque was experienced at 175.0 mbsf (depth of a major unconformity at the bottom of the elusive Megasequence C), and a total of three wiper trips were made to maintain the integrity of the hole. The final depth of 674.9 mbsf was 25 m below the Pollution Prevention and Safety Panel imposed limit of 650.0 mbsf; approval to exceed this depth was received from ODP/Texas A&M University headquarters. The interval 54.6 to 203.8 mbsf, which had an average recovery of 0.48% with the XCB in Hole 1197A, had 1.56% recovery in Hole 1197B. The total average recovery for the entire hole was 213.64 m (34.2%).

On 15 February, a planned rendezvous with the *Wyllaway* from Mackay took place. The vessel brought various supplies and returned Operations Engineer Leon Holloway to the mainland. In addition, a Transocean Sedco Forex employee required evacuation for medical reasons.

The hole was flushed and replaced with sepiolite mud, and the bit was released in preparation for the logging program. The tool string could not be advanced past the end of the open pipe and was recovered. The pipe was repositioned and the tool was redeployed and advanced to 81.6 mbsf, where the tool contacted an obstruction. When the tool was recovered, the compensating section of the DITE was missing, suggesting a mechanical failure of the bit release top connector at the end of the pipe. Logging was cancelled after attempts to clear the blockage with the drill string were unsuccessful. The drill string was recovered, both beacons were retrieved by 2335 hr on 17 February, and the vessel was slowly offset with the dynamic positioning system to Site 1199 (proposed Site CS-16A).

## Principal Scientific Results

The initial, early Miocene, transgression over acoustic basement at Site 1197 was characterized by an interval of skeletal floatstone rich in oysters deposited on a shallow platform in water depths <30 m. Overlying this interval are the first periplatform sediments deposited at this location. This thick middle Miocene sequence was deposited in water depths >200 m and is dominated by fine-grained skeletal material shed from the earliest growth phase of the adjacent platform. These sediments are overlain by two units of coarser neritic sediments reworked from the platform and also deposited at depths >200 m. A major hardground surface overlies these deposits and marks the cessation of sediment shedding from the SMP and the onset of hemipelagic drift sedimentation, which continues to the present day.

The 674.9-m-thick sedimentary succession and underlying basement drilled at Site 1197 were subdivided into six lithologic units. Sediments at Site 1197 consist of predominantly periplatform and hemipelagic deposits of wackestone to grainstone texture, formed in water depths >150 m with the exception of the lowermost sedimentary unit, which was deposited in depths of <100 m.

Sediments recovered in lithologic Unit I (0–59.6 mbsf; late Pleistocene to Holocene in age) consist of grainstone rich in planktonic foraminifers and sponge spicules, with minor bivalve fragments, echinoderms, rare scaphopods, and abundant pteropods. This unit coincides with seismic Megasequence D. The low proportion of neritic skeletal components and clay suggests that the drift deposits of lithologic Unit I were accumulated in a distal setting removed from platform input. Upper bathyal benthic foraminiferal taxa are common and diverse through lithologic Unit I. In addition, bioclastic debris from deep hard substrate communities are common in this interval. At ~55 mbsf there is a marked transition from predominantly pelagic components to neritic components. Mineralogical analyses show that aragonite is present in Unit I from ~0 to 43 mbsf with decreasing abundance downcore, reflecting aragonite production of pteropods. Once deposited, this aragonite underwent dissolution resulting in decreased downcore concentrations. Sediment bulk density within lithologic Unit I is nearly constant at ~1.7 g/cm$^3$, whereas porosity decreases from ~68% to 60%. MS shows

a peak near 9 mbsf and then decreases downcore. NGR shows cyclic variations on an increasing downcore trend.

Core recovery in lithologic Unit II (59.6–175.0 mbsf; late Miocene to early Pliocene? in age) was very low (0.6% in Hole 1197A and 1% in Hole 1197B). The recovered sediments are characterized by dolomitized skeletal grainstone rich in planktonic and larger benthic foraminifers and coralline algae fragments. Lithologic Unit II contains abundant neritic debris including well-preserved specimens of larger benthic foraminifers indicating a middle neritic origin. The prevalence of outer neritic and upper bathyal benthic foraminifers indicates that the neritic material was transported to a proximal periplatform setting at outer neritic to upper bathyal depths. The prolific shedding of platform sediments ceased in the late Miocene or earliest Pliocene as relative sea level rose and deepened the site, allowing hemipelagic sedimentation to prevail. This change in sedimentation is marked by a major hardground surface at the upper boundary of lithologic Unit II, corresponding to the seismic Megasequence C/D boundary. This surface consists of a prominent, reddened hardground with a thin phosphate crust. Evidence for endolithic boring, the presence of gastropod molds, and distinct color changes from red stained to yellow to white downcore indicate a gradual decline in lithification. Dolomite is present within lithologic Unit II and increases in abundance downcore, as indicated by X-ray diffraction (XRD) analysis. The abundance of the benthic foraminifer *Amphistegina* sp., along with fragments of coralline algae, is reminiscent of lithologic Subunits IA and IB from Sites 1196 and 1199 on the SMP. Planktonic foraminifers of late Miocene age in lithologic Unit II indicate that SMP growth and shedding may have ended in the late Miocene or early Pliocene. The base of lithologic Unit II is defined by a hiatus and correlates with the Megasequence B/C boundary and possibly with the boundary between the NMP and SMP growth phases at Sites 1196 and 1199.

Core recovery in lithologic Unit III (175.0–261.5 mbsf; late middle Miocene in age), as with Unit II, was low (~3%). The recovered sediments have dolomite contents similar to lithologic Unit II and are characterized as skeletal grainstone dominated by larger benthic foraminifers (*Lepidocyclina* sp.) with planktonic foraminifers and smaller benthic foraminifers as minor to abundant components. Glauconite is present and becomes common toward the base of this unit. The abundance of larger benthic foraminifers filled by glauconite within lithologic Unit III is a result of sediment reworking from the nearby platform. Unit III represents the upper part of a progradational seismic package within seismic Megasequence B. The base of lithologic Unit III is defined by an abrupt decrease in the presence of coarse neritic detritus. The bioclastic sediments of Unit III were deposited in a distal periplatform setting in outer neritic to upper bathyal water depths as indicated by benthic foraminiferal assemblages. These sediments are a mixture of fine neritic and planktonic debris, with occasional pulses of slightly coarser sediments that originated from middle to inner neritic depths.

Lithologic Unit IV (261.5–601.7 mbsf; early to middle Miocene in age) was deposited in a distal periplatform environment at water depths >200 m. The sediments within this unit are predominantly silt-sized skeletal packstone/grainstone. Coarse neritic detritus is absent. This unit was divided into two subunits on the basis of carbonate mineralogy, the degree of bioturbation, and differences in the presence or absence of cyclic intervals within the succession. Subunit IVA (261.5–367.4 mbsf) is characterized by partially dolomitized, skeletal grain-

stone with moderate to high bioturbation. Dolomite, mainly contained in cements, decreases downcore in this subunit. On seismic data, Subunit IVA forms the basal part of an inclined, prograding slope package that interfingers with deeper drift deposits within seismic Megasequence B. Subunit IVB (367.4–601.7 mbsf) consists of fine sand- to silt-sized skeletal packstone, grainstone, and wackestone with alternating light and dark intervals. Dark portions of these intervals have increased clay contents. Grain size and skeletal composition are generally similar within an interval. Most of the fine skeletal particles are fragmented neritic grains, such as coralline algae and benthic foraminifers. These alternating intervals probably result from high-frequency sea level changes. In addition to the color alternations discussed above, small-scale fining-upward intervals with well-preserved parallel lamination, characteristic of turbidites, were also observed. These calciturbidites are enriched in coarse skeletal detritus, such as larger benthic foraminifers. Low recovery in lithologic Subunit IVA precluded the measurement of physical properties in this interval, but measurements from Subunit IVB show decreasing porosity (39%–22%) and increasing bulk density (2.1–2.3 g/cm$^3$) downcore. In addition, the cyclic variability observed in the sediments is also seen in NGR and MS data.

The sediments of Unit V (601.7–656.1 mbsf; early Miocene in age) consist of coarse skeletal packstone to fine rudstone exceptionally rich in larger benthic foraminifers and coralline algae with common bryozoans and bivalve remains. Glauconite is abundant, both as pellets and infills of intraskeletal porosity. Quartz grains are present and become particularly abundant at the base of the unit. The top of Unit V is defined by the first occurrence of coarse periplatform sediments. Initial flooding of basement is recorded by an interval of skeletal floatstone rich in articulated oysters, implying limited reworking across a shallow platform in water depths <30 m. Small- to medium-scale graded bedding and the strong laminar fabric of many of the deposits suggest deposition from unidirectional gravity flows, probably slope-proximal turbidites related to periplatform shedding. The base of lithologic Unit V is defined by a sharp transition to volcaniclastic breccia and basalt.

Unit VI (656.1–666.7 mbsf; age unknown) is characterized by a matrix-supported volcaniclastic breccia with coarse (up to 12 cm) angular clasts of basalt derived from the underlying basement. This unit was divided into two subunits. Subunit VIA (656.1–666.6 mbsf) consists either of a pyroclastic/ignimbrite flow or reworked, previously deposited volcanic rocks. Native sulfur mineralization is observed. The dark breccia is overlain by grainstone rich in larger benthic foraminiferal tests that were originally produced in middle neritic water depths, possibly in an open shelf setting where they were rounded and mixed.

Subunit VIB (666.6–666.7 mbsf) consists of a highly altered dark olivine basalt with plagioclase phenocrysts, small plagioclase laths, and pyroxenes comprising the groundmass. This rock was recovered in the core catcher of the final core at Site 1197. It is unclear whether this basalt was recovered in situ or whether it is a large breccia clast. The age and origin of this olivine basalt is uncertain, but is interpreted to have originated during synrift tectonic activity. The basaltic surface was most likely exposed for a significant period of time and then covered by a veneer of volcaniclastic breccia (Subunit VIA) that accumulated from a series of landslides. This continental surface likely maintained significant topography as indicated by the nature of the clasts in the breccia. Unit VI represents the acoustic basement at Site 1197.

Shipboard analyses of calcareous nannofossils and planktonic foraminifers provided a good age-depth resolution within lithologic Unit I of latest Pliocene to Pleistocene age. Below 60 mbsf, poor core recovery and likely downhole contamination hindered detailed age assignments. A broad late Miocene to early Pliocene age can be assigned to lithologic Unit II. Unconformities are present both at the top (59.6 mbsf) and the bottom (175.0 mbsf) of Unit II, which corresponds to Megasequence C. An early to middle Miocene age can be assigned to lithologic Units III–V. The majority of samples from Hole 1197B are poorly preserved, have low microfossil abundance, and often contain no age-diagnostic fauna.

Paleomagnetic analyses performed on APC cores collected with a nonmagnetic drill bit provided a good magnetic record for Hole 1197A, whereas cores from Hole 1197B obtained with the RCB showed the usual downward magnetic overprint. In Hole 1197A, natural remanent magnetization (NRM) intensity generally varies between $10^{-3}$ and $10^{-2}$ A/m with an average intensity of $10^{-2.5}$ A/m. An NRM intensity increase at 11 mbsf was interpreted as a hiatus. The NRM intensity for Hole 1197B is low (~$10^{-4.5}$ A/m). Intervals of negative and positive inclination corresponding to the Brunhes and Matuyama Chrons are evident in Hole 1197A. All early Miocene polarity intervals are identified in Hole 1197B although it was difficult to locate where polarity transitions occur. The NRM, anhysteretic remanent magnetization (ARM), isothermal remanent magnetization (IRM), and IRM demagnetizations were measured on discrete samples collected from 4 to 50 mbsf in Hole 1197A. These data show that the predominant minerals are magnetite and pyrrhotite. R values of 0.4 to 0.5 have been obtained, indicating a possible hemipelagic environment. The concentration of magnetite decreases downcore, suggesting dissolution of fine-grained primary magnetite.

The low gas content at Site 1197 is likely a function of appreciable pore water $SO_4^{2-}$ concentrations to total depth, limiting methanogenesis, and the lack of mature organic matter that could provide a thermogenic component to the gas fraction.

Carbonate ($CaCO_3$) content at Site 1197 ranges from ~4 to ~100 wt%. $CaCO_3$ content covaries inversely with TOC content, which ranges from 0.0 to 0.54 wt%. Sulfur content in Site 1197 sediments ranges from 0.0 to 1.56 wt%, and its distribution is similar to that of TOC. Variations in the generally high carbonate content and the inversely covariant relation between carbonate and TOC content at Site 1197 reflect variations in carbonate mineralogy (i.e., calcite or dolomite) and the ratio of biogenic carbonate and terrigenous sedimentation through time.

In lithologic Subunit IVB, TOC and carbonate content display a relationship of decimeter-scale inverse covariations. The amplitude of these covariations increases downsection and corresponds to alternations of white to yellow skeletal grainstone and packstone, and olive-gray packstone. These alternations are also reflected in variations of NGR. The highest S value (~1.56 wt%) measured at Site 1197 was also obtained within this interval (at ~544 mbsf). HI values suggest that lithologic Subunit IVB contains either terrestrial or oxidized organic matter. The presence of highly oxidized organic matter within an interval characterized by high S content is unlikely; therefore, organic matter deposition may have been dominated by terrestrial input.

Pore water sampling at Site 1197 was restricted to the upper 50 mbsf and 410–530 mbsf because of poor core recovery between these intervals. In the upper 50 mbsf, the concentrations of most ions are similar

to seawater values, and little change in pore water chemistry is observed. Only calcium shows marked changes, increasing in concentration with depth to a value of 20 mM at 50 mbsf. In the lower sampled interval, the pore water profiles are more typical of those observed in near surface sediments. Sulfate, magnesium and potassium decrease, and ammonium and strontium increase in concentration. Calcium remains at ~20 mM. Although the data set is limited, the results suggest active seawater circulation through seismic Megasequence C.

## Site 1198

Site 1198 (proposed Site CS-05A) is located in 319 m water depth at the intersection of regional seismic lines MAR07 (shotpoint 2262) and MAR54 (shotpoint 900). This site lies ~10 km northeast of the modern south-central Great Barrier Reef and 13.5 km northwest of Site 1196 (Figs. **F1, F2**). Site 1198 is located adjacent to the current-swept margin of the Miocene SMP ~5 km from the Miocene platform escarpment.

The main goal of this site was to recover platform proximal sediments that record the growth phases of the adjacent SMP. Deposition of material shed from the SMP on the Marion Plateau is predominantly controlled by current flow in a similar fashion to the Nicaraguan Rise, as opposed to the generally wind-dominated system of the Great Bahama Bank. To investigate sediment and subsequent deposition resulting from current processes, Site 1197 was located off the southeast margin of the SMP, which, with Sites 1196/1199 and 1198, forms a transect from the leeward, depositional side to the top of the platform and to the current-dominated margin. A comparison of the two marginal sites shows that the lower energy site has significantly thicker sediment sequences.

In their offbank setting, the sediments at Site 1198 were expected to contain both platform and open marine sedimentary signals. In addition to the primary objective listed above, other objectives were to recover the proximal sequences adjacent to the SMP and to determine the age of both the initiation and demise of the SMP. Also, the Megasequence D sediment drift, which overlies the unconformity marking the end of the SMP growth phase, is expected to provide information on the Pliocene–Holocene paleoceanography of the Marion Plateau region. A further objective was to investigate the potential of fluid flow in a platform proximal setting.

### Operations

Operations at Site 1198 began at 1636 hr on 7 February 2001. Hole 1198A was APC cored to refusal at 203.0 mbsf, and average recovery for this interval was 102.2%. Cores were oriented starting with Core 194-1198A-3H. Four downhole temperature measurements with the APC temperature tool at 33.5, 62.0, 119.0, and 147.5 mbsf and three measurements with the DVTP at 176.0 and 203.0 mbsf were unsuccessful.

Subsequent coring with the XCB deepened the hole to 251.5 m. The first XCB core had 29% recovery, and the subsequent four cores had zero recovery. Based on a similar zero-recovery experience with XCB coring at Site 1197 in the same stratigraphic unit (seismic Megasequence C), the hole was abandoned in favor of a new hole to be cored with the RCB.

The vessel was offset 20 m east of Hole 1198A. After drilling with the RCB to 195.7 mbsf, coring resumed to a total depth of 522.6 mbsf (Ta-

ble T2). During the process, the drill string became stuck and was subsequently worked free. To reduce the potential for further hole problems, coring was interrupted twice for wiper trips and the annulus was frequently flushed with sepiolite. Average recovery for the intervals from 195.7 to 359.1 and from 359.1 to 522.6 mbsf was 6.1% and 65.2%, respectively. The average recovery for the entire hole was 35.7%.

Once coring was completed, the bit was released on bottom, the hole was flushed and displaced with sepiolite, and the pipe was pulled back to 91.8 mbsf for logging. The triple combo tool was unable to descend below 235.5 mbsf because of a collapse of the upper part of the borehole (corresponding to the interval poorly recovered in the cores). The tool became stuck and was subsequently freed. The hole was logged with one pass from 231 mbsf to the seafloor. Above 192 mbsf the hole was found to be significantly enlarged, adversely affecting log quality. It was decided not to make any additional logging runs because of the deteriorating hole conditions. The vessel departed at 0430 hr on 11 February, ending operations at Site 1198 to return to Site 1196.

## Principal Scientific Results

Site 1198 penetrated a 522.6-m-thick lower Miocene to upper Pleistocene sedimentary sequence that was nearly all deposited at water depths >200 m in a proximal periplatform to hemipelagic environment. At the bottom of the hole, a thin veneer of deep-euphotic foraminifer species and rhodolith floatstone (estimated paleowater depth of 100–150 m) was deposited under the influence of seafloor currents directly on top of the basaltic basement. This carbonate unit is capped by a thin hardground surface and overlain by 100 m of hemipelagic clay-rich carbonates (seismic Megasequence B). Above is a ~200-m-thick periplatform section that consists partly of talus that contains a record of variations in platform growth from the late middle Miocene until carbonate production was terminated in the late Miocene (~7.7 Ma). This unit may be hydrologically connected to the SMP edifice, because pore water chemistry indicates circulation of almost unaltered seawater within lithologic Unit II (seismic Megasequence C). After the termination of SMP platform growth, a submarine hardground formed on the slope. Subsequently, a 200-m-thick Pliocene–Pleistocene sediment drift (seismic Megasequence D) was deposited on top of the proximal periplatform sediments.

The lithostratigraphy at Site 1198 consists of five main units that are divided according to variations in sedimentary structures, texture, grain size, terrigenous content, and biotic assemblages. Lithologic Unit I (0–200.6 mbsf; upper Pliocene to Pleistocene) is characterized by a thick sequence of alternating mudstone and skeletal grainstone intervals with varying amounts of terrigenous constituents as indicated by cyclic changes in texture and carbonate content. The sediments of Unit I, coinciding with seismic Megasequence D, were deposited in a hemipelagic environment in water depths >200 m. Lithologic Unit I shows an unusual downhole trend of nearly constant velocity (1625 m/s), bulk density (1.75 g/cm$^3$), and porosity values (60%). The uniformly high porosity values throughout this interval indicate a lack of compaction that may result from elevated fluid pressures generated during deposition or induced by fluid migration. MS and NGR increase, on average, throughout lithologic Unit I. MS shows variations at the scale of 25–50 m that are superimposed on the average trend. The average MS and NGR trends

correlate with sediment lightness, which decreases downhole from ~70% to ~50%.

The lithologic Unit I/II boundary occurs at 200.6 mbsf at a 10-cm-thick brown phosphate nodule layer that is interpreted to be a reworked hardground surface. The middle to upper Miocene lithologic Unit II (200.6–397.6 mbsf) was divided into three subunits. The upper and lower of these subunits consist of fine-grained, neritic-rich skeletal packstone to grainstone deposited in a periplatform environment (Subunit IIA: 200.6–225 mbsf; Subunit IIC: 330.3–397.6 mbsf). Subunit IIB (225–330.3 mbsf) consists of coarse-grained skeletal grainstone to rudstone with abundant larger benthic foraminifers, rhodoliths, and hermatypic corals. Based on seismic interpretation, Subunits IIA, IIB, and part of IIC were deposited in a proximal slope environment or reef talus at the base of a nondepositional escarpment and correspond to seismic Megasequence C, which thickens toward the SMP, suggesting that the SMP is the source of the neritic carbonate sediment. Lithologic Unit II is separated from Unit III by a change from silt-sized packstone with minor identifiable neritic debris above and a unit of mudstone/wackestone deposits with no identifiable neritic detritus below 397.6 mbsf. Few velocity measurements were obtained between 200 and 400 mbsf (lithologic Unit II) because of poor recovery. Of the obtained data, the average velocity is 2225 m/s, with two high velocity measurements (4250 and 3750 m/s) corresponding to the hardground at ~200 mbsf (boundary of lithologic Units I and II), which is also characterized by high MS and NGR values.

The lower middle Miocene to early Miocene lithologic Unit III (397.6–503.6 mbsf) is characterized by meter-scale, gradational alternations of packstone and wackestone textures that coincide with color changes. Within lithologic Unit III, carbonate content increases overall from ~50 wt% at the top to ~95 wt% at the base. This unit was subdivided on the basis of small-scale fining-upward sequences at the base of wackestone intervals and an increased amplitude of variability in MS in Subunit IIIA.

At the top of lithologic Unit IV (503.6–513.2 mbsf), thin phosphatic laminae suggestive of a hardground surface are present. Below this hardground and just above basement, a skeletal floatstone to rudstone facies with thin red algal crusts and very large and flat benthic foraminifers indicate a paleowater depth of ~100–150 m.

Throughout lithologic Units III and IV, bulk density (2.1–2.4 g/cm$^3$) and velocity (2.0–2.8 km/s) increase with depth and porosity (40%–25%) decreases. Below 400 mbsf, MS gradually decreases, which is mirrored by a gradual lightness increase (45%–55%). NGR is highly variable throughout this interval.

At the base of Site 1198, 3.9 m of olivine basalt represents acoustic basement (Unit V; 513.2–518.1 mbsf), which is characterized by a darkish green matrix consisting of smectite, magnetite, hematite, and feldspars (plagioclase) and abundant mineral-filled fractures. Abrupt increases in MS, NGR, and velocity and a decrease in porosity characterize the basement lithology. A strong increase in NRM marks the transition from sediment to basement with average intensities of 0.5 A/m, a value 10 times less than the average intensities of both subaerial and submarine basalt.

Shipboard paleontological analyses show that lithologic Unit I is composed of planktonic microfossils with a minor component of reworked material. Upper bathyal benthic foraminifers are common throughout this unit. Calcareous nannofossils and planktonic foramin-

ifers indicate a hiatus of ~4 m.y. (~3.8–7.7 Ma) at the lithologic Unit I/II boundary. Subunit IIB contains abundant and well-preserved *Lepidocyclina* spp. that, based on seismic geometries, were (at least in part) shed from the SMP. Planktonic foraminifers and nannofossils indicate a middle to late Miocene age (~12–8 Ma) for that interval. Near the bottom of the cored sediment sequence, below the phosphatic hardground that marks the top of lithologic Unit IV (489.9 mbsf), nannofossil assemblages indicate an age of 18.2–18.5 Ma. Despite the expanded Pliocene–Pleistocene drift deposit of lithologic Unit I, the magnetic stratigraphy does not show the expected pattern of polarity reversals in part due to measurement difficulties. However, a tentative magnetostratigraphy was developed for the Brunhes and Matuyama Chrons. Below 205 mbsf, poor recovery and residual viscous remanent magnetization hindered interpretations. Rock magnetic analyses performed on representative discrete samples indicate that the dominant magnetic phase is magnetite, with some minor, indeterminate, high coercive magnetic mineral, possibly pyrrhotite. The low gas content (1.7 to 6.6 ppmv) at Site 1198, is likely a function of appreciable pore water $SO_4^{2-}$ concentrations limiting methanogenesis to total depth and the lack of mature organic matter that could provide a thermogenic component to the gas fraction.

Carbonate ($CaCO_3$) content at Site 1198 ranges from ~47 to 99 wt% and mostly covaries inversely with the TOC content, which ranges from 0.0 to 0.38 wt%. Sulfur content in Site 1198 sediment ranges from 0.0 to ~0.78 wt% and its distribution is similar to that of TOC. Lithologic Subunits IB, IC, and IIIA are notable for broad ranges in inversely covarying $CaCO_3$ and TOC values.

The pore water profiles for dissolved constituents at Site 1198 show distinctive patterns. In the hemipelagic sediments of lithologic Unit I, pore water profiles display typical deviations from seawater concentrations in the upper ~100 mbsf (e.g., bacterial sulfate reduction begins with a concomitant rise in ammonium concentration, and strontium concentration rises due to carbonate recrystallization). In the lower half of lithologic Unit I, however, these trends reverse. Sulfate concentration returns to a seawater value of 29 mM, whereas ammonium and strontium concentrations decrease to near-seawater concentrations. No pore fluids were recovered from lithologic Unit II. Pore waters from the top of lithologic Unit III at 350 mbsf have a chemistry remarkably close to seawater. Through lithologic Unit III, sulfate again decreases, strontium concentration rises, and calcium rises to very high values of ~140 mM. The pore water chemistry immediately above and below lithologic Unit II suggests active circulation of seawater through the unconsolidated sediments of Unit II. The mechanism causing this flow and the flow properties in the third dimension are not known, but an active hydraulic connection to the adjacent carbonate platform is hypothesized.

Downhole logging operations in Hole 1198B were limited to the interval from 231 mbsf to the seafloor. The natural gamma ray data are the most useful logs at Site 1198 because they are corrected for variations in the large borehole size. In the 135-m open-hole interval measured, two major changes in log response can be distinguished. Within logging Unit 1 (74–199 mbsf) natural gamma ray values are low at (~20 American Petroleum Institute gamma ray units [gAPI]) and show small-scale variability in the upper interval (74–110.5 mbsf). This interval can be roughly correlated with a carbonate-rich packstone to grainstone described in the recovered cores. The interval between 110.5 and 199 mbsf shows an increase in the natural gamma ray log to 30 gAPI with

small-scale variations superimposed on a nearly linear downhole trend. From the top of the hole until ~200 mbsf, the sediments record a gradual downhole increase in clay content that is observed in the logs by a change to higher potassium and thorium values below 110.5 mbsf. At 199 mbsf, a peak in natural gamma ray marks the hardground between the skeletal packstone with clay of lithologic Unit I, and the coarse-grained rudstone and floatstone of Unit II. The natural gamma ray log decreases sharply below 199 mbsf and stays low in logging Unit 2 (199–210 mbsf).

# LEG SYNTHESIS

## Seismic Stratigraphic Results of Leg 194

Drilling at all Leg 194 primary sites and two alternate sites penetrated and sampled a Neogene sedimentary record that can be used to calibrate the sequence stratigraphic architecture of the Marion Plateau megasequences. The recovered sediments calibrate the regional seismic stratigraphy by identifying the lithologic signature and providing a chronostratigraphic framework and thus constraining the carbonate platform history and the magnitude and timing of sea level changes on the Marion Plateau.

### Time-Depth Correlation

In order to correlate core and log information accurately with the seismic data, a time-depth curve was constructed for each site (Fig. **F11**). These curves were obtained by integrating velocity data from sonic logs and shipboard velocity measurements and by calibrating these curves with results from check-shot surveys when they were available (Sites 1194, 1195, and 1196). For the remaining sites, tie points were defined that link prominent high-amplitude reflections to unique horizons in the cores. These horizons are usually hardgrounds or exposure surfaces at megasequence boundaries. Near the bottom of the drill holes, the basement reflection was used as a tie point to fix the critical lower part of the time-depth curve. Variations in the slopes of the time-depth curve reflect the high sonic velocities in the platform sediments (Sites 1193, 1196, and 1199), the medium velocities in the proximal slope sections (Sites 1194, 1197, and 1198) and the lowest velocities in the most distal locations (Sites 1192 and 1195) (Fig. **F11**). Time-depth curves, combined with the age model curves (Fig. **F12**), were used to assign chronostratigraphic datums to the seismic sequence boundaries at each site, which then can be compared across the transect (Fig. **F13**). The age models are mostly based on core catcher analyses and therefore have limited depth resolution. An overall good match between the ages of the sequence boundaries at the different sites, within limits of seismic and shipboard biostratigraphic resolution, confirms the concept of seismic stratigraphic correlations, in which seismic reflections have a chronostratigraphic significance. Age differences at boundaries between sites may be reduced once a more refined chronostratigraphy is established postcruise. The following sections discuss the major findings for each of the megasequences. The ages and depths of seismic megasequence boundaries, as well as lithologic unit boundaries at each site are plotted in Figure **F13.**

**F11.** Correlation between seismic two-way traveltime and depth, p. 73.

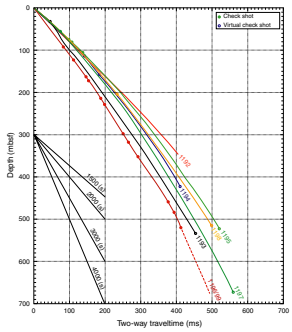


**F12.** Sedimentation rates at Leg 194 sites, p. 74.

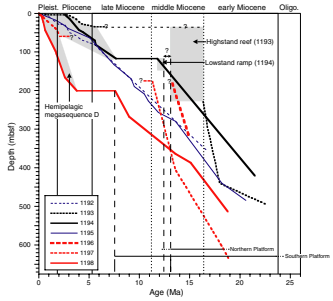


**F13.** Seismic correlation between Leg 194 sites, p. 75.

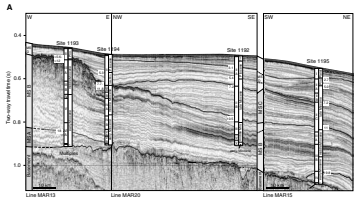

## Megasequence D

At all Leg 194 sites, Megasequence D, the youngest of the Marion Plateau megasequences, is composed of hemipelagic drift deposits. Megasequence D is only missing at the top of the southern platform edifice (Sites 1196 and 1999) where Megasequence C outcrops at the seafloor. The base of Megasequence D is a regional unconformity that is observed at all proximal platform sites (1193, 1197, and 1198) characterized by a hiatus lined with submarine hardgrounds, which provides an excellent link between seismic unconformities, biostratigraphic hiatuses, and nondepositional processes on the seafloor. At these sites, the age of the onset of Megasequence D sedimentation is dependent on the sites' locations relative to the depocenters of drift deposition. These ages are always younger than the ages of the base of Megasequence D in the distal areas where the sequence boundary is conformable. Sites 1192, 1194, and 1195 were drilled into the conformable succession at the base of Megasequence D, recovering the oldest sediments within this megasequence. At these sites, the base of Megasequence D was dated at 7.2 (Site 1192), 7.7 (Site 1194), and 7.2 Ma (Site 1195), respectively (Fig. **F13A**). Sites 1192 and 1195 are located in the most distal locations and have a well-constrained age model curve, so a basal age of ~7.2 Ma for Megasequence D is likely. Two smaller-scale seismic unconformities that represent current-controlled drift unconformities reflecting lateral shifts of depocenters and local hiatuses can be traced throughout the seismic grid. Their age range along the transect is 2.8–3.1 and 5.0–5.4 Ma, respectively (Fig. **F13**).

The C/D boundary at either side of the SMP coincides with the end of platform-derived shedding of neritic constituents onto the slopes (Fig. **F13B**). The age of ~7.2 Ma is thus assumed to reflect the end of the youngest phase of carbonate platform growth in this area and may date the drowning of the southern platform at least 1 m.y. earlier than originally predicted (Pigram, 1993).

## Megasequence C

Megasequence C is best developed near the southern carbonate edifice, where it records the platform-derived sedimentation of the youngest growth phase (Fig. **F13B**). Platform proximal sediments were drilled at Sites 1197 and 1198, and despite very low recovery, their age and platform-derived constituents indicate the existence of a late Miocene carbonate platform. Megasequence C at Site 1197 is characterized by relatively fine to medium grainstones (Unit II). At Site 1198, Megasequence C was deposited at the base of an escarpment and consists of coarse rudstone and floatstone (Subunits IIA and IIB) in the lower part of the section. Further from the platform, these proximal periplatform sediments interfinger with time-equivalent hemipelagic drift deposits. Based on the downlap of these Megasequence C drift deposits northwest of Site 1198 onto slope deposits of underlying Megasequence B, the southern platform edifice was thought to be entirely of late Miocene age. Drilling on the platform itself (Sites 1196 and 1199) revealed, however, that only the uppermost 100–180 m potentially consist of a late Miocene phase (lithologic Subunits IA–IC). Biostratigraphic dating below this depth gave a middle Miocene age. A low-amplitude, low-frequency reflection underneath the SMP top is a candidate for the boundary between these two carbonate platform-growth phases (Fig. **F13B**). This interval between the seafloor and ~110–130 mbsf dips gently to

the southeast and coincides approximately with Megasequence C sediments on the downcurrent slope at Site 1197. The age models for the B/C boundary indicate ages of 10.5 (Site 1192), 11.0 (Site 1195), 11.5 (Site 1198), <11.8 Ma (Site 1194) and <11.3 (Site 1197). Giving more weight to the open-plateau section with the best seismic coherency and age control, an age of ~11.0 Ma can be postulated for the B/C boundary. This boundary correlates with the karstic top of the northern platform, placing an upper age limit on middle Miocene platform growth of NMP.

## Megasequence B

Within the NMP, at Site 1193, Megasequence B consists, at the base, of inclined slope deposits that can be seen on seismic data as inclined reflections underneath the platform (Fig. **F13A**). At Sites 1193 and 1194, these early Miocene slope deposits were composed mostly of fine silt-sized carbonate debris, which became mixed with a pelagic fraction in a periplatform environment (lithologic Units IV and V at both sites). The top of these periplatform sediments immediately underneath the platform section at Site 1193 could be confined to ~16 Ma. No age-diagnostic markers were found in the platform section above. Considering that the top of Megasequence B (platform top) was dated through seismic correlation along the B/C boundary to ~11.0 Ma, the northern platform growth may span ~5 m.y. in the middle Miocene. The top of this platform at Site 1193 shows signs of meteoric diagenesis. Topographically below the northern platform, Site 1194 penetrated an upper-slope section in a margin proximal position adjacent to NMP. The top of Megasequence B at Site 1194 is represented by a hardground surface, which caps an interval interpreted as a neritic outer ramp deposited in 30–50 m paleowater depth (lithologic Subunit IIIA). The base of this interval, marked by another hardground surface, can be clearly mapped on the seismic data. The interval overlies neritic upper-slope and hemipelagic sediments, indicating a shallowing-upward trend and thus a sea level lowering in the latest middle Miocene.

Megasequence B on the open plateau is mostly composed of a mixture of distal periplatform and pelagic components. In the most distal Site 1195, the top of Megasequence B coincides with a 20- to 30-m-thick interval rich in glauconite overlying distal periplatform sediments. The absence of neritic components indicates a reduction of neritic carbonate production at the end of the middle Miocene.

At Site 1198, situated adjacent to the escarpment in a proximal position to the southern platform, the top 70 m of Megasequence B (lithologic Subunit IIC) thickens toward the platform escarpment, documenting shedding of neritic material at the end of the middle Miocene. These periplatform sediments overlie hemipelagic deposits (lithologic Unit III). At Sites 1196 and 1199 on the platform, the >500-m-thick platform sequence below the presumed B/C boundary cannot be further subdivided because of the transparent seismic facies. It is likely that after its initiation onto a substrate of latest Oligocene age, this southern platform complex was a product of several growth phases in the early and middle Miocene. Interestingly, at both sites on the slope (Site 1197 and 1198), no early Miocene platform shedding is indicated, neither by debris in the periplatform sediments, nor geometrically by a thickening toward the platform. This observation might be related to the strong influence of currents from north to south that shape the geometry of the platform. The paleo platform shape can be estimated by tracking the weak reflection assumed to be the top of Megasequence B (equivalent to

the top of the NMP) at a subsurface depth of ~100–130 mbsf. This reflection can be partly traced on the seismic data and displays a topography with a rim at the northwest, upcurrent escarpment and a gentle dip toward the southeastern, downcurrent slope at Site 1197. At Site 1197 the B/C boundary caps the coarsest interval at that site (lithologic Unit III) and forms a thick prograding slope unit that forms a downcore transition from steeper-dipping slope to almost flat hemipelagic deposits (lithologic Units III–V).

### Megasequence A and Basement

In the northern survey area, Megasequence A consists of a siliciclastic substrate that directly overlies acoustic basement. Megasequence A has a highly variable thickness, infilling small-scale basement irregularities. Only Sites 1193 and 1195 were characterized as having siliciclastic sediments directly overlaying basement. Thus, Megasequence A is not easily traced seismically and lithologically through all Leg 194 sites. At Sites 1195 and 1198, basement was overlain by a thin veneer of coarse carbonate deposits of undefined age. These sediments at Site 1198 can be seen on the seismic data as a thin onlapping unit directly overlying the basement reflection. Acoustic basement itself is highly variable, as shown by its different seismic signature across the study area. At Leg 194 sites, it consists of altered basalt flows and volcaniclastic breccias/conglomerates.

## Sea Level Magnitude Recorded by Sediment Sequences on the Marion Plateau

A primary objective of Leg 194 was to establish the magnitude of the major late middle Miocene sea level fall based on the expected stratigraphic relationships between the northern and the southern platforms. The SMP was thought to be nucleated on the distal slope sediments of the NMP during the maximum sea level lowstand. However, drilling results at Sites 1196 and 1199 showed that the southern platform is composed of ~120–160 m of late Miocene platform sediments overlaying a middle to early Miocene platform. This stratigraphic architecture makes estimates of sea level variations difficult using the original proposed methodology. Nevertheless, sequence stratigraphic and facies relationships from Sites 1193 and 1194 allow an estimate of the magnitude of the sea level fall to be made. The top of the platform at Site 1193 (35 mbsf) was deposited during the middle Miocene (~12–16 Ma) at an estimated paleowater depth of 10–50 m (Table **T3**) and represents the middle Miocene highstand. Lithologic Subunit IIIA at Site 1194 (117–154 mbsf), deposited during the latest middle Miocene (~12–14 Ma), represents an in situ shallow-water (30–50 m) interruption of a generally deeper water sedimentation. The base of Subunit IIIA today lies 145 m below the top of the northern platform at Site 1193, and seismic correlation between the two sites suggests that Subunit IIIA was deposited after the platform top was exposed (top panel of Fig. **F14A**). Consequently, these sequences provide a means to estimate the amount of sea level drop needed to move the shallow-water depositional environment from the top of the platform at Site 1193 to the base of Subunit IIIA at Site 1194. Sediment and water loading that have occurred since the end of the middle Miocene compacted earlier deposited sediments, and perhaps resulted in differential isostatic adjustments between the two sites, and thus affected the sequence geometry. These ef-

**T3.** Parameters used for paleotopographic reconstructions and sea level estimates, p. 88.

**F14.** Diagrams illustrating calculations of late middle Miocene eustatic fall using Sites 1193 and 1194, p. 77.

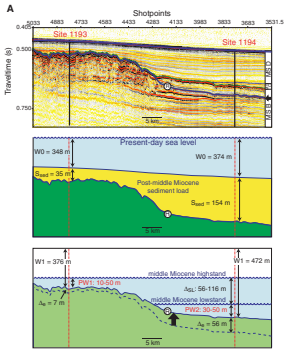

fects need to be removed in order to estimate the magnitude of the sea level drop.

First, the sediment rebound is considered relative to a basement with infinite flexural strength (Fig. F14A). As sediment is removed, the thickness of the underlying sediments must be adjusted to reflect the progressive decompaction of the sediment. The measure of compaction is sediment porosity, which was measured at both sites. Porosity ($\phi$) can be related to depth ($z$) using an exponential function and a porosity decay parameter with depth ($k$) (Athy, 1930) such that

$$\phi(z) = \phi_0^{-kz}. \quad (1)$$

A least-squares fit of this function to Site 1194 porosity data yields $\phi_0$ = 65% and $k$ = 0.002/m (correlation coefficient = 0.91). This normal compaction trend suggests hydrostatic fluid pressures were maintained during the deposition and compaction process and that the equation above can be used to simulate the compaction (and decompaction) of the sediment column. Removing lithologic Units I, II, and IIIA (a total thickness of 154 m) induces an expansion of $\Delta_e$ = 56 m. Porosity at Site 1193 shows a general decrease with depth, except within the platform sediments, where values are scattered, ranging from 10% to 45%, reflecting the various degrees of cementation in the carbonate rocks. Ignoring the porosity interval spanned by the cemented platform, the equivalent least-squares fit for Site 1193 porosity data yields $\phi_0$ = 61.2% and $k$ = 0.001/m (correlation coefficient = 0.60). Removing lithologic Units I and II (a total thickness of 35 m), expansion of the sediment packages below the cemented carbonate platform amounts to $\Delta_e$ = 7 m. Assuming infinite flexural strength of the lithosphere, the present-day geometry between Sites 1193 and 1194 is maintained except for the decompaction of underlying sediments. The reconstructed water depths W1 at Sites 1193 and 1194 without overlying sediment and $\Delta_e$ are 376 and 472 m, respectively. The corrected geometric relief between the platform and Site 1194 is thus 96 m. Given the paleowater depth estimates at Sites 1193 and 1194 of 10–50 m and 30–50 m, respectively, the corresponding range in the estimated eustatic fall is 56–116 m.

Second, local isostasy in response to sediment and water loading may have further affected the difference in elevation between the top of the platform at Site 1193 and the base of Subunit IIIA at Site 1194 (Fig. F14B). Isostatic correction is based on the density difference between the added water and sediment layers and an equivalent thickness of mantle at an assumed density of 3.3 g/cm$^3$. The special case of complete local isostasy (zero flexural strength in basement) is calculated in a three-step procedure (Fig. F14B).

The present-day water depth in the absence of sediment can be calculated using

$$\Delta_{water} = S_{sed}(\rho_m - \rho_s)/(\rho_m - \rho_w), \quad (2)$$

where $\Delta_{water}$ is the added water column thickness after the removal of the overburden sediment, $S_{sed}$ is the thickness of the post-middle Miocene sediment load on top of the NMP at Site 1193 (35 m) or on top of the base of Subunit IIIA at Site 1194 (154 m), and, $\rho_m$, $\rho_w$, and $\rho_s$ are the mantle, water, and average sediment densities, respectively (Table T3). Present-day water depths, W0, at Sites 1193 and 1194 are 348 and 374 m, respectively. Applying the above equation the calculated $\Delta_{water}$ for

Sites 1193 and 1194 are 25 m and 106 m, respectively, giving a reconstructed present-day water depth in the absence of sediment, W2, of 373 and 480 m. From these reconstructed water depths the previously calculated correction $\Delta_e$ is subtracted for the expansion of the underlying sediments. The corrected water depths W3 for the late middle Miocene stratigraphic reference levels at Sites 1193 and 1194, therefore, are 367 and 424 m, respectively (top panel of Fig. **F14B**).

Next, the water depth at the time of the middle Miocene highstand needs to be calculated. As the water column is reduced, basement and overlying sediments are unloaded and so will flexurally rebound. The following equation determines the sea level change ($\Delta_{SL}$) responsible for producing a given paleowater depth (*PW*) including the isostatic adjustment of basement associated with the sea level change:

$$\Delta_{SL} = (W3 - PW)(\rho_m - \rho_w)/\rho_m. \quad (3)$$

Considering the estimated 10–50 m paleowater depth at Site 1193 during the middle Miocene highstand, sea level must be decreased by 219–246 (233 ± 14) m (the middle panel of Fig. **F14B**). The water depth at Site 1194 at the time of the maximum highstand, W4, is given by the reconstructed water depth W3 of 424 m minus the $\Delta_{SL1}$ change of 219–246 m minus the isostatic adjustment (rebound) induced by the change in sea level, which is

$$\Delta_{m2} = \Delta_{SL1}\rho_w/(\rho_m - \rho_w) \quad (4)$$

Evaluating gives a rebound range of 98–110 m. The corresponding highstand water depth, W4, at Site 1194 is thus 67–107 m.

Finally, the middle Miocene sea level fall can be calculated. At the time of the maximum lowstand, the paleowater depth at Site 1194, PW2, is estimated from paleontological assemblages to be 30–50 m. Using PW2 and the reconstructed water depth at Site 1194, W4, and adjusting for the isostatic rebound induced by the lowering of sea level, the required sea level fall is 12–53 m (32 ± 20 m; equation 3) (the lower panel of Fig. **F14B**).

In summary, an extremely conservative estimate of the late middle Miocene eustatic fall based on Leg 194 drilling, considering both the effects of sediment compaction and the possible range in flexural behavior of the lithosphere, is 12–116 m (64 ± 52 m). The assumption of local isostasy minimizes the estimated eustatic fall. The relatively small distance (~20 km) between Sites 1193 and 1194, the undisturbed and consistently dipping sediments, as well as the horizontal basement geometry between the sites as seen on seismic data (Figs. **F7, F14A**), suggest that no significant differential subsidence occurred between the sites. Therefore, given the much more reasonable scenario of finite flexural strength of the lithosphere, our best estimate of the eustatic fall is 86 ± 30 m. Platform erosion at Site 1193 and overall tectonic subsidence during the sea level lowering were not considered. Both effects are much smaller than the error margin of the above calculations and would increase the sea level fall. It is also possible that a record of the lowest sea level was not preserved, cored, or observed in Subunit IIIA at Site 1194, which would also increase the magnitude of the eustatic fall.

## Platform Evolution

Two transects were drilled across the Miocene carbonate platforms of the Marion Plateau during ODP Leg 194. The northern transect includes the platform (Site 1193), proximal slope (Site 1194), and distal slope (Site 1195) sites composed of a mixed carbonate-siliciclastic depositional system adjacent to the Australian continent. The NMP drilled at Site 1193 represents the second phase of carbonate production that occurred during the Miocene on the Marion Plateau (Pigram et al., 1992; Pigram, 1993). The southern transect includes the platform (Sites 1196 and 1199), the leeward upcurrent slope (Site 1198), and the windward downcurrent slope (Site 1197) sites of an isolated carbonate bank ~65 km to the southeast of the NMP (Fig. F2). The SMP was labeled MP3 by previous investigators (Pigram et al., 1992; Pigram, 1993) because it was thought to be entirely composed of the third phase of carbonate platform sedimentation occurring on the Marion Plateau in the late Miocene. A primary discovery made during ODP Leg 194 is that this southern platform is a compound edifice that has undergone three main phases of carbonate accumulation.

The following sections reconstruct the evolution of these two platforms on the basis of lithologies recovered during ODP Leg 194 (Figs. F9, F15).

### Northern Transect (Sites 1192–1195)

Sedimentation on the Marion Plateau basement initiated on a topographically irregular surface consisting of volcanic and volcaniclastic rocks (Fig. F15A). The oldest sediments at Site 1195 include inner platform carbonates of possible Eocene age that could be transported clasts (not represented in Fig. F15A). During the early Miocene (23.8–16.4 Ma) siliciclastic estuarine sediments containing large oyster shells and larger benthic foraminifers accumulated at Site 1193. A subsequent sea level rise resulted in the deposition of a thick succession of mixed carbonate/siliciclastic material bearing glauconite and phosphate, which was also recovered at Site 1195. Between these two locations, a basement high at Site 1194 apparently formed an island in this time interval. Around 18 Ma (late early Miocene), silt-sized skeletal packstone/grainstone with quartz and terrigenous clays were deposited throughout the northern transect. They likely represent the mid- to distal slope sediments of a platform that was located to the north or north-northwest of the study area. This sedimentary package formed a gentle, eastward-facing ramp. Shallow-water facies, including skeletal rudstone/floatstone with bryozoans and larger benthic foraminifers first appeared in the northern transect in the early middle Miocene (~16 Ma) (Fig. F15B). Silt-sized skeletal wackestone/grainstone with clay and planktonic foraminifers accumulated downslope from these facies at Sites 1192, 1194, and 1195. During the middle Miocene (16.4–11.2 Ma), a carbonate platform consisting of shallow-water grainstone/floatstone with bryozoan fragments and larger benthic foraminifers grew on the previous ramp morphology (Site 1193; Subunit IIIA; Fig. F15B). Sediment shedding was directed eastward, as shown by seismic data and the presence of upper-slope skeletal packstones at Site 1194 (Subunit IIIB). Distal slope sediments were retrieved from Site 1195. However, these sediments may not originate from the NMP because the corresponding lithologic horizon at Site 1192 (Subunit III) consists of hemipelagic packstones with glauconite, clay, and no neritic components. During

F15. Schematic diagrams reconstructing the depositional history of the Marion Plateau sequences, p. 79.

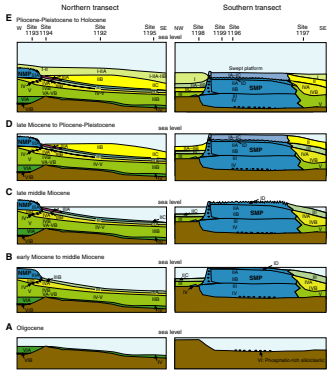

this time interval, the NMP had a flat-top morphology with a steep upper-slope between Site 1193 and 1194 (Fig. F15B).

An important sea level fall, possibly related to a major ice-building phase in Antarctica, occurred in the late middle Miocene. The Marion Plateau carbonate platforms were exposed and karstified (Fig. F15C). A 30-m-thick succession of skeletal packstone/floatstone dominated by bryozoans (Subunit IIIA; Site 1194) was deposited seaward of NMP between ~13 and ~11 Ma (Fig. F15C), likely corresponding to a lowstand carbonate ramp. Paleowater depth estimates of these sediments were used to calculate the amplitude of this major sea level change (see "Sea Level Magnitude Recorded by Sediment Sequences on the Marion Plateau," p. 47).

During the ensuing late Miocene sea level rise, the NMP was flooded (Fig. F15D), but platform growth did not reinitiate, as was observed on the SMP. A significant ferromanganese hardground was formed during this sea level rise on the top of the previously deposited lowstand platform sediments at Site 1194. From the late Miocene to the Pleistocene, a hemipelagic sediment drift consisting of greenish gray planktonic foraminiferal mudstone/wackestone with clay onlapped the middle Miocene slope lowstand platform and drowned the NMP (Fig. F15E).

## Southern Transect (Sites 1196–1199)

In this area, the irregular basement topography likely includes numerous basalt lava flows that formed an escarpment in the vicinity of Site 1198. The earliest deposits encountered are phosphate sands mixed with siliciclastic material of latest Oligocene age (24.6–24.2 Ma) recovered from Site 1196 (Fig. F15A). It is not clear whether these sediments were produced in situ, transported laterally, or reworked from older rocks. The presence of oysters in these beds indicates a water depth <30 m. During the early Miocene (23.8–16.4 Ma) a carbonate platform developed in a topographic low at Site 1196 (Fig. F15B) (SMP; Units IV and III), building a thick series of aggrading rhodalgal carbonates. Contrary to earlier hypotheses (Pigram et al., 1992; Pigram, 1993), this platform did not nucleate on the slope sediments from the NMP, but clearly predates them and thus likely corresponds to the earliest phase of carbonate production seismically imaged along the eastern margin of the Marion Plateau (Pigram, 1993). Facies homogeneity suggests that accommodation space remained more or less constant during this time interval. Numerous exposure surfaces within Subunit IIIC at Site 1196 (variegated dolostone) indicate that water depth was less than the amplitude of the early Miocene sea level fluctuations. Off-platform shedding was restricted, but included a thin package of coarse skeletal grainstone with benthic foraminifers at Site 1197 and stable deep-euphotic accumulations of rhodalgal-foraminiferal floatstone at Site 1198. The oldest phase of platform growth ceased near the early/middle Miocene boundary, corresponding to the first occurrence of shallow-water carbonate production on the northern transect.

The next phase of carbonate production initiated in the early middle Miocene (~16.4 Ma) (Site 1196; Unit II) (Fig. F15B). Red algal-dominated carbonate buildups formed during the renewed transgression, exporting detritus to the slopes of both Sites 1197 and 1198. The occurrence of reefs and possibly shoals or islands on the platform top is inferred from the variable depth in the sedimentary section at which these facies were recovered at Sites 1196 and 1199 (Figs. F9B, F15B). Shedding of silt-sized skeletal carbonate slope deposits was asymmetric,

with greater accumulation at Site 1197, probably related to the prevailing current directions. In the middle Miocene (~15.2–13.3 Ma), shallow-water carbonates accumulated in a ~150-m thick succession of fine grainstone rich in coralline algae, miliolid foraminifers, and seagrass remains. This facies filled the previously created irregular topography on the platform top in a shallow-water setting implying rapid and still unexplained creation of accommodating space. Vertically accreting reef-style growth was locally maintained, particularly on the northeast edge of the platform, where a buildup apparently existed as indicated by multichannel seismic data. At this stage, the platform was asymmetric with a flat-topped, rimmed western margin and an eastern margin showing a distally steepened ramp geometry (Figs. **F13B, F15B**). Platform shedding predominantly occurred in a downcurrent, downramp direction toward Site 1197 at the southeast of the section. Sediment shedding may also have taken place on the northwestern slope. The final pulse of the middle Miocene growth phase in this area was characterized by an increase in accommodation space expressed by the facies change from shallow (<20 m) seagrass-rich beds to rhodalgal floatstone (Subunit ID; Sites 1196 and 1199) (Fig. **F15B**) that suggest 60- to 100-m water depths. Reef growth speculatively continued on the northwestern side of the platform, where it acted as a marginal barrier system. Sediment shedding at this time was almost exclusively toward Site 1197 in the southeast.

Lithologic data from Site 1199 suggest that sea level retreat at the onset of the late Miocene was rapid because no evidence of shallowing could be observed in the depositional environment (60–100 m) of the rhodalgal floatstone forming Subunit ID, which occurs directly below an exposure horizon (Fig. **F15C**). Sediments produced during this regression may have also eroded and been exported downslope.

During the late Miocene (11.2–5.3 Ma), the platform was again flooded and carbonate production resumed in this area (Fig. **F15D**). The northwestern edge of the edifice was again occupied by a potential reef buildup. Sediments shed toward the west were possibly swept away by the strong currents flowing parallel to the platform flanks. In the platform center, this sedimentary pulse began with a phase of reef construction (Subunit IC) followed by a shallowing-upward succession consisting of rhodalgal floatstone (Subunits IB and IA; Fig. **F15D**). The latter accumulated in water depths that did not exceed 100 m. The uppermost sediments of Subunit IA include intertidal (beachrock) cements indicating extremely reduced accommodation space near the end of this depositional episode. Sediments were predominantly exported toward the southeast. The geometry of the southeastern margin evolved from a distally steepened to a more homoclinal ramp. The platform was exposed again during the latest Miocene as shown by the occurrence of a karst surface recovered at Site 1196 and the development of a pedogenic profile at Site 1199.

The southern platform was drowned during the latest Miocene or early Pliocene and thereafter was swept by bottom currents that contributed to the formation of a well-developed hardground surface with a laminated ferromanganese crust (Fig. **F15E;** also, see the volume **cover photograph**). The adjacent slope areas of Sites 1197 and 1198 were the locus of extensive hemipelagic drift deposition dominated by pelagic foraminifer remains, which filled the topographic lows adjacent to the platform leading to the modern bathymetrically nearly uniform seafloor (Fig. **F15E**).

## Discussion

Lithologic and biostratigraphic data obtained during Leg 194 from the Neogene carbonate platforms of the Marion Plateau reveal that platform architecture was controlled by a series of complexly related factors including sea level change, bottom-current action, and biological assemblages.

### *Northern Marion Platform*

The NMP platform initiated in the late early Miocene on low-angle, southward-dipping clinoforms. What is most striking in the evolution of this platform is the rapid onset of carbonate growth in a distal periplatform setting (Fig. **F15B**). The initiation of neritic sedimentation over midslope deposits suggests a major sea level fall at that time. The nearly flat surface at the base of the platform further shows that the onset of carbonate production was nearly simultaneous along the area seismically imaged near Site 1193. During the subsequent growth, the platform was predominantly aggradational producing a steep-sided margin (Fig. **F15B**). Carbonate production ceased when sea level dropped, exposing the platform at the end of the middle Miocene. This sea level drop shifted neritic sediment production onto the former slope, producing a lowstand carbonate ramp (Fig. **F15C**). The high-relief margin and insufficient water depth inhibited the establishment and growth of a "healthy" platform. Consequently, the subsequent sea level rise was able to outpace neritic sediment production and a hardground developed on this lowstand edifice. Why the younger carbonate production phases observed on the southern platform did not initiate on the NMP is still unclear.

### *Southern Marion Platform*

This compound carbonate edifice was initiated during the earliest Miocene and became inactive during the latest Miocene or early Pliocene. It apparently nucleated in a topographic low, questioning the paradigm that carbonate-platform nucleation requires positive antecedent topography. During its growth, this platform developed an asymmetrical architecture with an escarpment-like margin on the northwestern side and impressive high-angle prograding clinoforms on the southeastern margin. Little sediment was transported off the escarpment to the northwestern slope despite significant platform aggradation during the early and middle Miocene (Fig. **F15B**).

### *Biological Factors*

The steep-sided geometry of both the NMP and SMP originally suggested that they were constructed by tropical to subtropical faunal assemblages including corals (Figs. **F7, F8, F13**). In contrast, cores retrieved during Leg 194 document a cool subtropical faunal assemblage consisting primarily of red algae, bryozoans, and larger benthic foraminifers. These calcite-dominated biogenic sediments have a lower diagenetic potential than their aragonite-dominated counterparts in the tropical realm. They can therefore be reworked more easily as they undergo less cementation. In addition, the fragmentation of these sediments leads to the formation of silt- to fine sand-sized particles rather than mud which is typical for aragonite-dominated systems.

### *Physical Energy*

The carbonate platform architecture observed on the Marion Plateau can be best explained by the dominance of currents. Exposure to pre-

dominant wind direction results in different platform margin geometries (e.g., leeward and windward margins of the Great Bahama Bank). The Marion Plateau example demonstrates that, similarly, exposure to bottom currents also results in asymmetric platform architecture (Figs. F8, F13). Seafloor currents influence sedimentation on the periplatform apron as they inhibit sedimentation in the upcurrent position and form wide low-angle clinoforms in a downcurrent position.

The results of Leg 194 suggest that sea level in conjunction with current-dominated sedimentation is a possible cause for rapid carbonate platform growth. The fact that the observed cool subtropical faunal assemblage produces platform geometries reminiscent of tropical carbonates further indicates that physical parameters may be as or more important for producing a given platform architecture than biological ones.

## Regional Acoustic Basement

Acoustic basement was penetrated at five sites during Leg 194 drilling (Sites 1193, 1194, 1195, 1197, and 1198). Prior to Leg 194 drilling, no direct information existed concerning the basement composition of the Marion Plateau.

Leg 133 drilling on the Queensland Plateau recovered altered and deformed metasedimentary and metavolcanic rocks that comprised acoustic basement (Davies, McKenzie, Palmer-Julson, et al., 1991). These metasedimentary rocks consisted of detrital quartzofeldspathic assemblages and igneous rock fragments. Low-grade quartz-muscovite-feldspar schists were also recovered. Recovered igneous rocks were determined to be altered granodioritic to tonalitic in composition and dominated by feldspars and quartz (Feary et al., 1993). Those assemblages were considered a straightforward continuation of the onshore Hodgkinson Formation, predominantly Devonian in age, consisting of thick, monotonous cleaved graywacke, siltstone, shale, and slate successions that in turn were cut by late Paleozoic–early Mesozoic dike swarms.

Basement rocks recovered during Leg 194 differ greatly from those drilled on the Queensland Plateau, although prior to drilling they were assumed to be similar in composition. Rather than metasedimentary rocks, highly altered lava flows and volcaniclastics were collected (Figs. F16, F17, F18, F19). The lack of deformation suggests that these volcanics may have been emplaced during the Late Cretaceous–Paleocene rifting of northeastern Australia from the Papuan Plateau in the north to the Lord Howe Rise in the south.

Planation of basement supposedly occurred during subaerial exposure in the Mesozoic and Paleogene. Site survey multichannel seismic reflection data suggest that the top of basement of the Marion Plateau is a topographic surface with tens to hundreds of meters of relief (Fig. F3) and often a major erosional unconformity. In particular, a north-south–trending, eastward-facing ramp exists toward the eastern edge of the plateau. The ramp has a maximum relief of 225 m and a dip of ~1°. Initiation of the oldest early Miocene reef/platform systems (and perhaps earlier systems) was focused along the eastern edge of this ramp (Pigram, 1993). Given the progression of the shallow-water early reef systems to the present water depths of the drilling sites (304–420 m), it is clear that postrift thermal subsidence remains the controlling factor on the long-term accommodation. The postrift subsidence of the region occurs even though unambiguous rift structures (e.g., high-angle nor-

F16. Multichannel seismic reflection profile, Site 1194, p. 80.

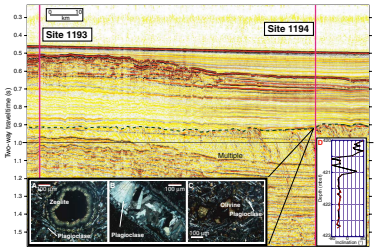


F17. Multichannel seismic reflection profile, Site 1197, p. 81.

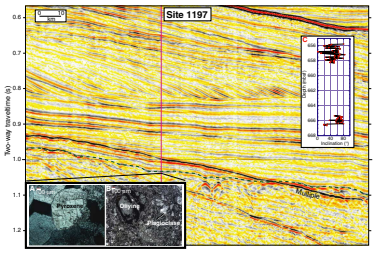


F18. Multichannel seismic reflection profile, Site 1193, p. 82.

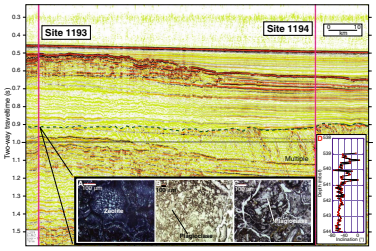


F19. Multichannel seismic reflection profile, Site 1198, p. 83.

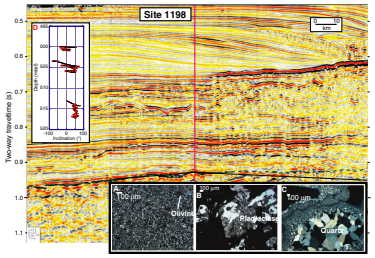

mal faults, rotated fault blocks, synrift wedge packages) are not observed across the plateau.

Site 1194 was drilled on the flank of a topographic basement high (Fig. F16). Recovered volcanic rocks consist of altered amygdaloidal olivine basalts, in which the olivines are large phenocrysts within a fine matrix of pyroxenes and plagioclase laths (Fig. F16). Many of the olivines have been altered to iddingsite and opaques, probably magnetite. Occasional veins are filled with feldspars that are zoned from fine to coarse, whereas the vugs are infilled with zeolites, most likely natrolite.

Site 1197 was located in a similar setting to Site 1194 (Fig. F17). Recovered basal units of this site are polymictite volcanic breccias (tuffs) deposited in a nonmarine paleoenvironment. Glass shards are also present and vugs are filled with feldspars. At the base of the breccias is an olivine basalt (Fig. F17) showing similar characteristics as the basalts from Site 1194.

Site 1193, a volcanic flow, is highly altered even compared with Sites 1194 and 1197 (Fig. F18). Vug infilling is natrolite, characterized by fine radiating fibers (Fig. F18). Crystal outlines are well represented under normal light.

The recovered basement rocks at Site 1198, although again highly altered, are different from the basalts at the other sites, being composed principally of plagioclase (albite?) lathes. Quartz is observed to infill veins (Fig. F19).

The paleomagnetic response of basement is characterized by both relatively high intensity and consistent normal and reversed inclinations (Figs. F16, F17, F18, F19). In general, the inclination polarity is almost exactly 180° apart, implying the existence of a clean, primary thermal remanent magnetization. In the upper part of the recovered basement section, the inclination has a greater variation, implying that a magnetic overprint exists. This leads to the possibility that the inclinations, when the corresponding paleomagnetic pole is compared with the Australian apparent polar wander path, may provide age estimates for both the emplacement of the basalts and the timing of low-temperature alteration.

## Fluid Flow in Carbonate Platform and Periplatform Sediments of the Marion Plateau

One of the main objectives of Leg 194 was to study fluid circulation in the Marion Plateau carbonate platforms using the sediments and pore fluids recovered from the Leg 194 drill cores. The dolomitization found in both the north and south platforms is itself indirect evidence for past fluid circulation. Dolomite formation on a large scale requires fluid flow to deliver the required magnesium to the precursor calcium carbonate sediments. But when and how fluids may have circulated and the nature of the fluids, whether they were normal seawater or hypo- or hypersaline, are open questions. It was also thought that the present-day pore waters might hold evidence of past or even continuing fluid movement. In that regard, the pore fluid sampling program on Leg 194 has yielded intriguing results. Although sampling of pore waters from within the southern platform was not possible, samples taken from sediments above and below the adjacent periplatform facies provide clear evidence that seawater continues to circulate through these sediments even though they are overlain by ~200 m of hemipelagic deposits. By inference, seawater is likely to be circulating through the southern platform at present. Similarly, the pore water samples from directly above

and below the carbonate platform facies of the NMP at Site 1193 are also close to seawater in composition, suggesting seawater circulation. Site 1198 drilled through seismic Megasequences D, C, and B to basement 5 km northwest of the margin of the SMP (Fig. F20). In seismic Megasequence D, which is equivalent to lithologic Unit I, 24 samples were taken at ~10-m intervals to a depth of 196.6 mbsf, the base of lithologic Unit I. From 197 to 350 mbsf, poor recovery of the unconsolidated sediments of lithologic Subunits IIA and IIB (seismic Megasequence C and the upper ~60 m of Megasequence B) precluded pore water sampling. Sampling resumed in Megasequence B at 350 mbsf, with samples taken at ~10-m intervals to a depth of 505.0 mbsf, just above basement.

For most of the pore water constituents, nearly symmetrical, arcuate pore water profiles are found in the upper 200 mbsf. From essentially seawater values near the sediment surface, concentrations in the interval from 0 to 100 mbsf either increase or decrease depending on the ion measured. In the interval from 100 to 200 mbsf, the trends of the upper 100 mbsf reverse and concentrations return to values close to those of normal seawater. This pattern is found for alkalinity, sulfate, ammonium, strontium, potassium, and magnesium.

Two profiles, sulfate and strontium, are illustrated in Figure F20. These two constituents were chosen because they are affected by completely independent processes. The two profiles are shown plotted on top of the seismic section that crosses the platform margin and continues across the adjacent periplatform sediments now buried beneath the hemipelagic sediments of seismic Megasequence D. Note that the data points all lie on the line showing the location of Site 1198; the x-axis is concentration, not distance. Sulfate concentration initially decreases as a result of bacterial sulfate reduction. At ~100 mbsf, however, sulfate concentration increases, returning to ~29 mM at the transition from hemipelagic sediments of seismic Megasequence D to Megasequence C. A cessation of sulfate reduction in the lower part of Megasequence D is an unlikely cause for the increase in sulfate concentration because there is no decrease in the organic carbon content within this unit. At the base of seismic Megasequence C, the sulfate concentration is also ~29 mM and thereafter decreases with depth.

The strontium concentration profile found in the upper ~100 mbsf is typical of pelagic or hemipelagic, carbonate-rich sediments. Strontium is added to the pore fluids by carbonate dissolution and recrystallization. Usually, this process continues for many hundreds of meters and high strontium concentrations (500 to 1000 µM) are a standard feature of sediment pore waters below 100–200 mbsf. At Site 1198, however, the concentration of strontium in the lower portion of seismic Megasequence D reverses the trend seen in the upper ~100 mbsf and is close to the seawater value at the contact with seismic Megasequence C. The strontium concentration is also low in the uppermost sample from seismic Megasequence B and then increases with depth to the bottom of the sampled interval. As for sulfate, there is no sedimentological reason for the reversal in trend. The carbonate content of seismic Megasequence D is relatively constant and in fact increases in Megasequence C.

The strontium profile is in many ways similar to sulfate, although the chemical reaction controlling strontium concentration is independent of that which affects sulfate. The pore water profiles of both constituents in seismic Megasequence D suggest diffusion-reaction control without fluid flow. The shape of the upper portion of the pore water

**F20.** Multichannel seismic line MAR07 at Site 1198, p. 84.

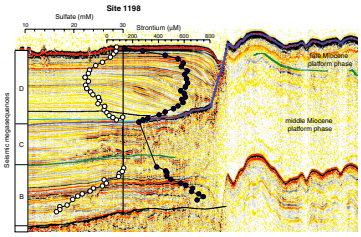

profiles is typical for pore waters in many parts of the ocean, but the changes in concentration seen in the lower half of lithologic Unit I are unusual. They are most easily explained by relatively constant rates of reaction in the sediments, with diffusion acting upon both the upper and lower bounds of this sediment package. The fact that the concentrations at the lower boundary of Unit I are close to seawater values implies that the fluid that fixes the concentration at the lower boundary condition is also close to seawater in composition. The near-seawater concentration of sulfate and strontium (and other constituents) at the base of seismic Megasequence D strongly suggests active circulation of seawater through the sediments of seismic Megasequence C, between 200 and 350 mbsf. Neither the mechanism nor direction of fluid flow can be determined from the available data. Based on the seismic profiles of the Marion Plateau, sequence C is not exposed on the seafloor and thus has no direct connection to seawater. The unit is in contact with the SMP; thus a hydraulic connection between the platform and the periplatform sediments of seismic Megasequence C seems likely.

Figure F21 is similar to Figure F20 but shows the concentrations of sulfate and strontium for Site 1193, drilled through the NMP. The ~200-m-thick sequence of platform facies are overlain by a thin cover of hemipelagic sediments of seismic Megasequence D and underlain by several hundred meters of hemipelagic sediments of seismic Megasequence B. Both sulfate and strontium concentration profiles of the upper 40 mbsf of Megasequence D faintly suggest the curved profiles found in Site 1198. More importantly, the pore fluids from the surface down to the base of the NMP at 230 mbsf are close to seawater in composition. The similarity was initially interpreted to be the result of a near lack of chemical reaction in highly stabilized lithologies, low-magnesium calcite and dolomite, of the platform. Although this explanation remains a possibility, a second possibility also exists. Chemical reaction may be continuing in the platform, but the resulting changes to pore fluid chemistry could be swept away by active fluid circulation. Chemical reactions certainly continue below the platform facies, in Megasequence B, where concentrations of sulfate decrease and concentrations of strontium increase with depth. The evidence for fluid circulation at Site 1193 is perhaps not as strong as found at Site 1198. Fluid circulation is, however, a viable explanation for the observed pore water profiles.

F21. Multichannel seismic line MAR13 at Site 1193, p. 85.

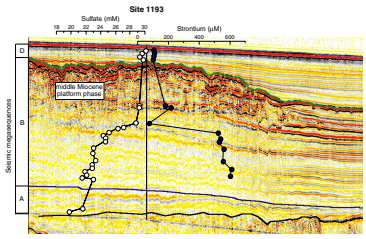

# REFERENCES

Athy, L.F., 1930. Density, porosity, and compaction of sedimentary rocks. *AAPG Bull.,* 14:1–24.

Buddemeier, R.W., and Oberdorfer, J.A., 1986. Internal hydrology and geochemistry of coral reefs and atoll islands: key to diagenetic variations. *In* Schroeder, J.H., and Purser, B.H. (Eds.), *Reef Diagenesis:* Berlin (Springer-Verlag), 91–111.

COSOD II, 1987. *Rep. 2nd Conf. Scientific Ocean Drilling:* Washington/Strasbourg (JOIDES/European Sci. Found.).

Davies, P.J., McKenzie, J.A., Palmer-Julson, A., et al., 1991. *Proc. ODP, Init. Repts.,* 133 (Pts. 1, 2): College Station, TX (Ocean Drilling Program).

Davies, P.J., Symonds, P.A., Feary, D.A., and Pigram, C.J., 1989. The evolution of the carbonate platforms of northeast Australia. *In* Crevello, P.D., Wilson, J.L., Sarg, J.F., Read, J.F. (Eds.), *Controls on Carbonate Platform and Basin Development.* Spec. Publ.—Soc. Econ. Paleontol. Mineral., 44:233–258.

Eberli, G.P., Swart, P.K., Malone, M.J., et al., 1997. *Proc. ODP, Init. Repts.,* 166: College Station, TX (Ocean Drilling Program).

Elderfield, H., Swart, P.K., McKenzie, J.A., and Williams, A., 1993. The strontium isotopic composition of pore waters from Leg 133: northeast Australian margin. *In* McKenzie, J.A., Davies, P.J., Palmer-Julson, A., et al., *Proc. ODP, Sci. Results,* 133: College Station, TX (Ocean Drilling Program), 473–480.

Feary, D.A., Champion, D.C., Bultitude, R.J., and Davies, P.J., 1993. Igneous and metasedimentary basement lithofacies of the Queensland Plateau (Sites 824 and 825). *In* McKenzie, J.A., Davies, P.J., Palmer-Julson, A., et al., *Proc. ODP, Sci. Results,* 133: College Station, TX (Ocean Drilling Program), 535–540.

Feary, D.A., Hine, A.C., Malone, M.J., et al., 2000. *Proc. ODP, Init. Repts.,* 182 [CD-ROM]. Available from: Ocean Drilling Program, Texas A&M University, College Station, TX 77845-9547, U.S.A.

Gaina, C., Müller, R.D., Royer, J.-Y., and Symonds, P., 1999. The evolution of the Louisiade Triple Junction. *J. Geophys. Res.,* 104:12927–12940.

Halley, R.B., and Ludwig, K.R., 1987. Disconformities and Sr-isotope stratigraphy reveal a Neogene sea level history from Enewetak Atoll, Marshall Islands, Central Pacific. *Geol. Soc. Am. Abstr. Progr.,* 19:691.

Haq, B.U., Hardenbol, J., and Vail, P.R., 1987. Chronology of fluctuating sea levels since the Triassic. *Science,* 235:1156–1167.

Hayes, D.E., and Ringis, J., 1973. Seafloor spreading in the Tasman Sea. *Nature,* 243:454–458.

Heck, P., Anselmetti, F., and Isern A., 1999. Sediment description and physical property analyses of seafloor and shallow subsurface. Unpubl. Rep., JOIDES/ODP Site Survey Databank.

Isern, A.R., McKenzie, J.A., and Feary, D.A., 1996. The role of sea-surface temperature as a control on carbonate platform development in the western Coral Sea. *Palaeogeogr., Palaeoclimatol., Palaeoecol.,* 124:247–272.

JOIDES Planning Committee, 1996. *Understanding our Dynamic Earth through Ocean Drilling: Ocean Drilling Program Long Range Plan into the 21st Century:* Washington (JOI).

Katz, M.E., and Miller, K.G., 1993. Neogene subsidence along the northeastern Australian margin: benthic foraminiferal evidence. *In* McKenzie, J.A., Davies, P.J., Palmer-Julson, A., et al., *Proc. ODP, Sci. Results,* 133: College Station, TX (Ocean Drilling Program), 75–92.

Lincoln, J.M., and Schlanger, S.O., 1987. Miocene sealevel falls related to the geological history of Midway Atoll. *Geology,* 15:454–457.

————, 1991. Atoll stratigraphy as a record of sea level change: problems and prospects. *J. Geophys. Res.,* 96:6727–6752.

Major, R.P., and Matthews, R.K., 1983. Isotopic composition of bank margin carbonates on Midway Atoll: amplitude constraint on post-early Miocene eustasy. *Geology,* 11:335–338.

McKenzie, J.A., Isern, A., Elderfield, H., Williams, A., and Swart, P., 1993. Strontium isotope dating of paleoceanographic, lithologic, and dolomitization events on the northeastern Australian margin, Leg 133. *In* McKenzie, J.A., Davies, P.J., Palmer-Julson, A., et al., *Proc. ODP, Sci. Results,* 133: College Station, TX (Ocean Drilling Program), 489–498.

Miller, K.G., Fairbanks, R.G., and Mountain, G.S., 1987. Tertiary oxygen isotope synthesis, sea-level history, and continental margin erosion. *Paleoceanography,* 2:1–19.

Moore, T.C., Jr., Loutit, T.S., and Greenlee, S.M., 1987. Estimating short-term changes in eustatic sealevel. *Paleoceanography,* 2:625– 637.

Müller, R.D., Lim, V.S.L., and Isern, A.R., 2000. Late tertiary tectonic subsidence on the northeast Australian passive margin: response to dynamic topography? *Mar. Geol.,* 162:337–352.

Mullins, H.T., Heath, K.C., Van Buren, M., and Newton K., 1984. Anatomy of a modern open-oceanic carbonate slope: northern Little Bahama Bank. *Sedimentology,* 31:141–168.

Mutter, J.C., and Karner, G.D., 1980. The continental margin off northeast Australia. *In* Henderson, R.A., and Stephenson, P.J. (Eds.), *The Geology and Geophysics of Northeast Australia*. Geol. Soc. Aust., Queensl. Div., 47–69.

Pigram, C.J., Davies, P.J., Feary, D.A., and Symonds, P.A., 1992. Absolute magnitude of the second-order middle to late Miocene sea-level fall, Marion Plateau, Northeast Australia. *Geology,* 20:858–862.

Pigram, C.J., 1993. Carbonate platform growth, demise and sea level record: Marion Plateau, Northeast Australia [Ph.D. dissert.]. Australian National Univ., Canberra.

Sahagian, D.L., and Watts, A.B., 1991. Introduction to the Special Section on measurement, causes and consequences of long-term sea level changes. *J. Geophys. Res.,* 96:6585–6589.

Schlanger, S.O., and Premoli Silva, I., 1986. Oligocene sea-level falls recorded in mid-Pacific atoll and archipelagic apron settings. *Geology,* 14:392–395.

Shaw, R.D., 1978. Seafloor spreading in the Tasman Sea: A Lord Howe Rise—eastern Australian reconstruction. *Aust. Soc. Explor. Geophys. Bull.,* 9:75–81.

Simms, M., 1984. Dolomitization by groundwater-flow systems in carbonate platforms. *Trans. Gulf Coast Assoc. Geol. Soc.,* 34:411–420.

Struckmeyer, H.I.M., and Symonds, P.A., 1997. Tectonostratigraphic evolution of the Townsville Basin, Townsville Trough, offshore northeastern Australia. *Aust. J. Earth Sci.,* 44:799–817.

Symonds, PA., Davies, P.J., Feary, D.A., and Pigram, C.J., 1988. Geology of the northeastern Australian margin basins. *In* Harrison, P.L. (Ed.), *Queensland 1988 Exploration and Development.* Pet. Explor. Soc. Aust. Symp.

Vail, P.R., and Hardenbol, J., 1979. Sea-level changes during the Tertiary. *Oceanus,* 22:71–79.

Vail, P.R., Mitchum, R.M., Jr., Todd, R.G., Widmier, J.M., Thompson, S., III, Sangree, J.B., Bubb, J.N., and Hatlelid, W.G., 1977. Seismic stratigraphy and global changes in sea level. *In* Payton, C.E. (Ed.), *Seismic Stratigraphy: Applications to Hydrocarbon Exploration*. AAPG Mem., 26:49–212.

Varenkamp, V.C., 1991. Episodic dolomitization of late Cenozoic carbonates in the Bahamas. *J. Sediment. Petrol.,* 61:1002–1014.

Watts, A.B., and Thorne, J., 1984. Tectonics, global changes in sea level and their relationship to stratigraphical sequences at the U.S. Atlantic continental margin. *Mar. Pet. Geol.,* 1:319–339.

Weissel, J.K., and Hayes, D.E., 1977. Evolution of the Tasman Sea reappraised. *Earth Planet. Sci. Lett.,* 36:77–84.

Williams, D.F., 1988. Evidence for and against sea-level changes from the stable isotopic record of the Cenozoic. *In* Wilgus, C.K., Hasting, B.S., Kendall, C.G.St.C., Posa-

mentier, H.W., Ross, C.A., and Van Wagoner, J.C. (Eds.), *Sea-Level Changes: An Integrated Approach*. Spec. Publ.—Soc. Econ. Paleontol. Mineral., 42:31–36.

**Figure F1.** Map showing the location of DSDP Site 209 (solid square), ODP Leg 133 sites (open circles), and ODP Leg 194 sites (solid circles) off northeastern Australia. The box at the lower right indicates the location of Figure F2, p. 62.

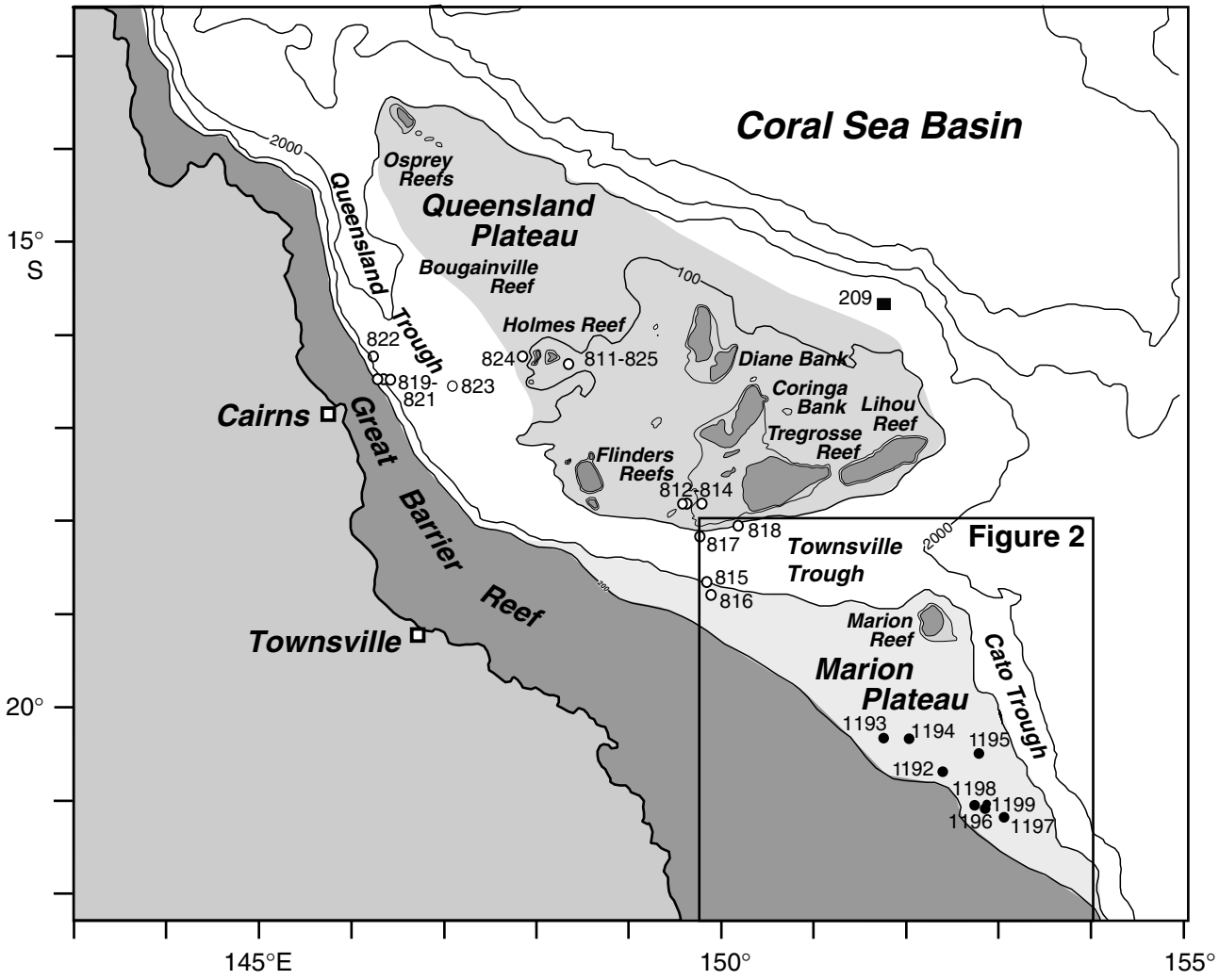

**Figure F2.** Map showing locations of Leg 194 sites (solid circles) and two Leg 133 sites (open circles). Thin solid lines = location of multichannel seismic lines from the Australian Geological Survey Organization (Survey 75). Heavier lines = location of multichannel seismic lines from the Leg 194 site survey (MAR data). Shaded areas = estimated extent of the NMP and the southern platforms. Dashed line = boundary of the Great Barrier Reef Marine Park.

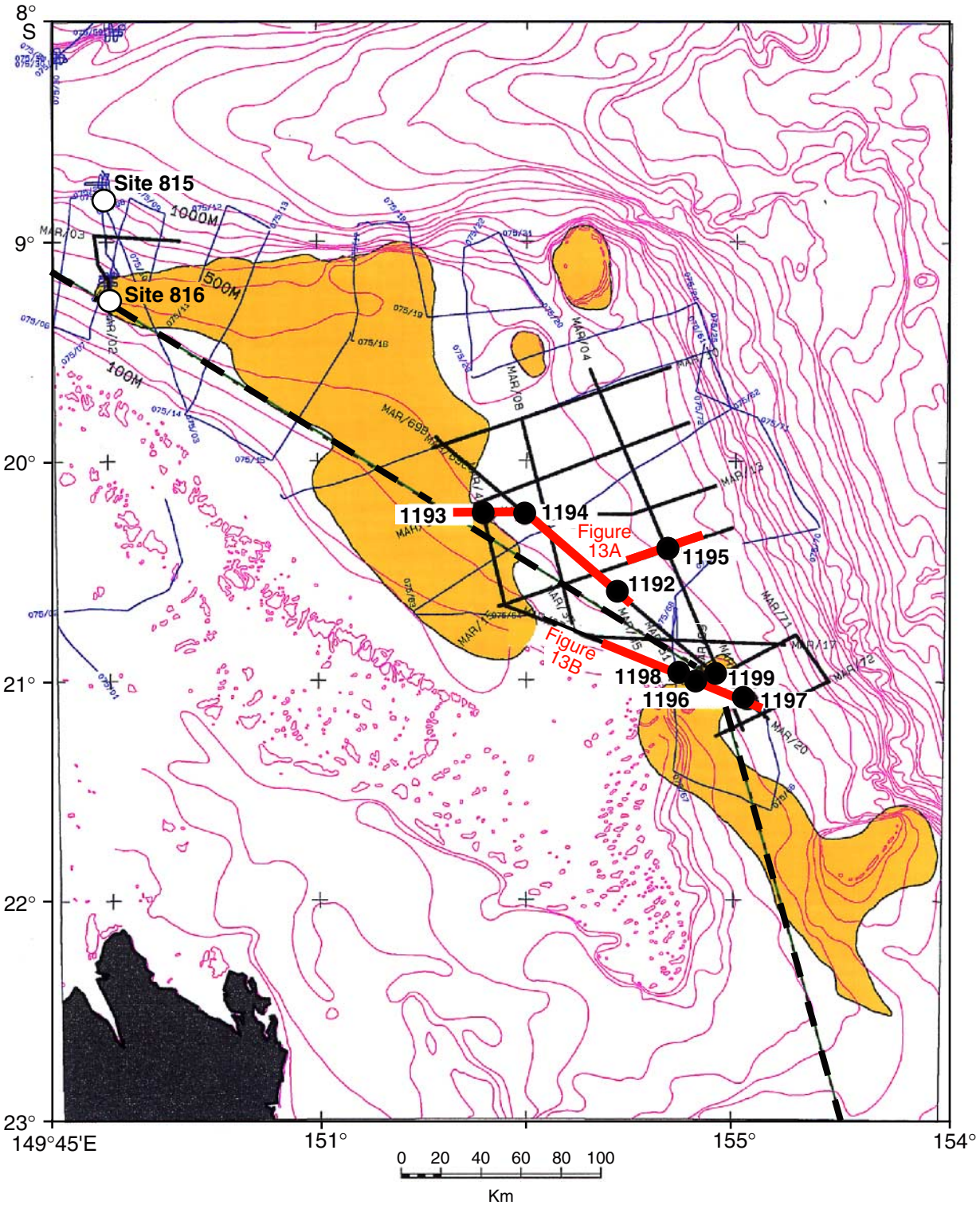

**Figure F3.** Topography of acoustic basement in the area covered by the Leg 194 site survey. Topography is given in two-way traveltime and is not depth corrected. Basement cannot be mapped below the carbonate platforms because scattering and attenuation of the platform top hinders penetration of the seismic signal. Fine lines are spaced every 20 ms, which equals ~20 m.

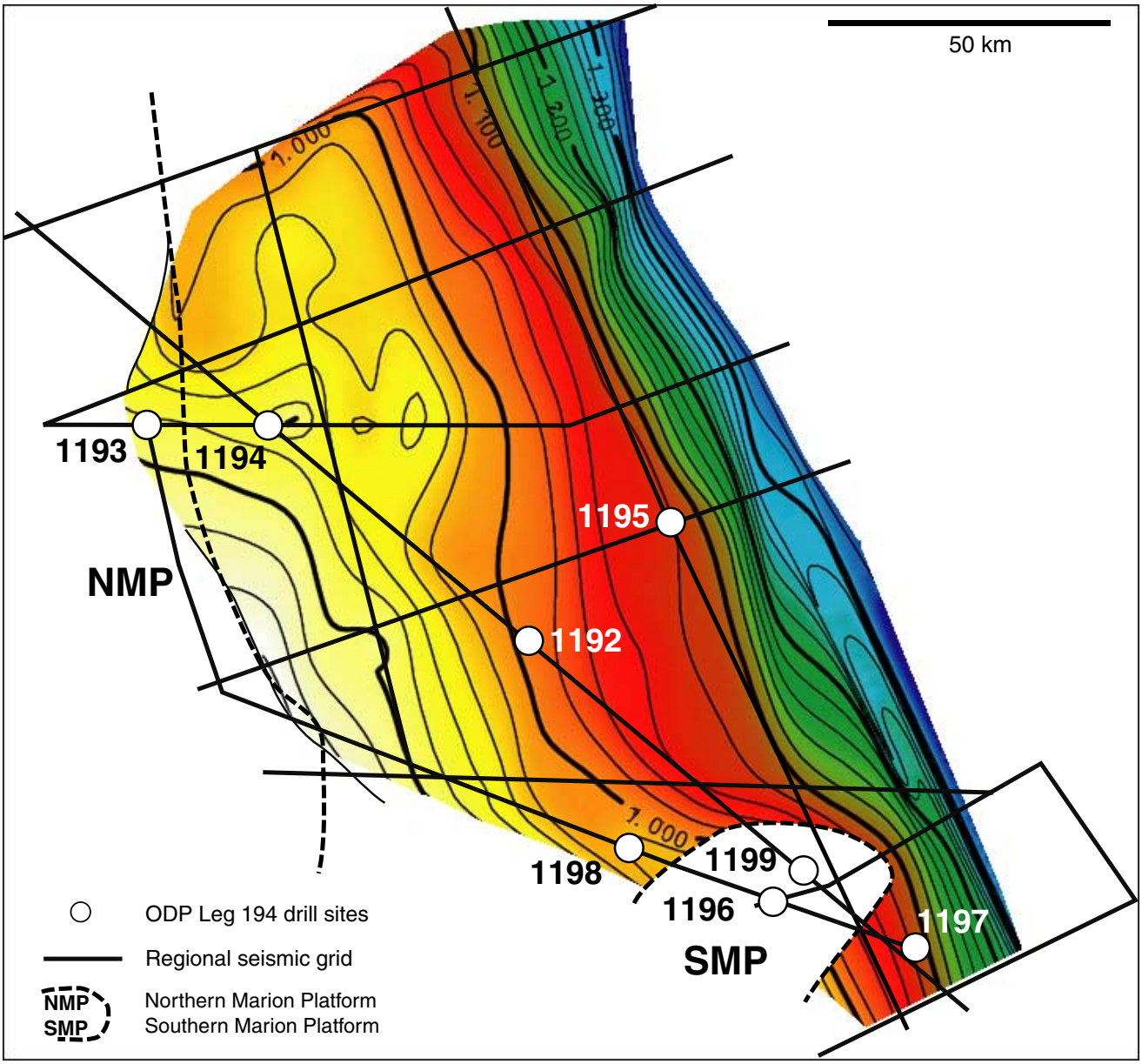

**Figure F4.** Water-loaded tectonic subsidence (i.e., with the isostatic sediment load removed) for ODP Leg 133 Sites 812, 814, 811/825, 815, and 823, assuming constant eustatic sea level (shown on left) and using eustatic sea level variations of Haq et al. (1987) (shown on right). The latter is not shown for Site 823, as the errors in water depth (vertical error bars) are much larger than eustatic sea level variations. Shading around error bars indicates the area in which the true subsidence curve should occur. Comparisons between constant and varying eustatic sea levels allow evaluation of the potential effect of eustatic variations on tectonic subsidence models. For instance, the first model (left) for Site 814 shows a gently subsiding platform until ~5 Ma, whereas the second model (right), including eustasy, shows a tectonic subsidence pulse between 14 and 12 Ma. Therefore, the latter may be entirely due to the input of an ill-constrained eustatic sea level curve.

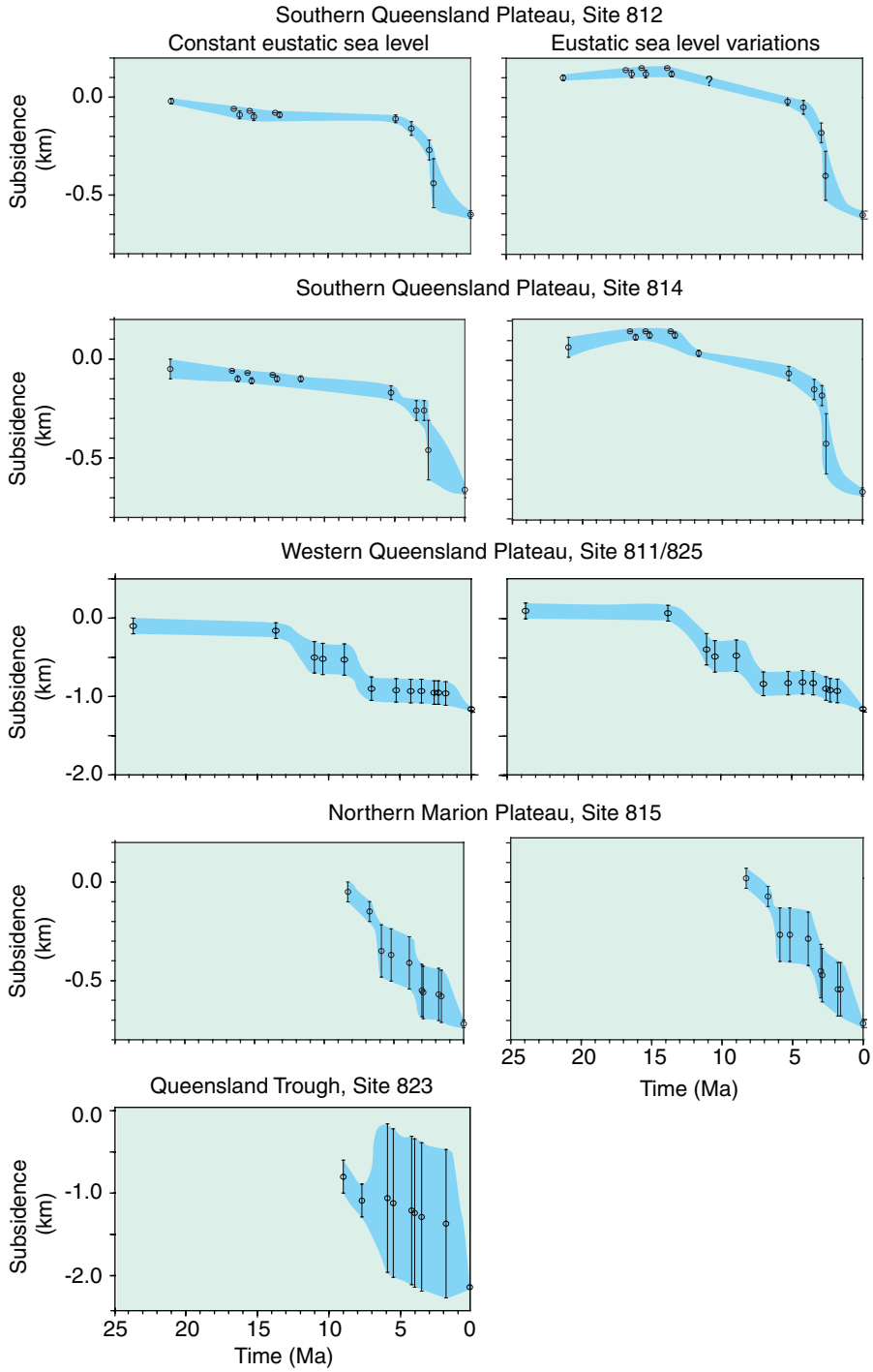

**Figure F5.** Stratigraphic summary of previously cored sites located near Leg 194 sites. All sites were cored during Leg 133 except for Site 209, which was cored during DSDP Leg 21.

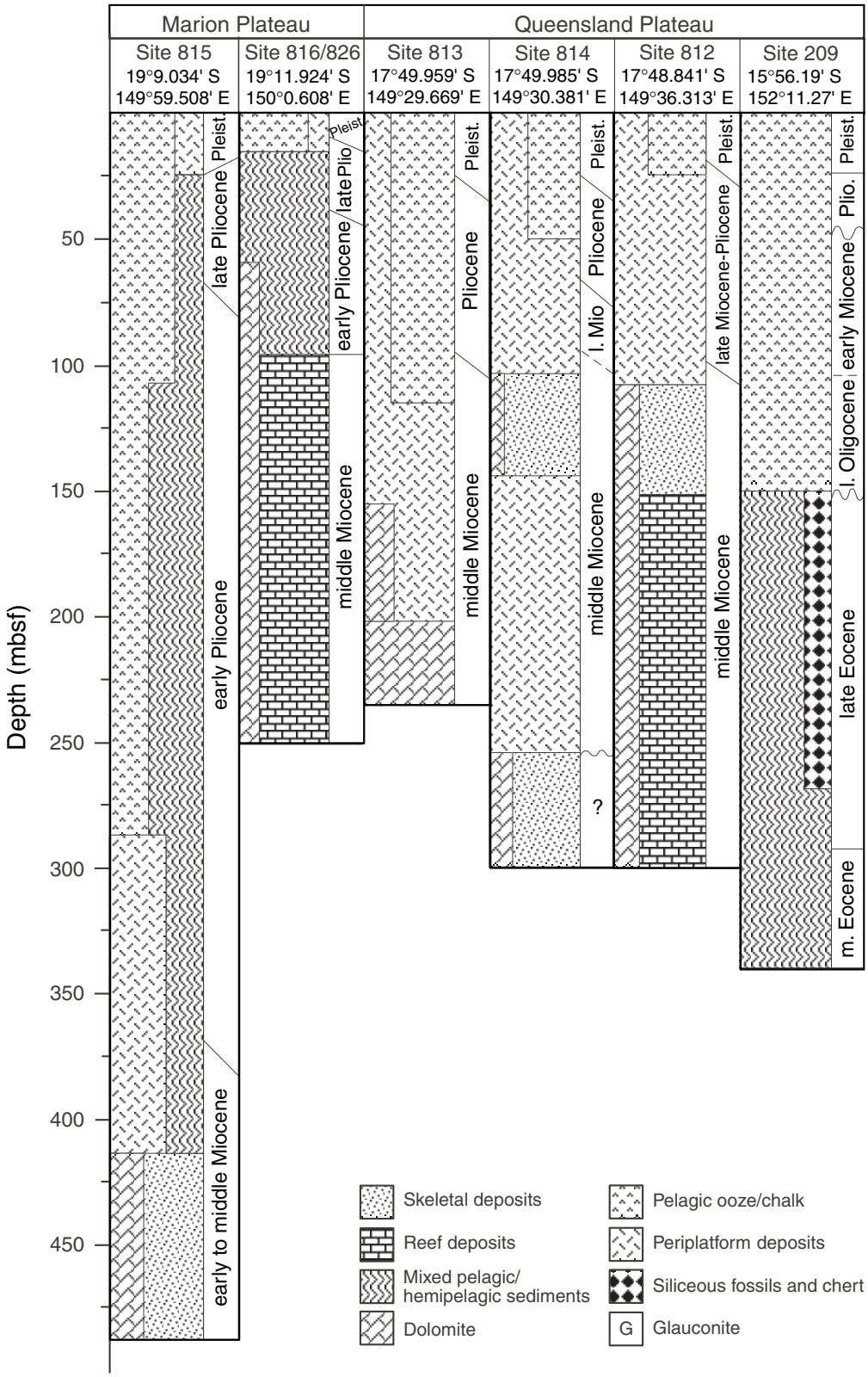

**Figure F6.** Seafloor photographs from Leg 194 sites. Phototrigger at upper right of each photograph is 10 cm in diameter. **A.** Seafloor photograph near Site 1194 at 374 meters below sea level (mbsl) shows decimeter-range sediment ripples and cemented pieces. The cut section of a dredged cemented piece reveals a burrow heavily encrusted by sponges, suggesting early cementation occurring on the seafloor. **B.** Dredged submarine crust from the location of Site 1196. The photo shows the underside of a 2- to 3-cm-thick reddened crust colonized by bryozoans and serpulids. **C.** Seafloor photographs near Site 1196 at 304 mbsl, showing patchy distribution of the hardground crust on the drowned southern platform top. **D.** Seafloor photograph near Site 1193 at 348 mbsl. Abundant decimeter-scale ripples document strong bottom currents.

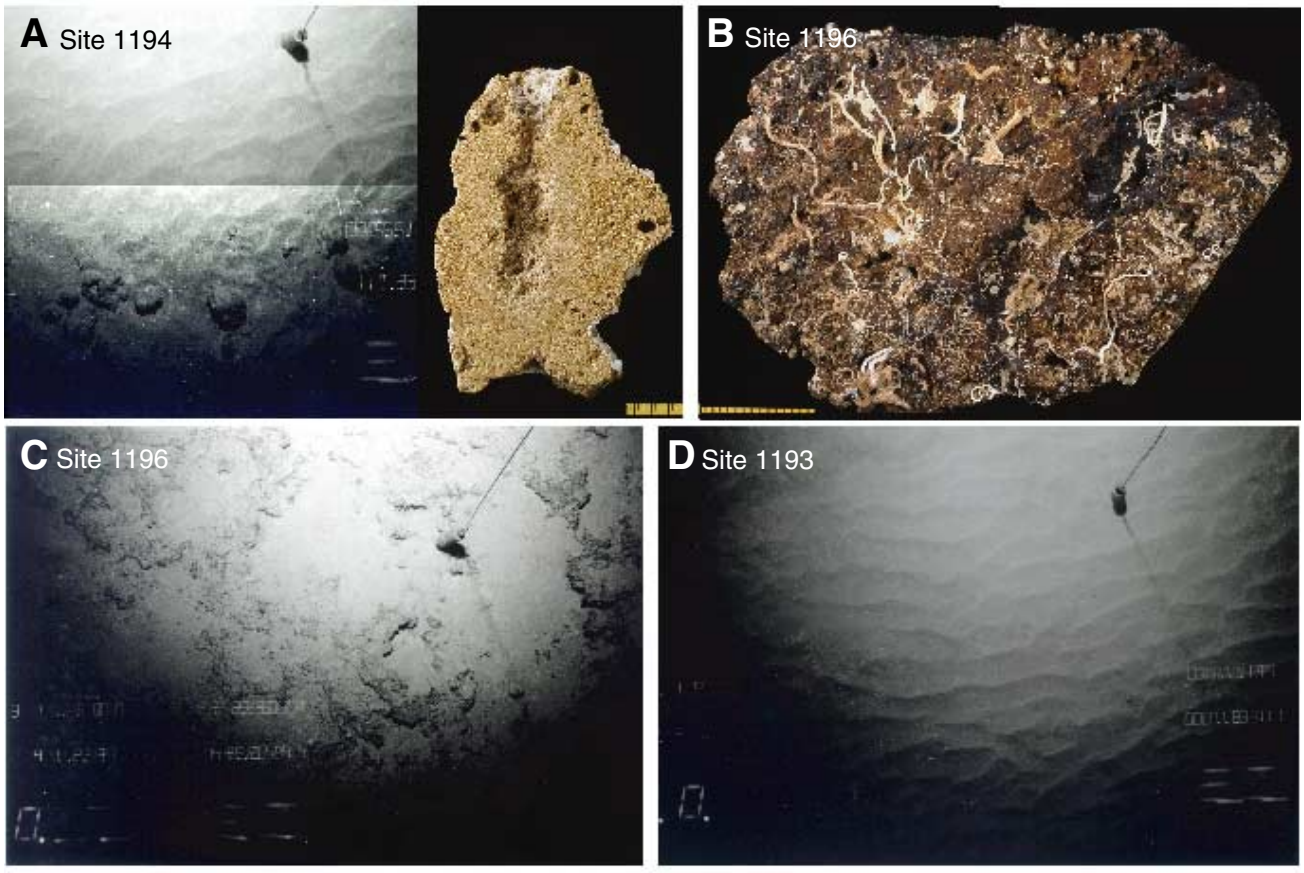

**Figure F7.** Seismic overview displaying characteristics of megasequences along the northern transect with seismic lines MAR13, MAR20, and MAR15 linking Sites 1193, 1194, 1192, and 1195 (see Fig. F2, p. 62, for location of profiles). (This figure is also available in an **oversized format.**)

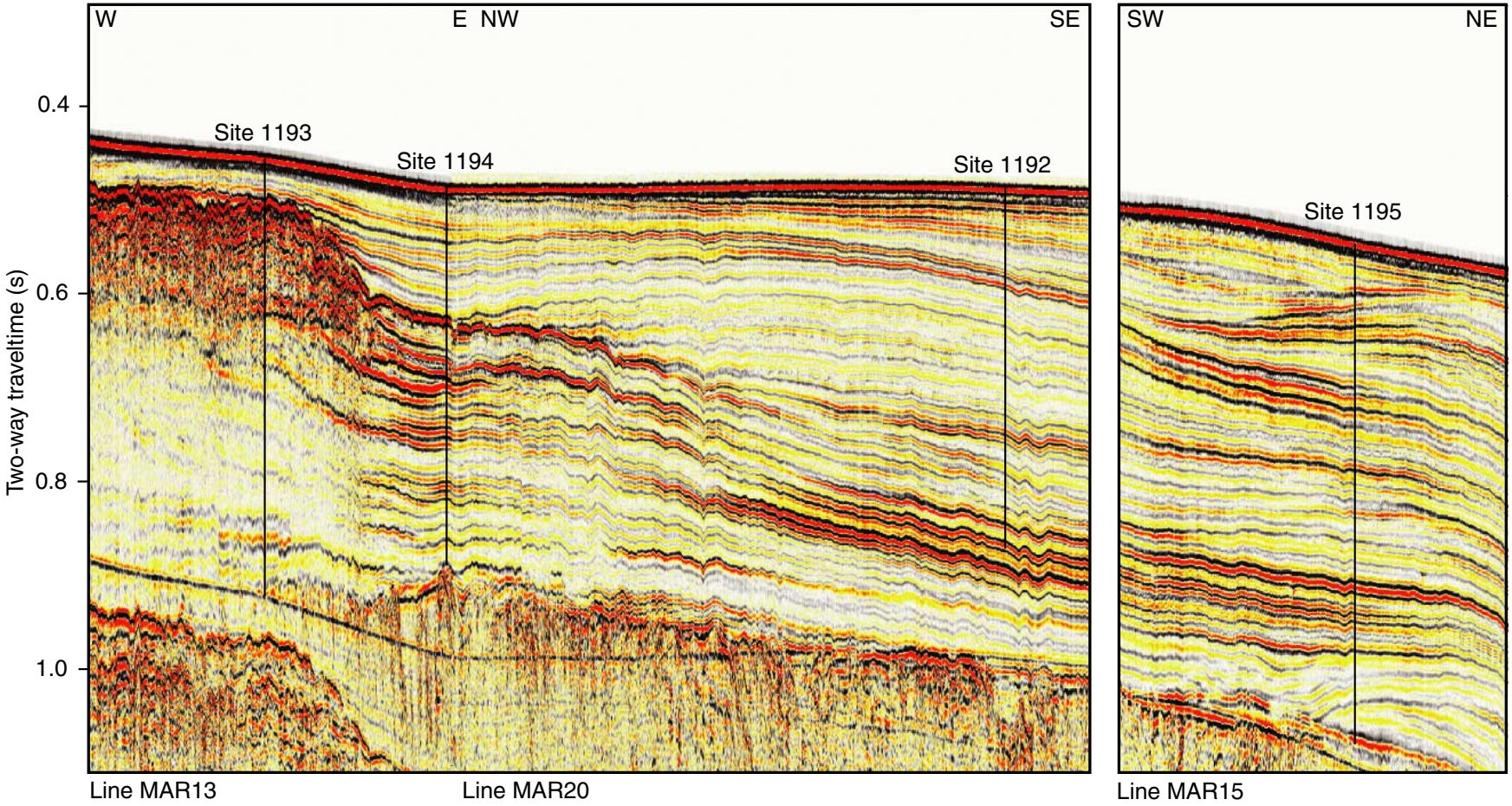

**Figure F8.** Seismic overview displaying characteristics of megasequences along the southern transect with seismic line MAR07 linking Sites 1198, 1196, 1999, and 1197. The position of Site 1199 was projected into the seismic section parallel to the northwestern SMP margin (see Fig. **F2,** p. 62, for location of profiles). (This figure is also available in an **oversized format.**)

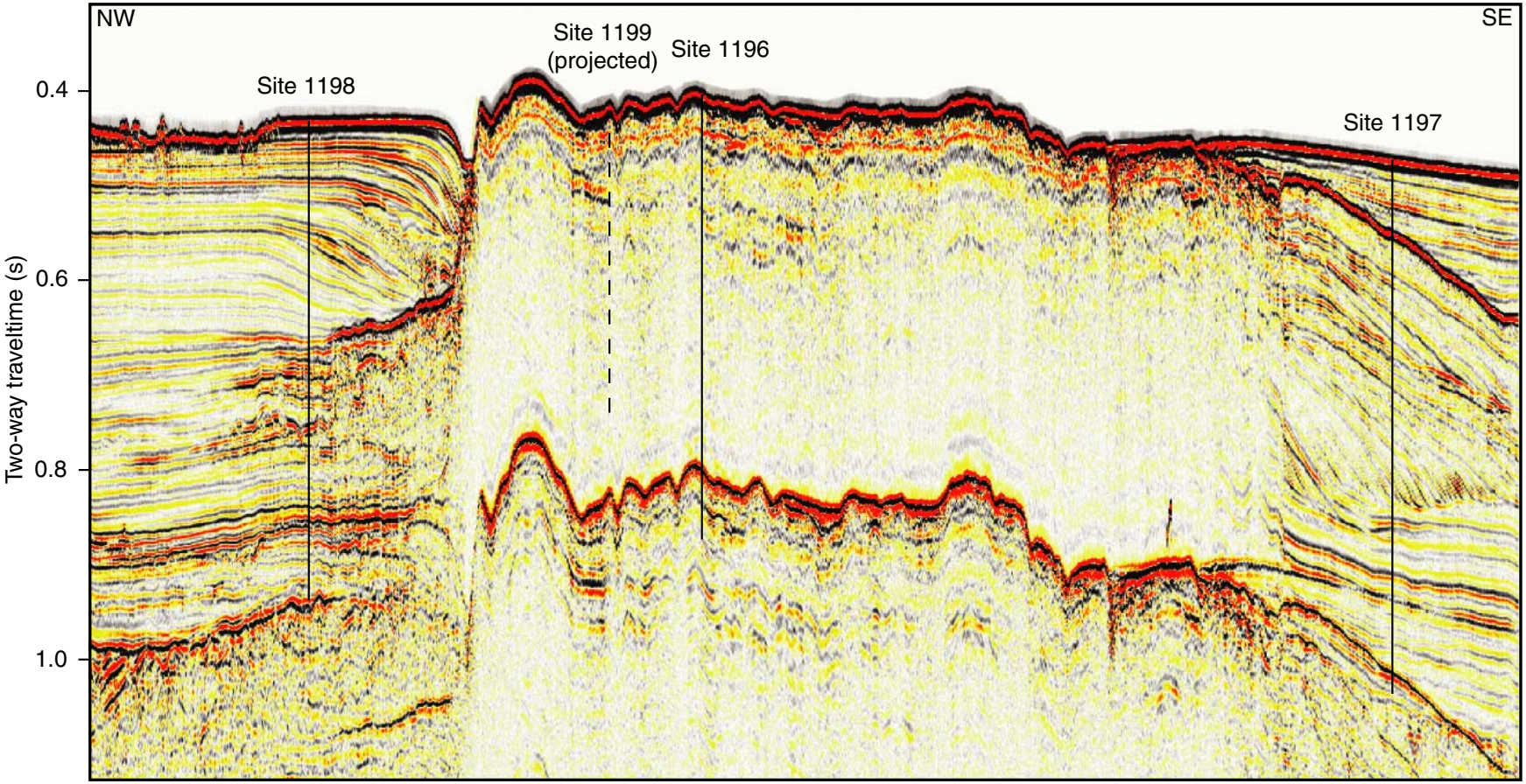

**Figure F9.** Stratigraphic correlation summary for Leg 194. **A.** Correlation between Sites 1193, 1194, 1192, and 1195, which represent the northern drilling transect from the northern platform to the distal periplatform/hemipelagic setting. **B.** Correlation between Sites 1198, 1199, 1196, and 1197, which represent the southern drilling transect extending across the southern platform from the northwest, across the platform top, to the southeast. **C.** Seven data panels are presented for each site and an explanation is provided describing the data and symbols used. Data sets include depth downhole in mbsf, core number, core recovery, lithologic units with age derived from biostratigraphy and magnetostratigraphy, a graphic display of lithologies, mineralogy based upon XRD analysis, natural gamma ray profiles from downhole logging and core-based physical properties measurements, and the megasequences defined from seismic reflection data. MS = megasequence, wd = water depth. (Continued on next two pages.) (This figure is also available in an **oversized format.**)

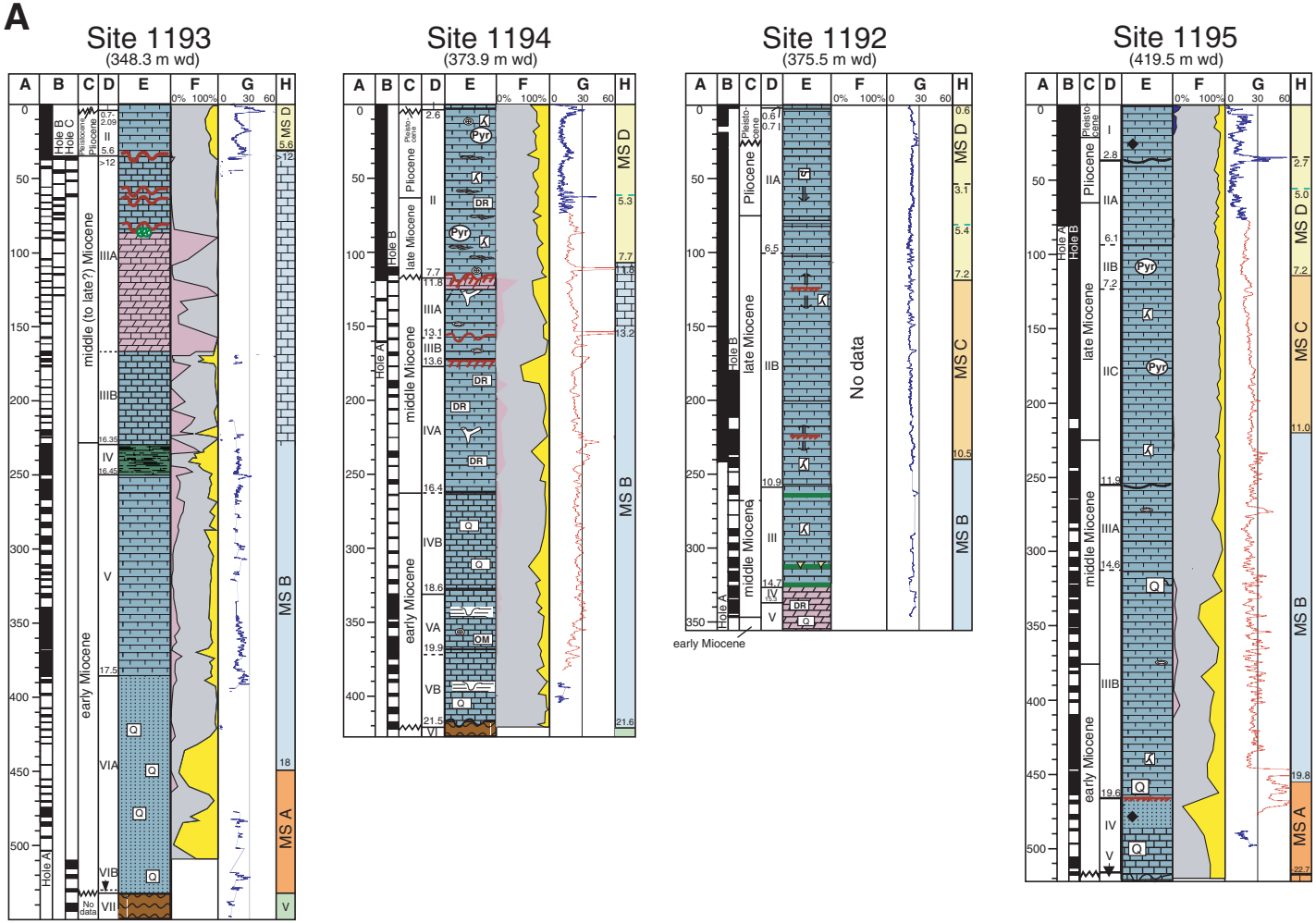

**Figure F9 (continued).**

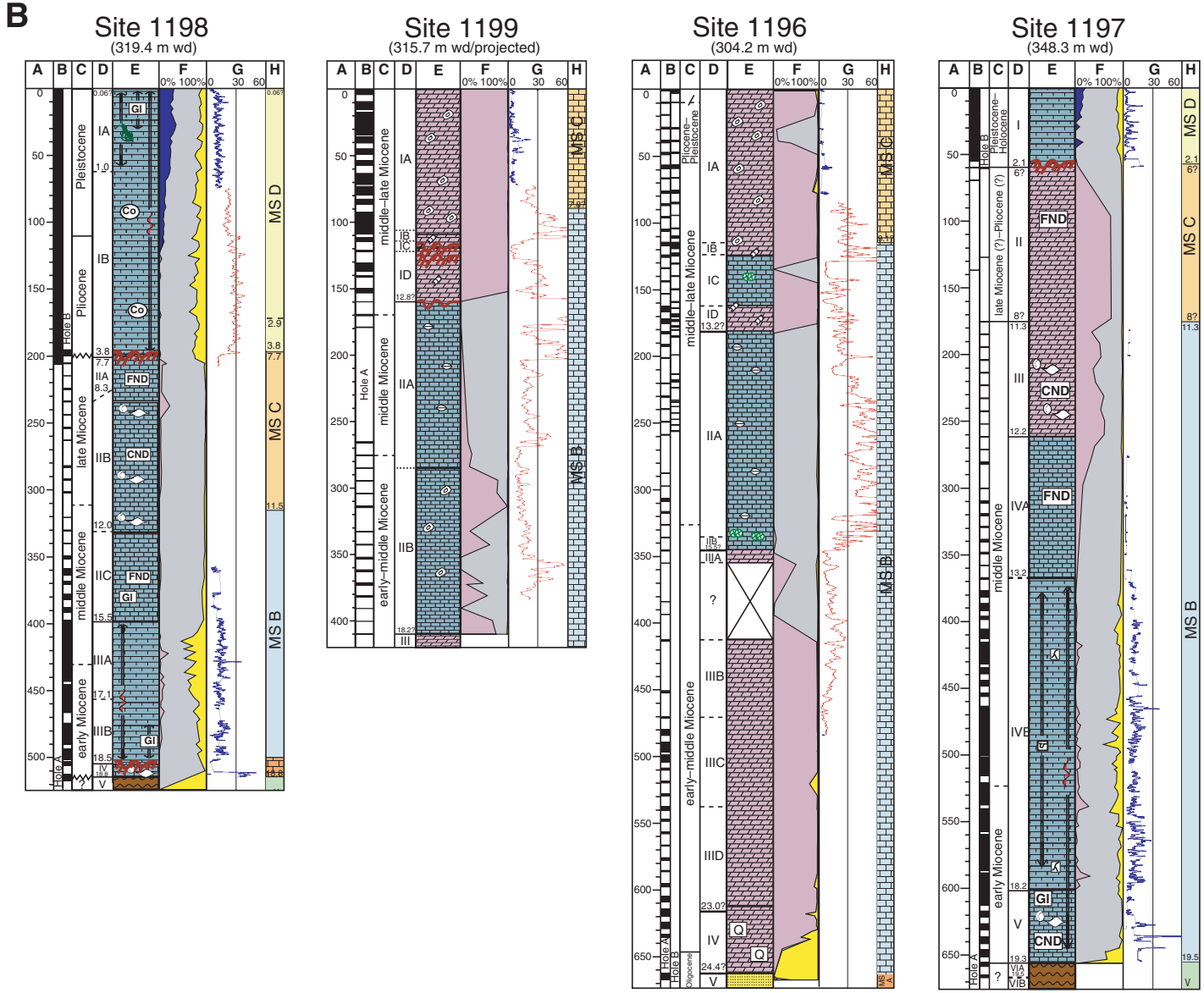

Figure F9 (continued).

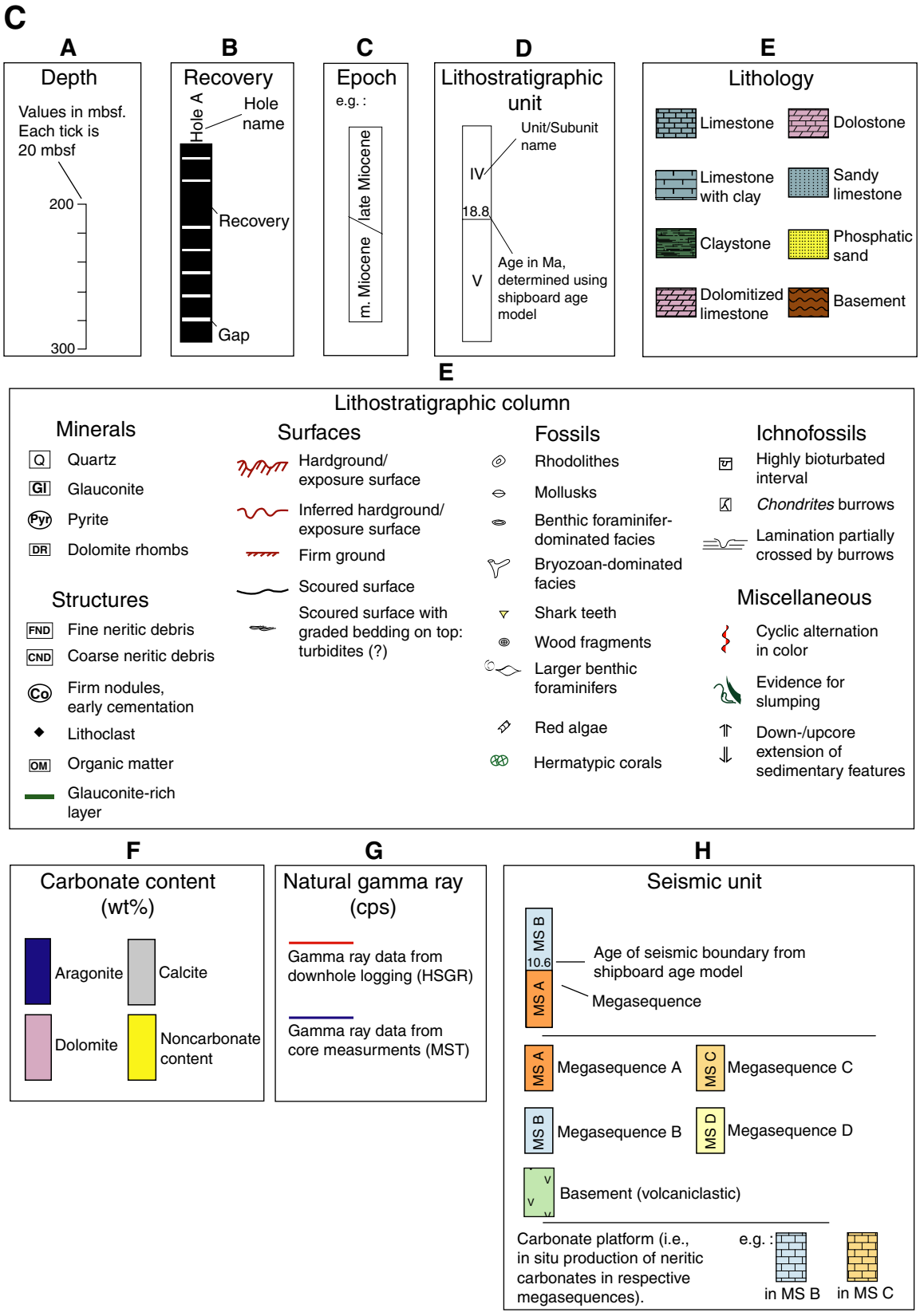

**Figure F10. A.** Parts of seismic sections MAR13, MAR20, MAR15, and MAR07 with locations of all Leg 194 sites. Uninterpreted sections with site locations are plotted in the upper half of the figure. Note that Line MAR07 (at left) has different horizontal scale than other lines. The position of Site 1199 was projected into the seismic section parallel to the northwestern SMP margin. Superimposed on the seismic sections in the lower half of the figure are the seismic stratigraphic interpretation and correlation, as well as shipboard core data converted from mbsf to two-way traveltime. Seismic Megasequences A–D and basement are color coded and match colors of stratigraphic correlation below (Fig. F10B). Roman numbers in left columns are lithologic boundaries. They do not correlate from site to site, as unit definition was based upon shipboard sedimentologic description of the drilled cores. Right columns indicate epoch boundaries defined with the shipboard age models. Numbers on the seismic section next to the sites indicate the age of seismic sequence boundaries, derived from time-depth conversion and shipboard age models. MS = megasequence. **B.** Stratigraphic correlation summary for Leg 194. The upper part of the figure shows a geological transect (sketch) representing all sites of Leg 194, from the Northern Marion Platform to the Southern Marion Platform and its talus. In the middle portion of the figure, seven data panels are presented for each site. In the bottom portion of the figure, an explanation is provided describing the data and symbols used. Data sets include depth downhole in mbsf, core number, core recovery, lithologic units with age derived from biostratigraphy and magnetostratigraphy, a graphic display of the lithologies, mineralogy based upon XRD analysis, natural gamma ray profiles from downhole logging and core-based physical properties measurements, and the megasequences defined from seismic reflection data. MS = megasequence, wd = water depth. (This figure is available in an oversized format.)

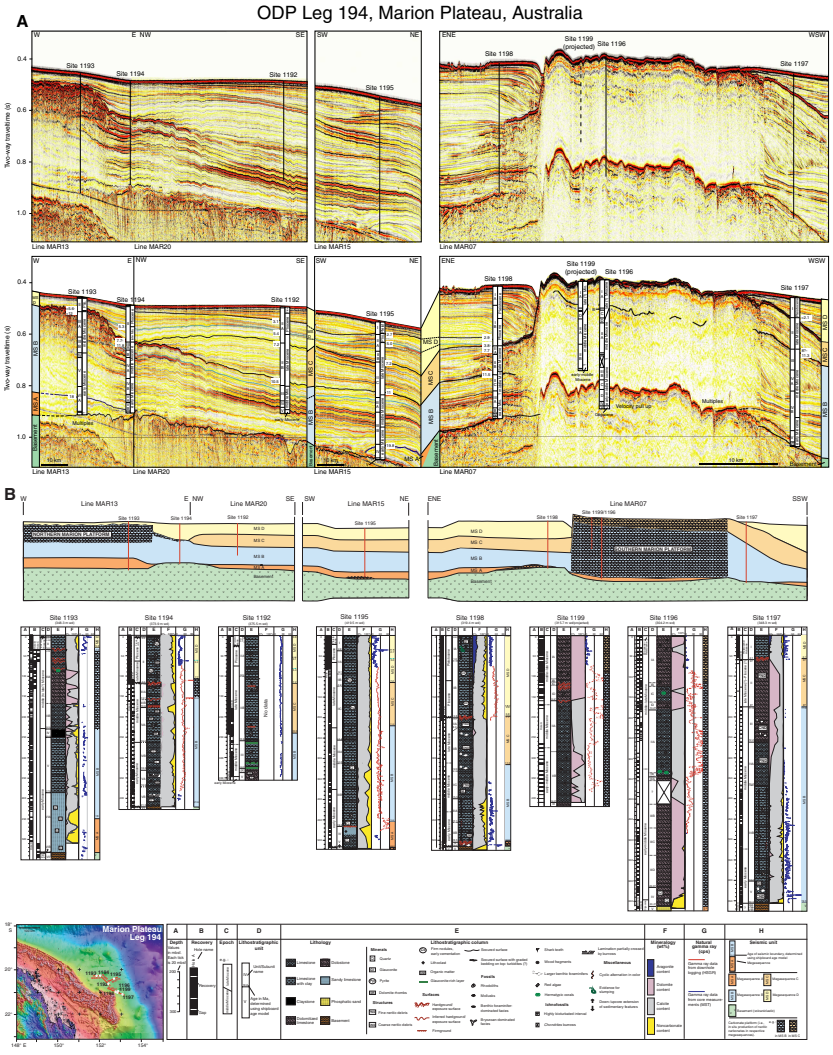

**Figure F11.** Correlation between seismic two-way traveltime (ms) and depth for all Leg 194 sites. These data were obtained by check-shot surveys (solid circles), virtual check shots (open circles), and integration of sonic log and shipboard velocity data between check shots. Virtual check shots are provided by obvious links between high-amplitude reflections on the seismic data and unique petrophysical horizons in the cores (e.g., basement and hardgrounds).

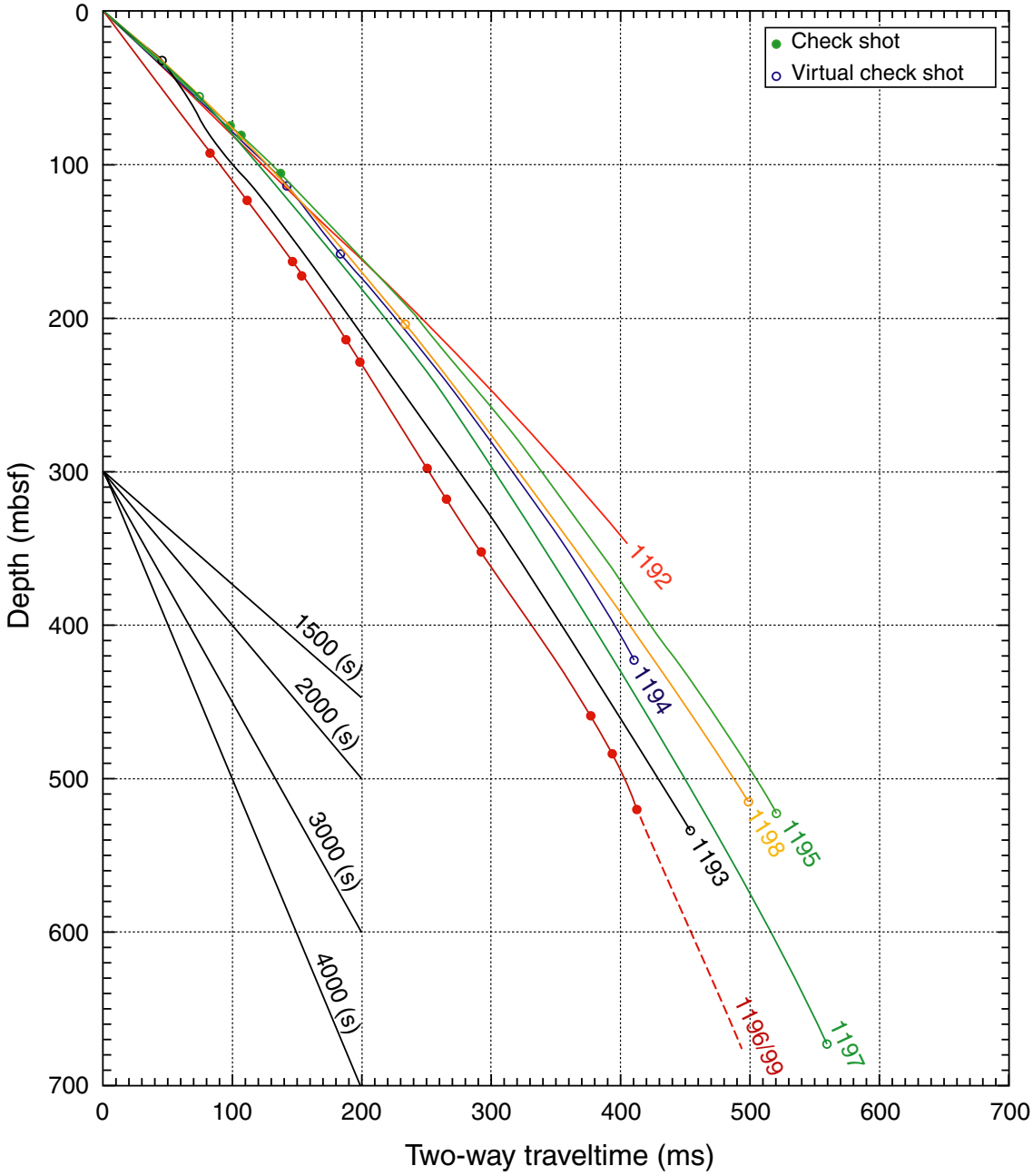

**Figure F12.** Sedimentation rates at Leg 194 sites. Trends at Sites 1195 and 1192 are similar and represent distal, drift-dominated deposition at rates of ~30 m/m.y. during the Miocene and 15 m/m.y. during the Pliocene–Pleistocene. The decrease in depositional rates at ~5 Ma probably reflects the decrease in nearby carbonate shedding. Carbonate platform Site 1193 shows a dramatic increase in depositional rates from 15 to 150 m/m.y. in the late early Miocene. Sedimentation rates in the overlying platform (initiated at ~16 Ma) are not directly defined. At Site 1196 (and Site 1199, not shown), platform growth rates of at least 80 m/m.y. are documented for an ~140 m thick middle Miocene interval, but subsequent growth rates could not be constrained. Adjacent slope Site 1197 shows increased depositional rates in the late middle Miocene, which is interrupted near the middle late Miocene boundary (11.1–? Ma; hiatus at 175 mbsf), a time of inferred sea level rise at Site 1194. Subsequent late Miocene (and early Pliocene?) platform shedding is only roughly constrained in time at Site 1197 (5–11 Ma); however, Site 1198 documents increased platform shedding (~50 m/m.y.) during the middle late Miocene, a time of apparent nondeposition at Sites 1193 and 1194. Deposition at Site 1198 ended at ~7.8 Ma (hiatus at 200 mbsf), which likely marks the end of carbonate growth at Site 1196. This starvation, lasting several million years, probably also occurred at Site 1197 (hiatus at 59 mbsf). The shaded area in the top left corner of the diagram highlights the records of the hemipelagic seismic Megasequence D, which fills in the topography created by the Miocene carbonate buildup. The oldest Megasequence D records (7.2–7.8 Ma) were recovered at Sites 1192, 1194, and 1195. This time coincides with the starvation of periplatform deposition at Site 1198 and could mark the onset of widespread drowning of the carbonate factory.

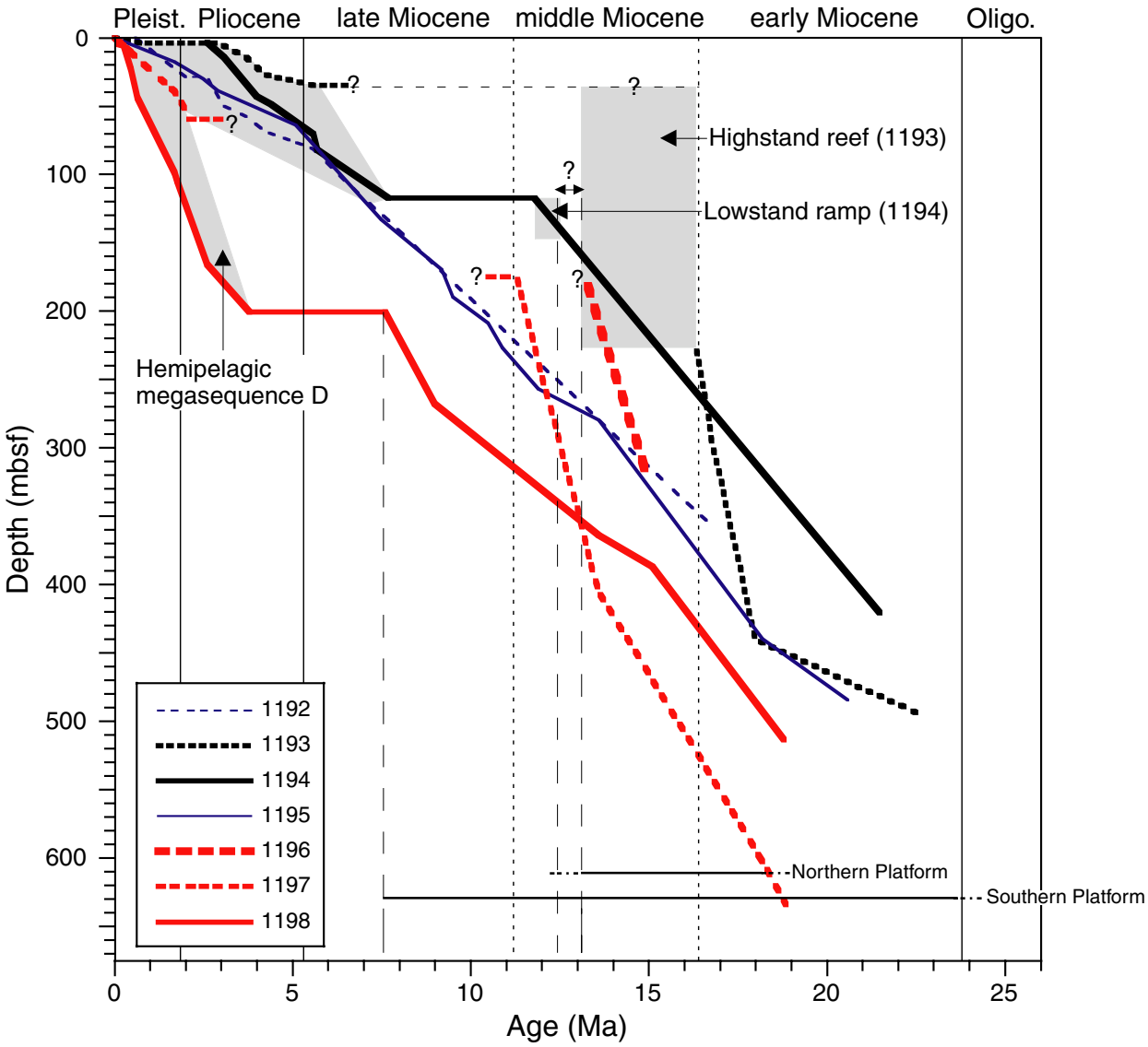

**Figure F13.** Seismic correlation between Leg 194 sites (see Fig. F2, p. 62, for location profiles). **A.** Northern transect along seismic lines MAR13, MAR20, and MAR15 linking Sites 1193, 1194, 1192, and 1195. (Continued on next page.) (This figure is also available in an **oversized format.**)

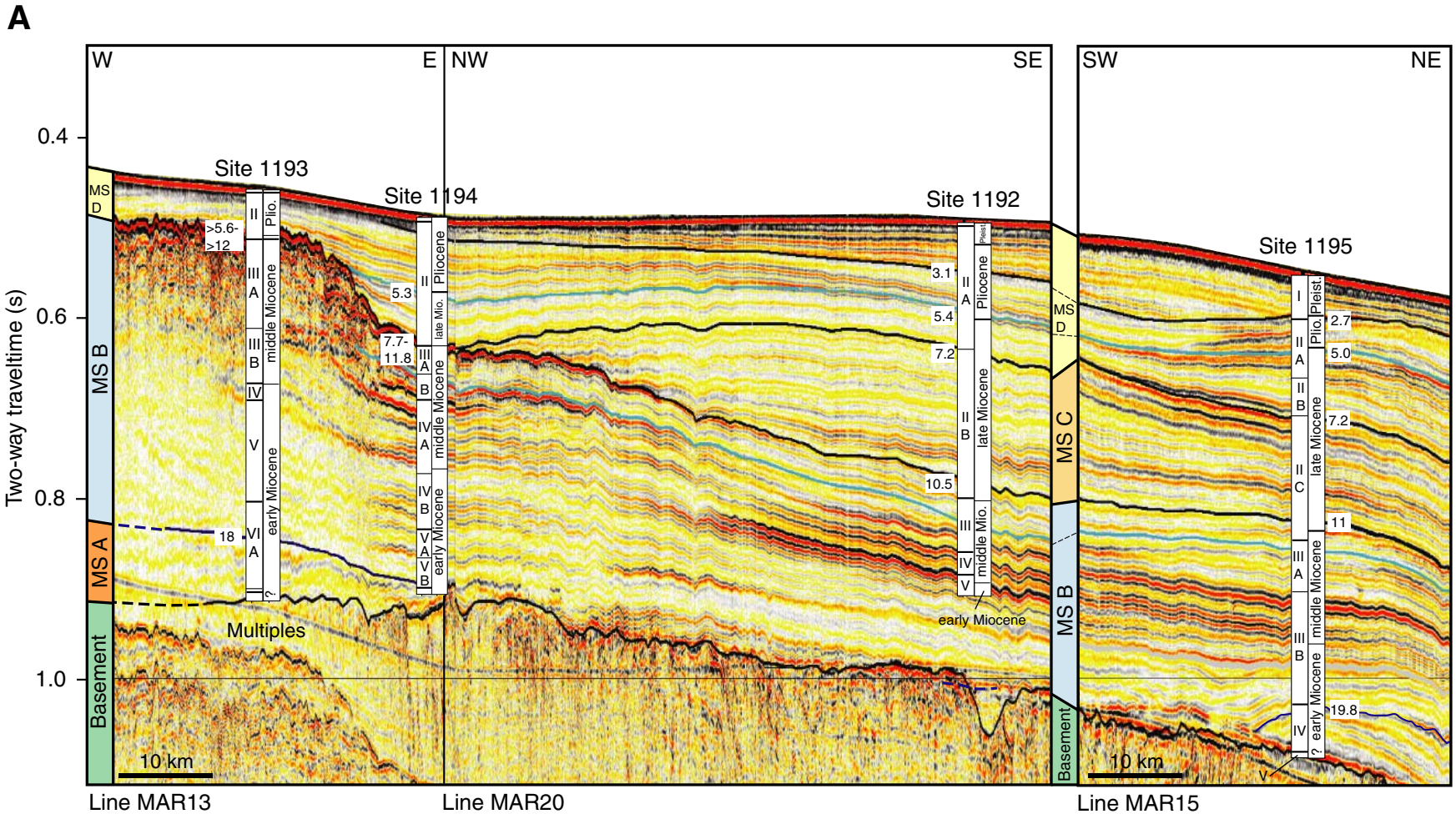

**Figure F13 (continued). B.** Southern transect along seismic line MAR07 linking Sites 1198, 1199, 1196, and 1197. The position of Site 1199 was projected into the seismic section parallel to the northwestern SMP margin. Roman numbers in left columns are lithologic unit boundaries. They do not correlate from site to site, as unit definition was based upon shipboard sedimentologic description of the drilled cores. Right columns indicate epoch boundaries defined with the shipboard age models. Numbers on the seismic section next to the sites indicate the age of seismic sequence boundaries, derived from time-depth conversion and shipboard age models. MS = megasequence. (This figure is also available in an **oversized format.**)

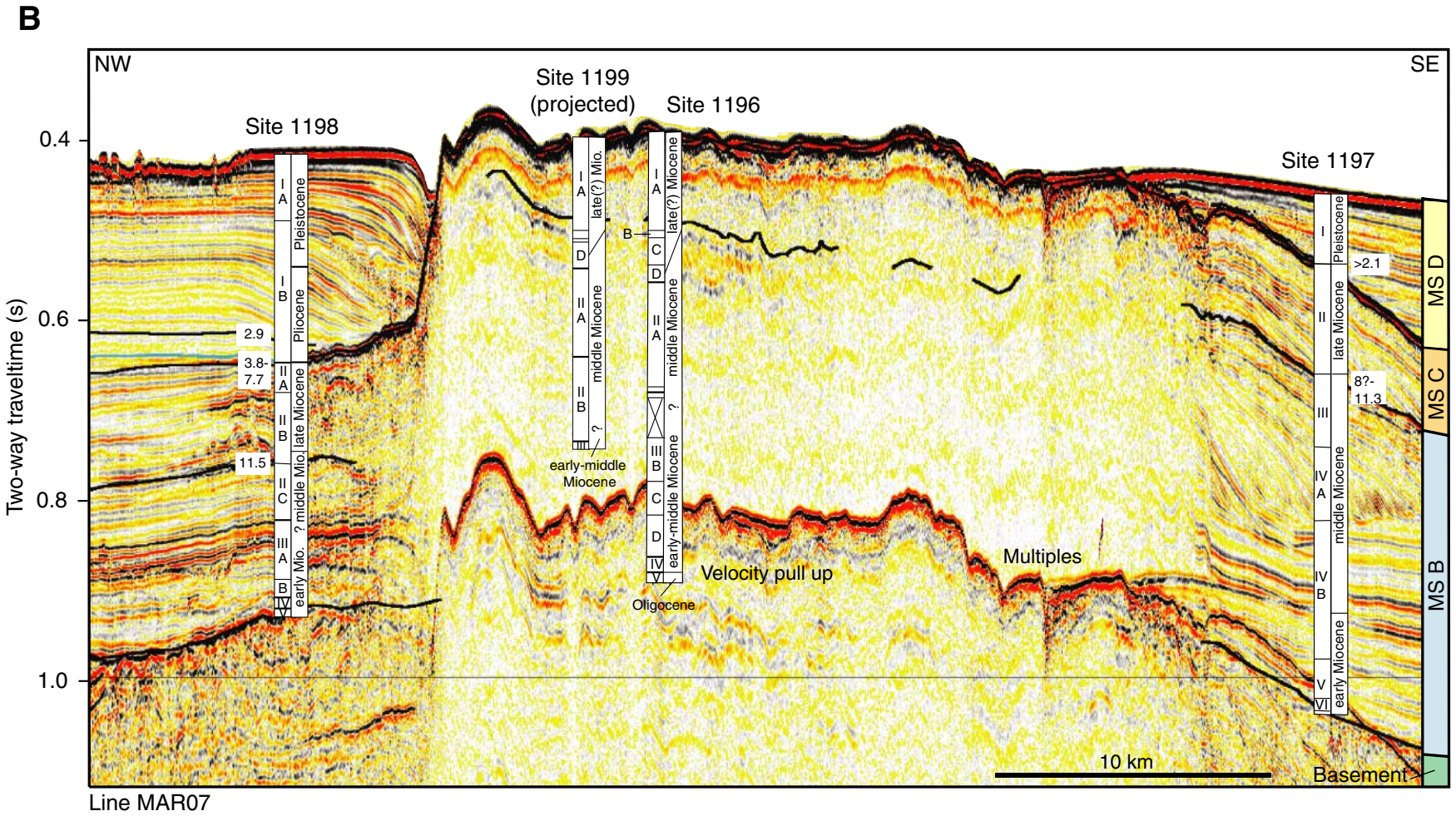

**Figure F14. A.** Diagram illustrating the calculation of the late middle Miocene eustatic fall using Sites 1193 and 1194, assuming infinite crustal strength (no differential subsidence) between the sites. The top panel displays the relevant seismic sequences on seismic line MAR13. The onlapping unit at Site 1194, below the Megasequence B/C boundary and above the onlap surface labeled R (sequence boundary; see arrow), was deposited during the middle Miocene lowstand, which exposed the platform top at Site 1193. The middle panel is a schematic presentation of the present-day configuration. The lower panel shows the geometric adjustment of the relevant sequence boundary (R) as a result of sediment expansion after removal of the post-middle Miocene sediment load. W1 = present day water depth, S = thickness of post-middle Miocene sediment load, PW = paleowater depth estimated from biotic assemblage, $\Delta_e$ = sediment expansion (reduced water depth), $\Delta_{SL}$ = magnitude of eustatic fall. (Continued on next page.)

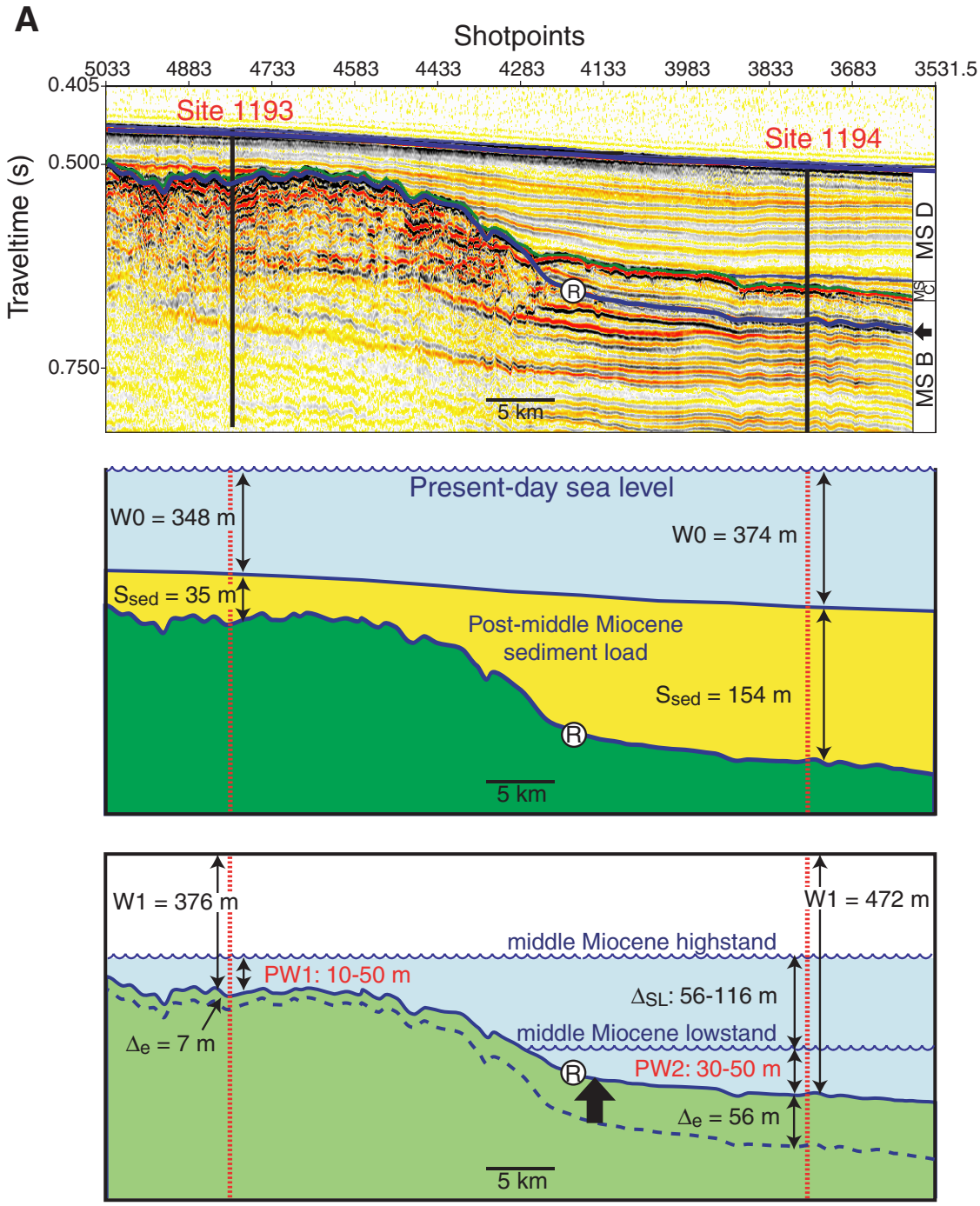

**Figure F14 (continued). B.** Diagram illustrating the calculation of the late middle Miocene eustatic fall using Sites 1193 and 1194, assuming zero flexural strength between the sites (i.e., local isostatic compensation at each site). Refer to the top two panels in Figure **F14A,** p. 77, for seismic line and schematic representation of the present-day configuration. The top panel illustrates geometric adjustments to sediment unloading (isostatic and sediment expansion). The middle panel shows the water depths adjustment for the middle Miocene highstand condition. The bottom panel shows the final adjustment for the middle Miocene lowstand parameters. W3 and W4 = reconstructed water depths, $\Delta_m$ = amounts of isostatic rebound, $\Delta_{SL1}$ = total sea level fall required for middle Miocene highstand paleowater depth PW1, $\Delta_{SL2}$ = eustatic fall required for middle Miocene lowstand paleowater depth PW2.

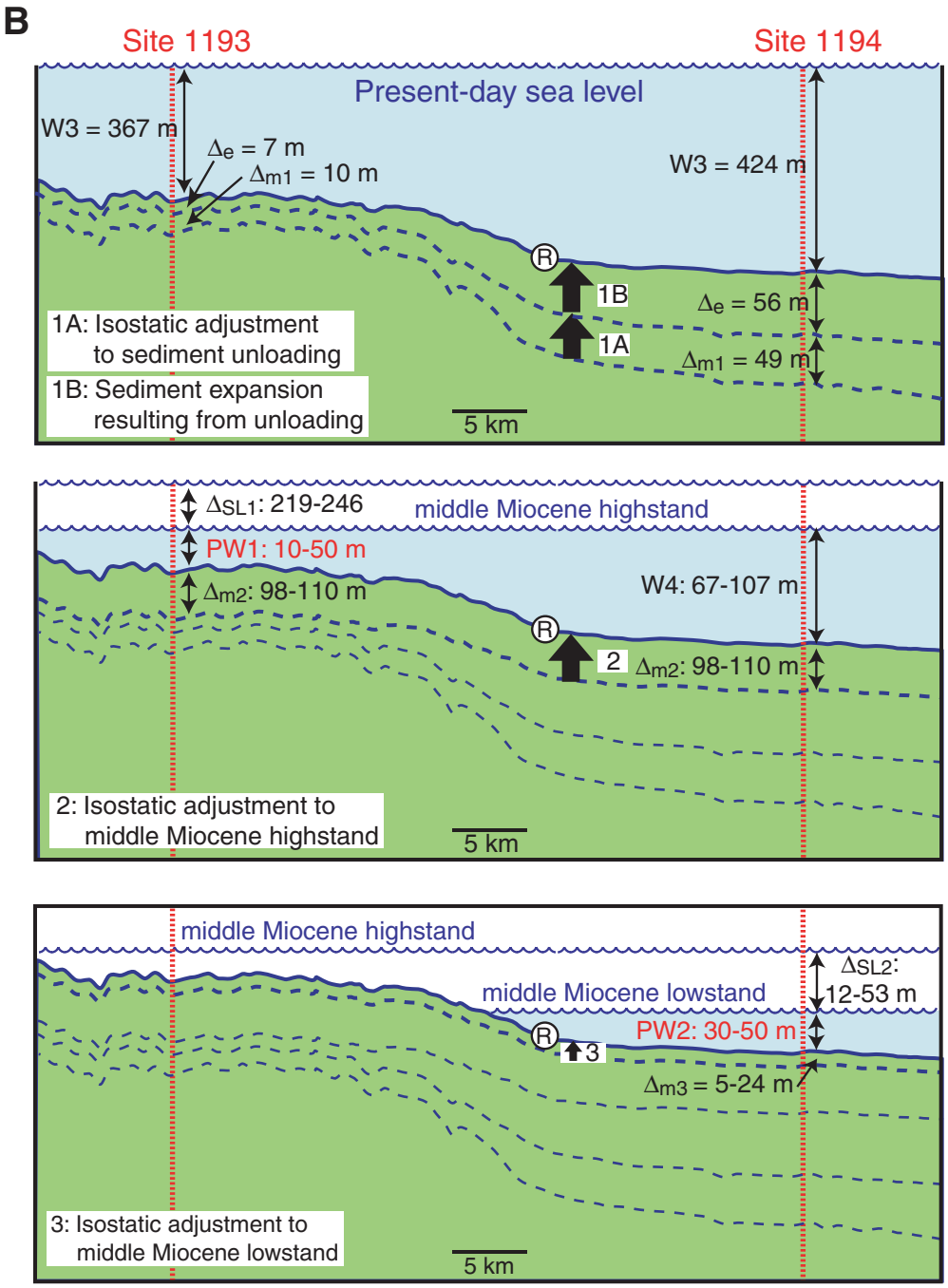

**Figure F15.** Schematic diagrams reconstructing the depositional history of the Marion Plateau sequences based on recovered lithologies (see "Platform Evolution," p. 50, for a description of the evolutionary sequence of depositional events). Diagrams on the left represent the transect across the Northern Marion Platform (Sites 1192, 1193, 1194, and 1195). Diagrams on the right represent the transect across the Southern Marion Platform (Sites 1196, 1197, 1198, and 1199). Time slices are (from bottom to top) (**A**) Oligocene, (**B**) early Miocene to middle Miocene, (**C**) late middle Miocene, (**D**) late Miocene to Pliocene–Pleistocene, and (**E**) Pliocene–Pleistocene to Holocene. Subseafloor depth on the southern drilling transect has been adjusted to account for differential subsidence since the middle Miocene.

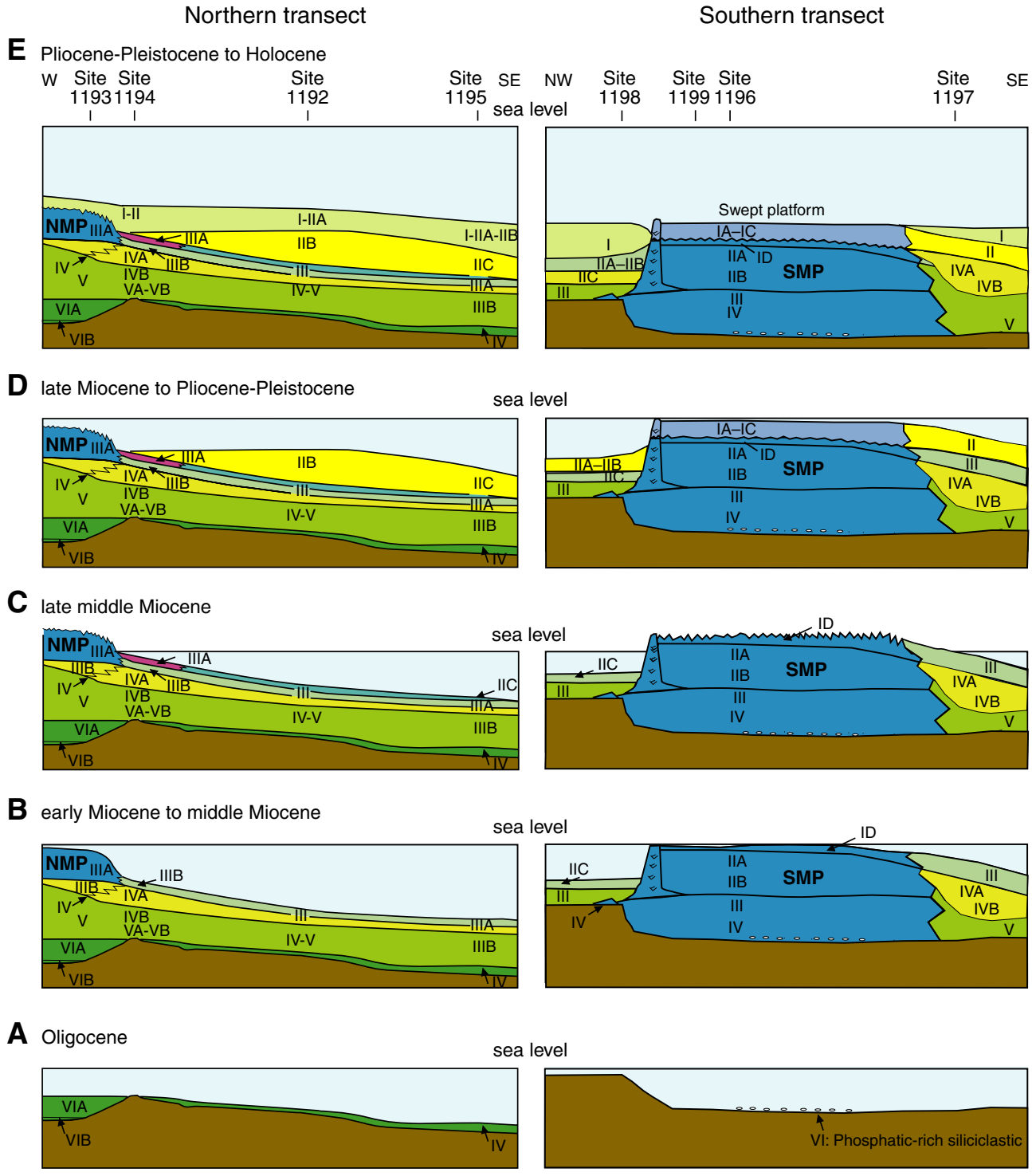

**Figure F16.** Multichannel seismic reflection profile (MAR13) showing the location of Site 1194 and basement reflection (dashed line). Shown are examples of thin sections of altered olivine basalts that comprise basement in this region. **A.** Thin section view showing the products of alteration (zeolites-natrolite) infilling an amygdaloid under cross-polarized light. **B.** Thin section view showing the infilling of veins with plagioclase under cross-polarized light. **C.** General thin section view under cross-polarized light showing olivine phenocrysts and plagioclase lathes. **D.** Magnetic inclination data from the basement sequence.

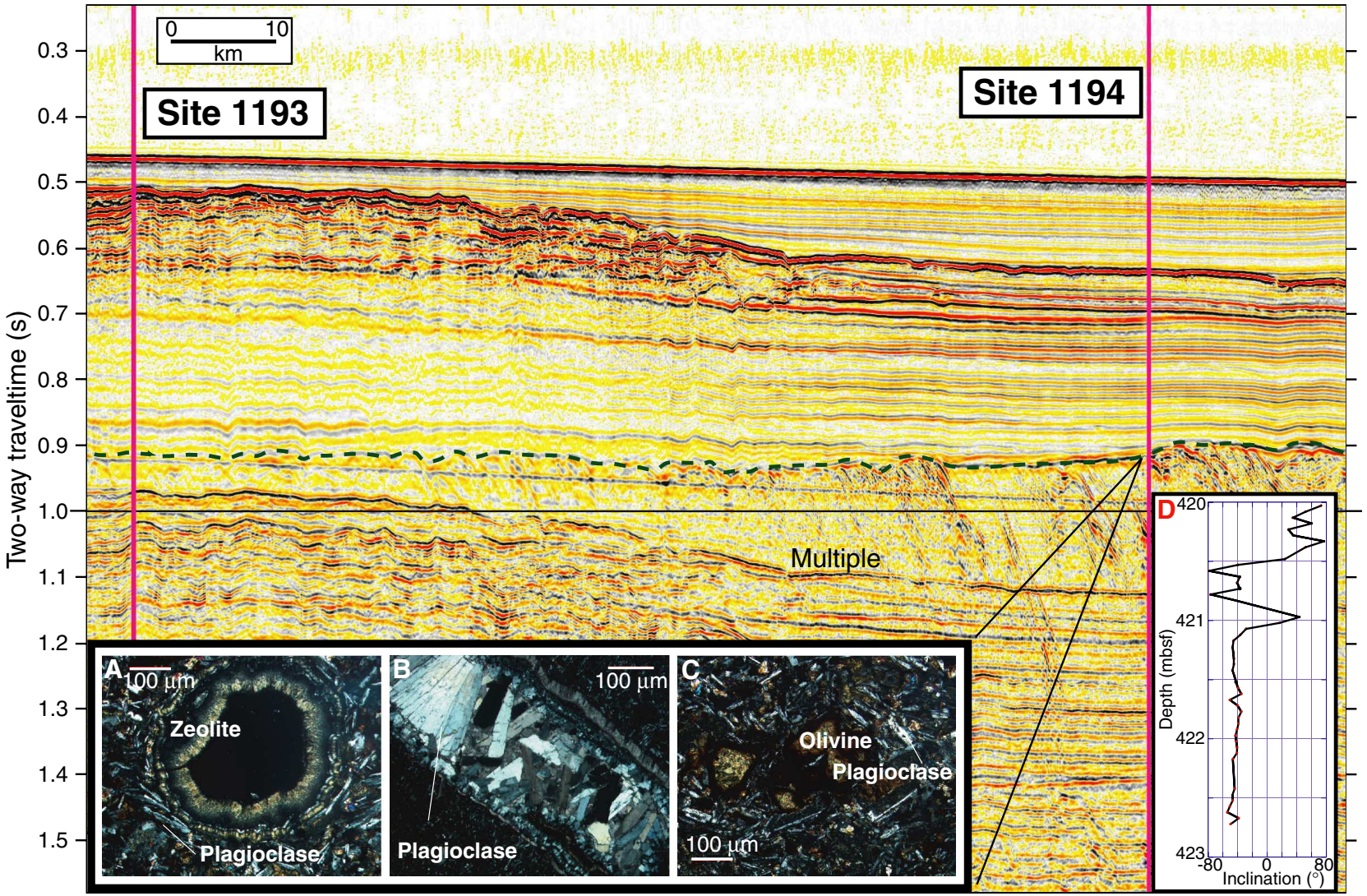

**Figure F17.** Multichannel seismic reflection profile (MAR07) showing the location of Site 1197 and basement reflection (dashed line). Shown are examples of thin sections of altered olivine basalts that comprise basement in this region. **A.** Thin section view under cross-polarized light showing pyroxene phenocrysts. **B.** Thin section view under cross-polarized light showing olivine phenocrysts and plagioclase lathes. **C.** Magnetic inclination data from recovered basalts.

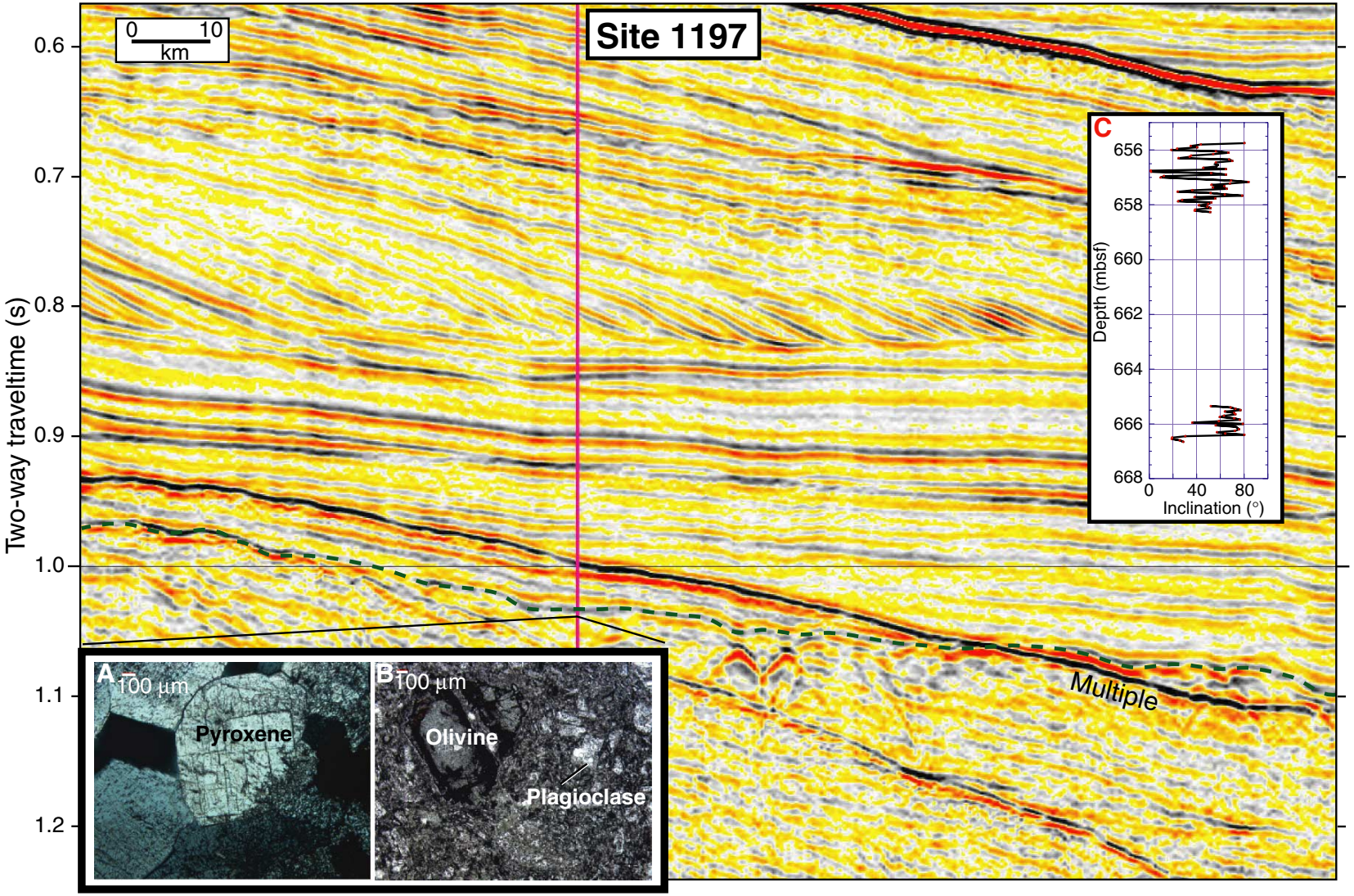

**Figure F18.** Multichannel seismic reflection profile (MAR13) showing the location of Site 1193 and basement reflection (dashed lines). Shown are examples of thin sections of altered olivine basalts that comprise basement in this region. **A.** Thin section view showing the products of alteration (zeolites–natrolites) infilling an amygdaloid under cross-polarized light. **B.** Thin section view under normal light showing the "ghost" residuals of plagioclase lathes and pyroxenes. **C.** Thin section view under cross-polarized light showing the "ghost" residuals of plagioclase lathes and pyroxenes. **D.** Magnetic inclination data from recovered basalts.

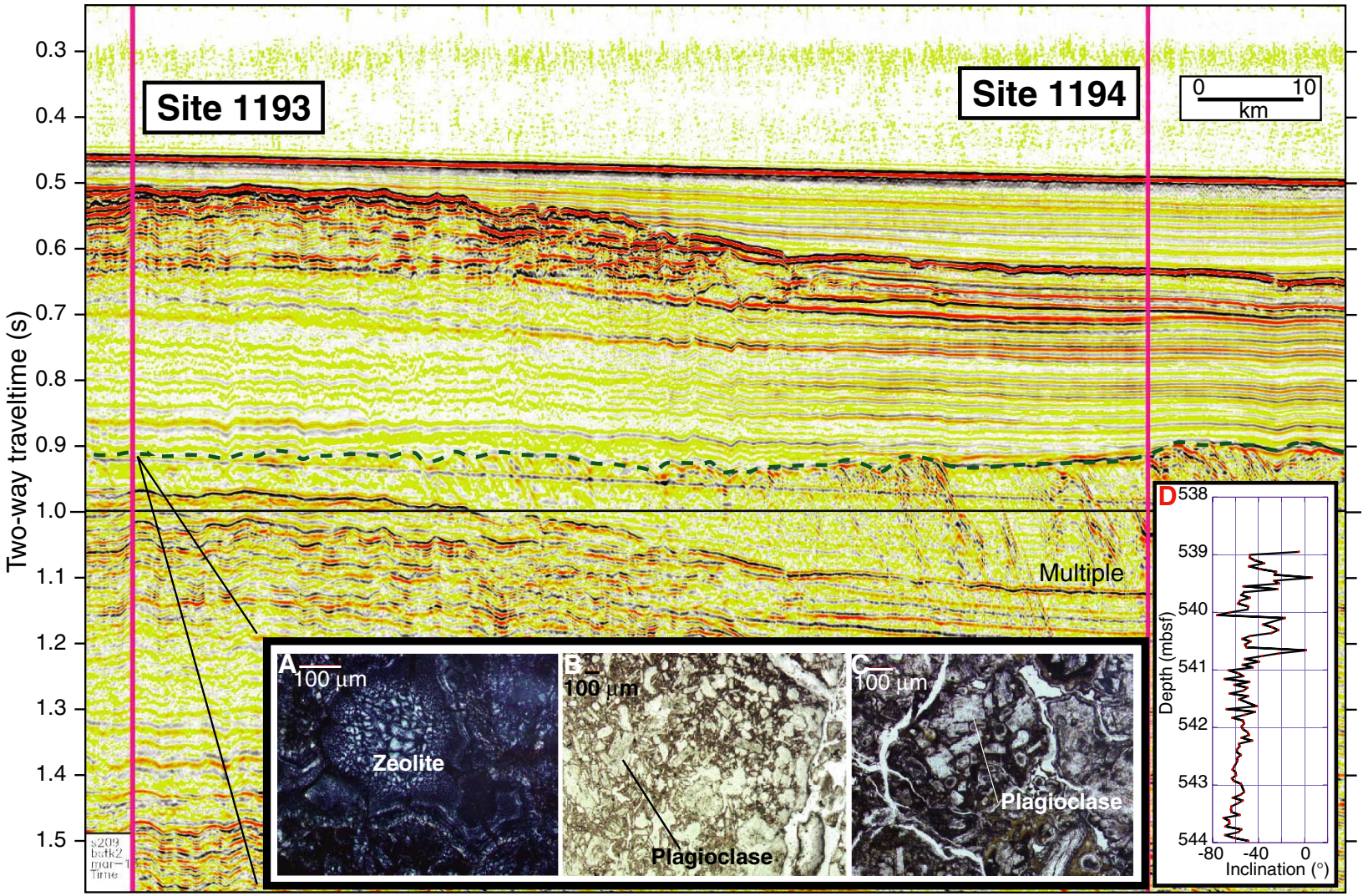

**Figure F19.** Multichannel seismic reflection profile (MAR07) showing the location of Site 1198 and basement reflection (dashed line). Shown are examples of thin sections of altered olivine basalts that comprise basement in this region. **A.** Thin section view under cross-polarized light showing the groundmass, olivine phenocrysts and plagioclase lathes. **B.** View of altered plagioclase phenocrysts under cross-polarized light showing olivine phenocrysts and plagioclase lathes. **C.** Thin section view showing the products of alteration (quartz) infilling an amygdaloid under cross-polarized light. **D.** Magnetic inclination of recovered basalts.

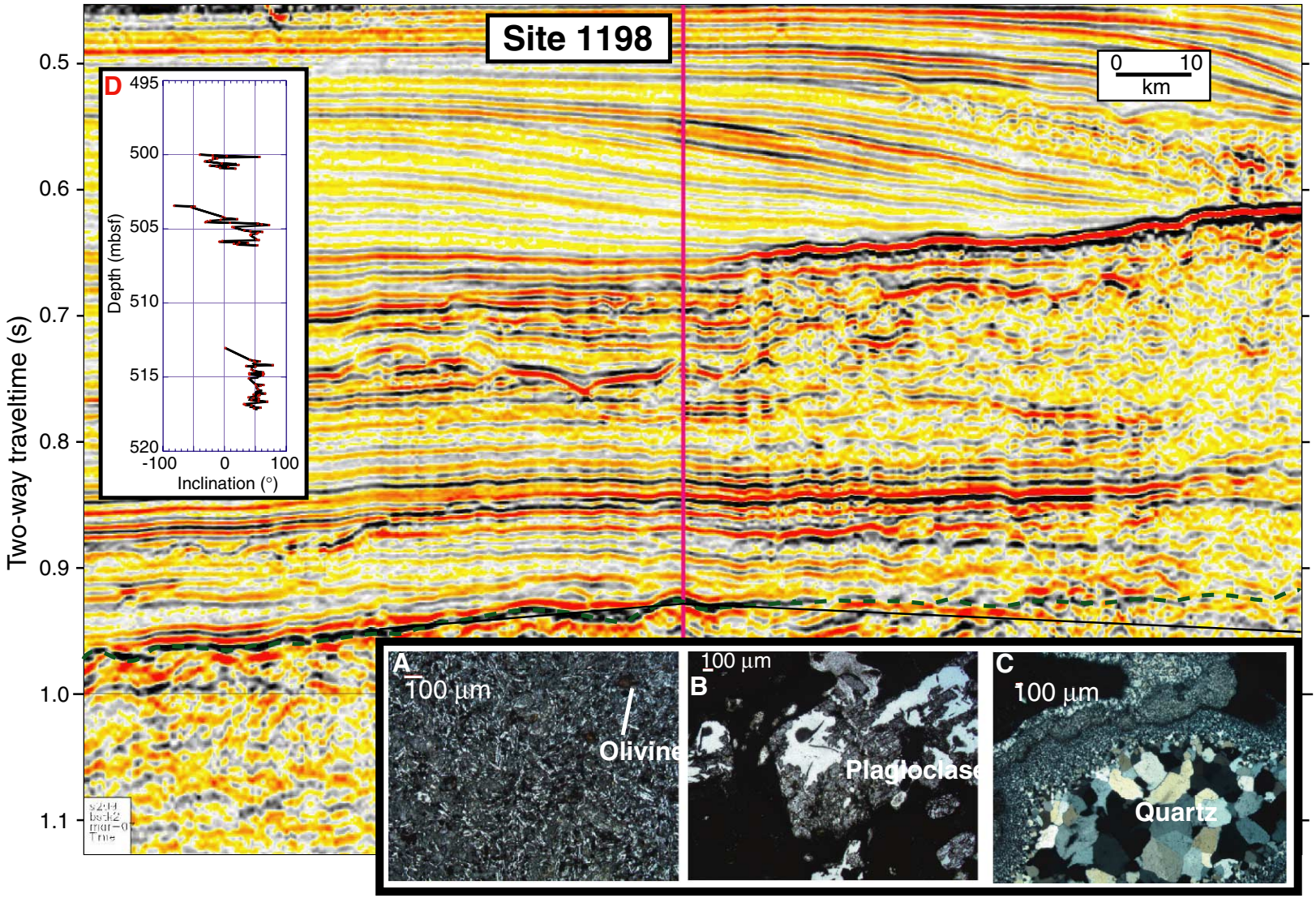

**Figure F20.** Multichannel seismic line MAR07 at Site 1198. Strontium (solid circles) and sulfate (open circles) concentrations are plotted on the location of Site 1198 vs. depth (in two-way traveltime). Note the near-seawater values of strontium and sulfate in Megasequence C, indicating circulation of seawater, possibly through a hydraulic connection with the southern platform.

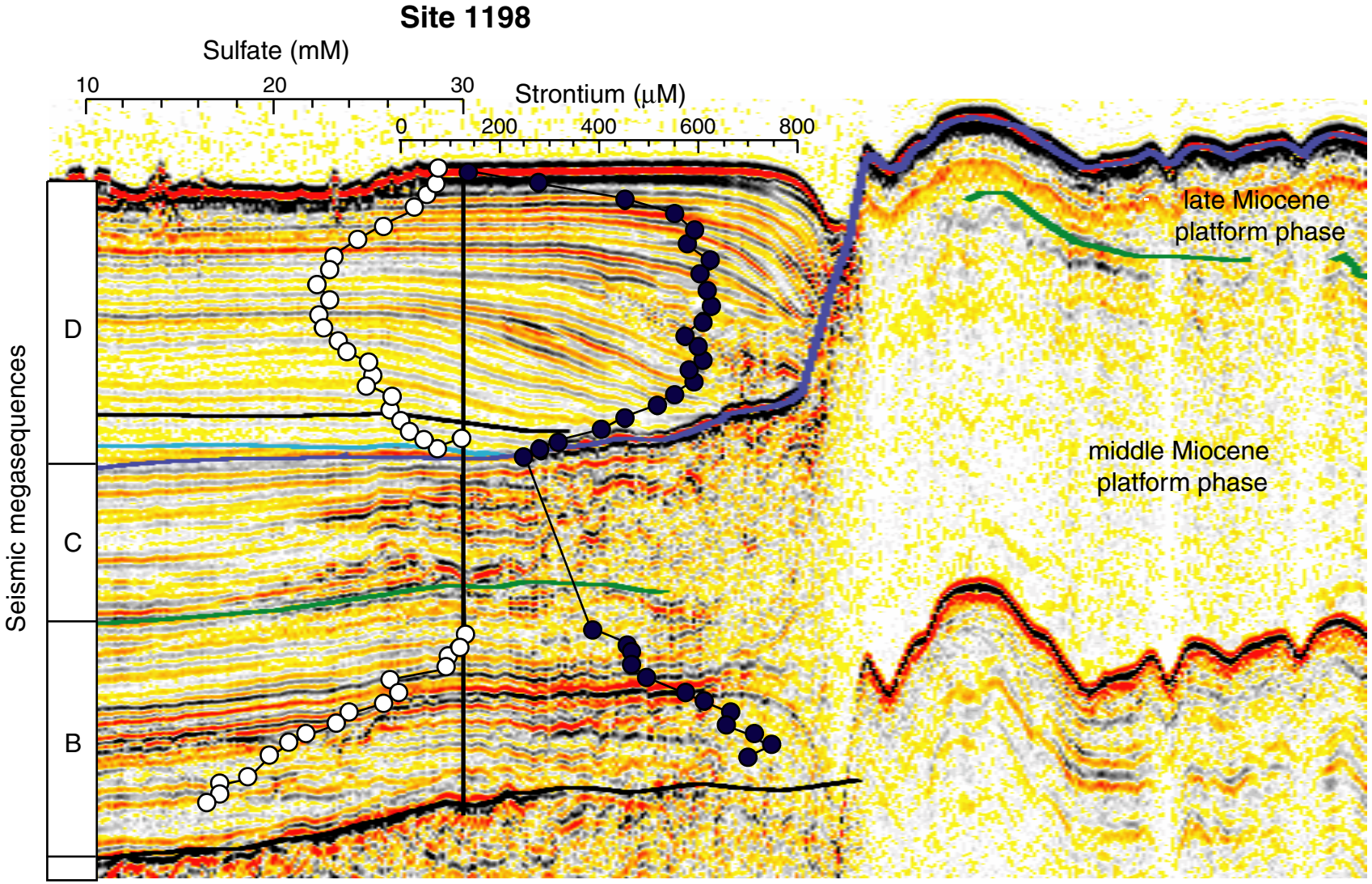

**Figure F21.** Multichannel seismic line MAR13 at Site 1193. Strontium (solid circles) and sulfate (open circles) concentrations are plotted on the location of Site 1193 vs. depth (in two-way traveltime). Note the near-seawater values of strontium and sulfate above and below the northern platform, indicating circulation of seawater within this platform.

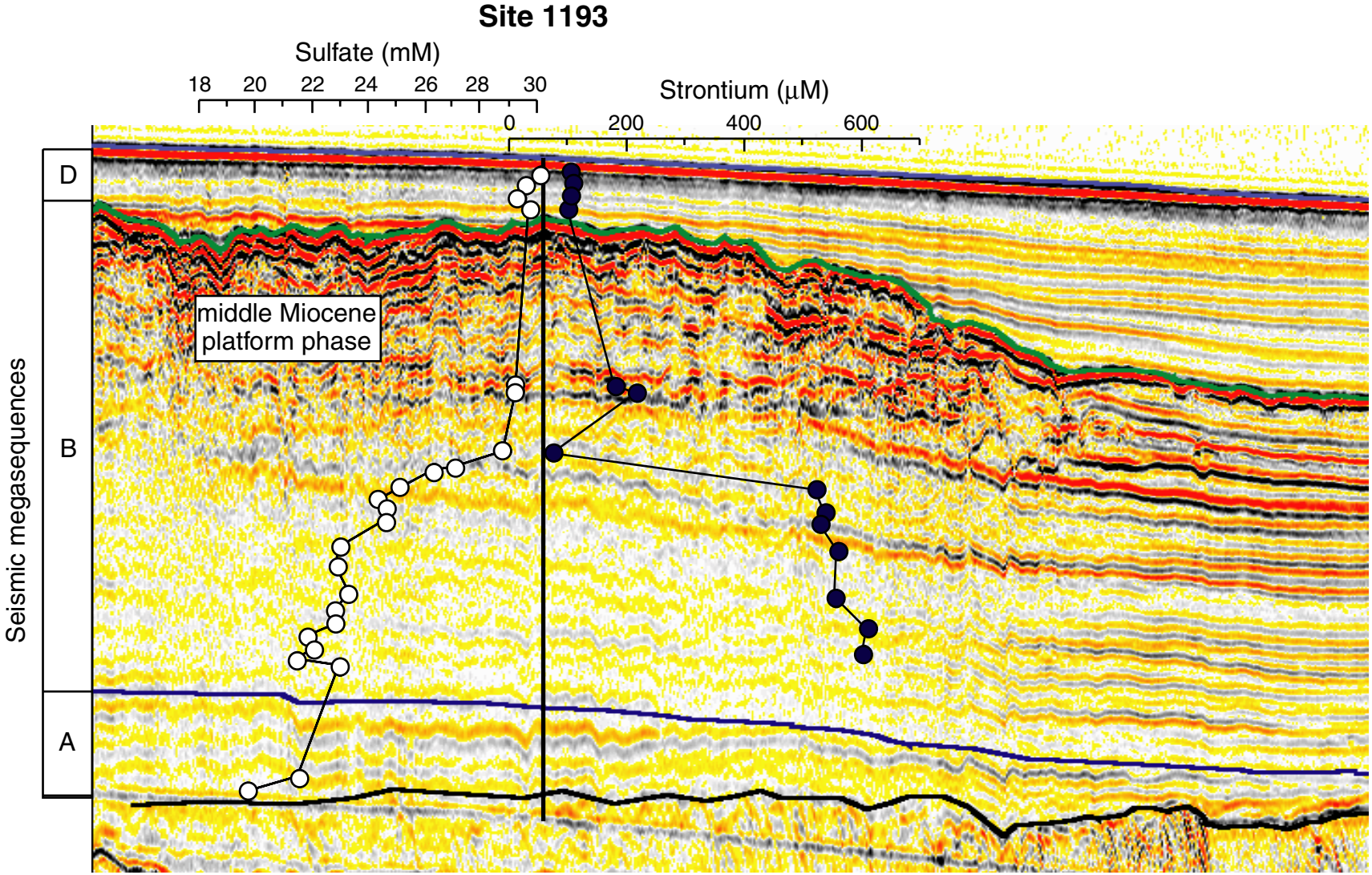

**Table T1.** Acquisition and processing parameters for seismic site survey data.

| | |
|---|---|
| Seismic source | Two generator-injector guns (45/105 $in^3$) |
| Streamer | 24-channel Innovation Transducers Inc. |
| | 12.5-m group spacing, six hydrophones/channel |
| | 30-m deck leader, 105-m tow leader |
| | 2 x 150-m active sections |
| | Three digicourse 5010 active birds set to 5 ± 1 m |
| Navigation | DGPS reference station Optus Townsville |
| Shot spacing | 25 m |
| Acquisition system | Geometrics 24-channel |
| Sample interval | 1 ms |
| Recording length | 3 s |
| Processing parameters | F-K filter, water-depth dependent gain |
| | Bandpass filter 20–25/400/500 Hz |
| | 250-ms automatic gain control |

**Table T2.** Operations summary, Leg 194.

| Hole | Latitude | Longitude | Water depth (m) | Number of cores | Interval cored (m) | Core recovered (m) | Recovery (%) | Interval drilled (m) | Total penetration (m) | Time on hole (days) |
|---|---|---|---|---|---|---|---|---|---|---|
| 1192A | 20°34.306′S | 152°24.257′E | 374.4 | 30 | 242.5 | 243.5 | 100.4 | 0.0 | 242.5 | 1.7 |
| 1192B | 20°34.310′S | 152°24.260′E | 376.5 | 22 | 178.0 | 105.1 | 59.1 | 177.5 | 355.5 | 1.3 |
| | | Site 1192 totals: | | 52 | 420.5 | 348.6 | 82.9 | 177.5 | 598.0 | 3.0 |
| 1193A | 20°14.502′S | 151°47.531′E | 348.3 | 84 | 515.0 | 173.9 | 33.8 | 0.0 | 515.0 | 4.6 |
| 1193B | 20°14.501′S | 151°47.542′E | 348.3 | 21 | 103.0 | 12.8 | 12.4 | 35.0 | 138.0 | 3.1 |
| 1193C | 20°14.495′S | 151°47.538′E | 348.3 | 8 | 73.6 | 21.1 | 28.6 | 474.9 | 548.5 | 2.2 |
| | | Site 1193 totals: | | 113 | 691.6 | 207.7 | 30.0 | 509.9 | 1201.5 | 10.0 |
| 1194A | 20°14.552′S | 151°58.983′E | 373.9 | 20 | 169.9 | 126.2 | 74.3 | 0.0 | 169.9 | 1.0 |
| 1194B | 20°14.554′S | 151°58.991′E | 373.9 | 33 | 317.1 | 89.2 | 28.1 | 0.0 | 427.1 | 2.1 |
| | | Site 1194 totals: | | 53 | 487.0 | 215.4 | 44.2 | 0.0 | 597.0 | 3.2 |
| 1195A | 20°24.283′S | 152°40.231′E | 419.9 | 9 | 80.7 | 79.3 | 98.2 | 0.0 | 80.7 | 0.5 |
| 1195B | 20°24.283′S | 152°40.243′E | 419.2 | 55 | 521.2 | 399.3 | 76.6 | 0.0 | 521.2 | 3.1 |
| | | Site 1195 totals: | | 64 | 601.9 | 478.6 | 79.5 | 0.0 | 601.9 | 3.6 |
| 1196A | 21°0.371′S | 152°51.512′E | 304.2 | 70 | 672.2 | 86.4 | 12.8 | 0.0 | 672.2 | 5.3 |
| 1196B | 21°0.372′S | 152°51.523′E | 304.2 | 51 | 265.3 | 29.4 | 11.1 | 0.0 | 265.3 | 4.3 |
| | | Site 1196 totals: | | 121 | 937.5 | 115.7 | 12.3 | 0.0 | 937.5 | 9.6 |
| 1197A | 21°4.570′S | 153°3.929′E | 348.3 | 23 | 203.8 | 56.2 | 27.6 | 0.0 | 203.8 | 1.3 |
| 1197B | 21°4.574′S | 153°3.943′E | 348.3 | 65 | 624.9 | 213.6 | 34.2 | 50.0 | 674.9 | 4.3 |
| | | Site 1197 totals: | | 88 | 828.7 | 269.8 | 32.6 | 50.0 | 878.7 | 5.5 |
| 1198A | 20°57.930′S | 152°43.994′E | 319.4 | 27 | 251.5 | 210.2 | 83.6 | 0.0 | 251.5 | 1.1 |
| 1198B | 20°57.930′S | 152°44.005′E | 319.4 | 34 | 326.9 | 116.6 | 35.7 | 195.7 | 522.6 | 2.4 |
| | | Site 1198 totals: | | 61 | 578.4 | 326.9 | 56.5 | 195.7 | 774.1 | 3.5 |
| 1199A | 20°58.692′S | 152°54.947′E | 315.7 | 45 | 419.5 | 92.2 | 22.0 | 0.0 | 419.5 | 4.4 |
| | | Site 1199 totals: | | 45 | 419.5 | 92.2 | 22.0 | 0.0 | 419.5 | 4.4 |
| | | Leg 194 totals: | | 597 | 4965.1 | 2054.9 | 41.4 | 933.1 | 6008.2 | 42.7 |

**Table T3.** Parameters used for paleotopographic reconstructions and sea level estimates.

| Parameters | Site 1193 | Site 1194 |
|---|---|---|
| Site: | | |
| Present-day water depth (W1) | 348 m | 374 m |
| Depth below seafloor to the Megasequence B/C boundary | 35 mbsf | 154 mbsf |
| Paleowater depths at Megasequence B/C sequence boundary | 10–50 m | 30–50 m |
| Total sediment thickness | 531 m | 422 m |
| Decompaction: | | |
| Exponential fit to porosity data ($\phi_0$) | 61% | 65% |
| Exponential fit to porosity data (k) | 0.001/m | 0.002/m |
| Sediment thickness of postmiddle Miocene load ($S_{sed}$) | 35 m | 154 m |
| Coordinates of sediment to be decompacted | (229–531 mbsf) | (154–421 mbsf) |
| Present-day sediment thickness to be decompacted | 302 m | 268 m |
| Decompacted sediment thickness | 309 m | 323 m |
| Sediment expansion | 7 m | 56 m |
| Isostatic correction: | | |
| Density of seawater ($\rho_w$) | 1.02 g/cm$^3$ | 1.02 g/cm$^3$ |
| Bulk density of postmiddle Miocene sediment load ($\rho_s$) | 1.67 g/cm$^3$ | 1.75 g/cm$^3$ |
| Assumed mantle density ($\rho_m$) | 3.33 g/cm$^3$ | 3.33 g/cm$^3$ |
| Estimated sea level change: | | |
| Assuming local isostasy (no flexural strength) | 12–53 m (32 ± 20 m) | |
| Assuming rigid basement (high flexural strength) | 56–116 m (86 ± 30 m) | |